Universitat Autònoma de Barcelona

Non-linear elastic response of scale invariant solids

Víctor Cáncer Castillo

Universitat Autònoma de Barcelona

Institut de Física d'Altes Energies

Non-linear elastic response of scale invariant solids

A thesis presented for the degree of
Doctor of Physics by

Víctor Cáncer Castillo

Supervised by:

Prof. Oriol Pujolàs Boix

October 16, 2020

Acknowledgments

First off, I would like to start thanking my supervisor Oriol Pujolas, for the countless hours that he devoted to teach me and help me through these four years of PhD (plus the year where we worked in the Bachelor's thesis as well!).

Secondly, but not less important, I would like to thank my parents Manoli and Rafa, who had always supported my decision on pursuing this career on theoretical physics. Without their contribution this thesis (and much more) would never have been possible.

To my fiance, Bea, who has had to put up with all my ups and downs through all this journey. Thank you.

Of course, thanks also to all my friends and family. I hope we get the chance to get together soon and celebrate this is finally done.

Finally, I would like to express my gratitude to Matteo, my main collaborator in all publications.

Abstract

The goal of this thesis is to apply modern field theory methods to understand the non-linear elastic (NLE) response of solids. The NLE response contains a large number of low-energy observable quantities, not always easy to derive from the microscopic composition of the material. An essential actor in the elastic response are the phonons, which can be described as the Goldstone bosons of the spontaneously broken space-time symmetries. As such, their low energy dynamics (including non-linearities) can be captured systematically by standard low energy Effective Field Theory (EFT) methods. This offers naturally a novel approach to tackle NLE phenomenology. One main conclusion is that indeed the low energy effective methods can provide nontrivial information, as relations among various different NLE observables. We illustrate this by obtaining bounds on the maximum deformation that a material can tolerate, which can be expressed in function of other NLE observables.

A case of special interest is that of scale invariant (SI) solids. This includes two distinct sub-cases, since SI can be realized either as a manifest symmetry or a spontaneously broken symmetry. The former case corresponds to a non-trivial fixed point and requires the use of holographic (AdS/CFT) techniques. The latter case instead can be described with more standard EFT methods. We compare the results obtained in the two cases, and find that the obtained elasticity bounds differ significantly in the two sub-cases.

List of publications

1. **Elasticity bounds from Effective Field Theory**
   Lasma Alberte, Matteo Baggioli, Victor Cancer Castillo, Oriol Pujolas
   arxiv.org/abs/1807.07474
   Published in Phys. Rev. D 100, 065015 (2019)
   This publication is covered in Section 4.

2. **Scale invariant solids**
   Matteo Baggioli, Victor Cancer Castillo, Oriol Pujolas
   arxiv.org/abs/1910.05281
   Published in Phys. Rev. D 101, 086005 (2020)
   This publication is covered in Section 5.

3. **Black Rubber and the Non-linear Elastic Response of Scale Invariant Solids**
   Matteo Baggioli, Victor Cancer Castillo, Oriol Pujolas
   arxiv.org/abs/2006.10774
   Published in J. High Energ. Phys. 2020, 13 (2020)
   This publication is covered in Section 5 (mostly on subsections 5.2 and 5.3) and an Appendix of the paper is reproduced in Section 4.3.

* *In Appendix A I add some results that are not part of any publication.*

Contents

Chapter 1

Introduction

Solids and its elastic properties have been thoroughly studied for many centuries due to its many applications and uses. The theory of elasticity treats the mechanical response of solids considering such material as a continuum media, including its sound wave excitations - the phonons. We can consider this theory as an early example of an EFT. Similarly to hydrodynamics, the theory of elasticity can be formulated as a derivative expansion (low-energy expansion) of some effective degree of freedom - in this case, the displacement vector of the solid elements from its equilibrium configuration.

The classic theory of elasticity can be extended in order to describe the non-linear regime, dealing with the response of solids to finite deformations [168, 170, 222]. This regime is characterized by the stress-strain relations at finite deformations (see Figure 1.1 as an example), which encodes a large number of observables and physical parameters [170]. However, these parameters are not easy to derive from a microscopic theory, thus we consider EFT methods that might help us understand the nonlinear elasticity phenomena.

From the QFT perspective, it is a very interesting question whether one can apply modern EFT methods to describe the non-trivial features of the non-linear elastic response of materials. This particular issue is one of the central points that we want to deal with throughout the thesis. We hope that via these methods we can have a better understanding of the elastic response of solid materials at finite deformation.

As in any EFT we must require a clear separation of scales: here we regard low frequency (acoustic) phonons as the only degrees of freedom, whereas heavier modes are integrated-out. We can exploit the fact that phonons can be considered to be the Goldstone bosons of translational symmetry breaking [74, 139, 163]. Due to this, we can obtain the fully non-linear effective action through the coset construction [164].

Once we have constructed the form of the EFT out of the symmetry breaking pat-

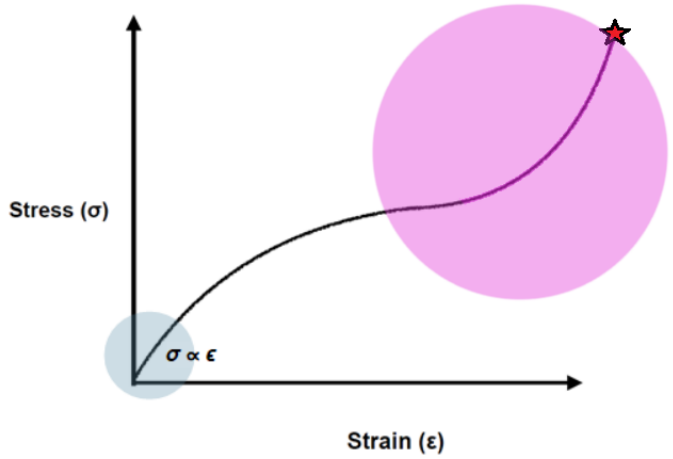

Figure 1.1: Cartoon of a typical stress-strain curve of a very elastic material. In blue we have the linear region, where the stress-strain relation is $\sigma \sim \epsilon$. At large deformations, displayed in pink, the stress-strain relation deviates from its linear form. Typically materials break or fracture at some finite deformation, which translates in the stress-strain curves to terminating at some point. This breaking point is indicated with a red star.

tern we attempt to understand how materials that can sustain very large deformations behave. These type of elastic materials are precisely the ones that allow us to explore a large enough range of deformations in order to investigate their non-linear response. By imposing self-consistency and stability conditions on the theory we will extract constraints on physical quantities, such as the maximum stress that can be applied to the material. Remarkably, from such constraints we will be able to establish correlations among multiple non-linear physical observables. This will show the predictive power that these EFT methods can have when studying solid materials.

There is also a case of special interest that is provided by the set of materials that exhibit scale invariance (SI). We will devote a large part of the manuscript on discussing and studying this type of solids, which we consider to be a very intriguing subject. Solids that exhibit SI represent a much more sophisticated scenario, but the problem is a well defined one and it is worth dedicating some effort on figuring out their non-linear elastic properties. Although it is not our goal to identify exactly which kind of physical systems accomplishes this we should note that these cases appear to be similar to some real world materials. Typical examples of materials related with these SI solids are those which display criticality in the form of a Quantum critial point. Among these

materials we can mention, for instance, the so-called high-T_c superconductors whose non-linear mechanical characterization has got growing interest in the last years due to their technological applications [189, 191].

The way this SI is realized in the solid can be divided into two principal categories, as we will see in Chapter 5: either the SI is a spontaneously broken symmetry (SBS) or it is manifest. Depending on what case we focus on the methods we will need to apply to describe them are going to be entirely distinct.

In the case of SI being a SBS we expect to have a gapped spectrum, where the phonons will be isolated low energy excitations. Thus, in such a case, we are going to be able to apply the EFT methods we described above, imposing SI in the theory. Let us point out that being SI here does not translate into being conformally invariant, as it usually happens. We must mention that this model represents a new example of SI theory that does not realize the full conformal group, which is achieved by breaking Lorentz invariance spontaneously.

On the other hand, if the SI is a manifest symmetry of the theory then we assume there is a non-trivial infrared fixed point (IRFP) that realizes an emergent SI. Here the phonon modes are no longer isolated degrees of freedom and we expect to have dispersion relations with an imaginary part. To describe such a theory we are going to take advantage of the gauge/gravity dualities, which through bottom-up AdS/CFT constructions will allow us to study the theory very efficiently. These type of theories are a bit more cumbersome to deal with, and we will need to introduce the methods of such models in Chapter 2.

Therefore, we may classify the SI solids in these two categories

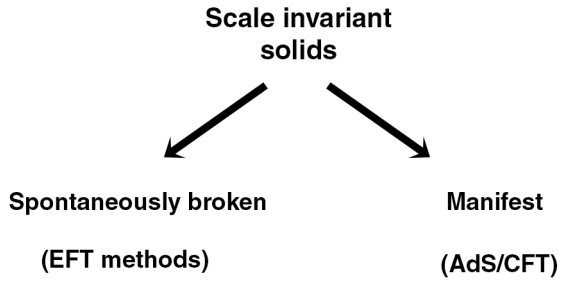

We are going to analyze the elastic response in these materials with SI from the low energy perspective and compare the results between the options considered. It is a very interesting question how does the elastic response of the solid depend on the

SI realization on the system. The constrains we find imply nontrivial relations among different physical observables of the material. To illustrate such constrains we have focused on the elasticity bounds of the solids, i.e. the maximum deformation a material may sustain in a reversible way. Moreover, for both cases we aim to characterize solid systems where the sound speeds can be realistic, that is, they are sufficiently small compared to the speed of light.

The thesis will be organized as follows:

- An introductory chapter to the gauge/gravity duality in Chapter 2 which will be useful to understand how the manifest SI solid theory is constructed.
- A short chapter with some condensed matter and solid physics aspects in Chapter 3. In this chapter we also introduce the Coset construction and how to derive the solid EFT theory from it.
- In Chapter 4 we discuss particular cases of the solid EFT, showing the potential of these methods. In this chapter we show the results obtained in [7]
- Chapter 5 is devoted to the study of SI solids, particularizing the results of Chapter 4 for the SI case and introducing the holographic case for the manifest SI solid. In this chapter we review the results from [23, 24].
- We end the thesis with a discussion of the results in Chapter 6.

Throughout the manuscript we will use natural units if not stated otherwise.

Chapter 2

Gauge-gravity duality

Gauge-gravity dualities have been an important field within theoretical physics in the last few years. As we will see in this chapter, these dualities make use of string theory, quantum field theory and general relativity and its applications are very diverse, from condense matter theories to nuclear physics.

The basic idea behind gauge-gravity dualities is that we can relate a gravity theory, defined in a D dimensional space-time (the so-called "bulk"), to a quantum field theory, defined in a $(D-1)$ space-time located in the boundary of this bulk. Therefore gauge-gravity dualities realise the *holographic principle* and that is why many people just refer to these theories as *holography*.

The most prominent example of this kind of dualities is the AdS/CFT correspondence, conjectured for the first time by Juan Maldacena [145]. Maldacena conjectured that a Type II String Theory on a $AdS_5 \times S^5$ background is equivalent to a $\mathcal{N} = 4$ Super Yang Mills theory in four dimensions.

In this chapter I will give an introductory view on gauge-gravity dualities and more particularly on AdS/CFT correspondence. There are plenty of reviews and references that have already given a great introduction to this topic from which I have been inspired by [13, 57, 73, 100, 123, 149, 160–162, 181, 225, 226].

2.1 Motivation

It was the study of black holes and D-branes in string theory what led Maldacena to propose the AdS/CFT correspondence. However, one can motivate its existence by pointing out certain aspects of gauge theories and gravity. Let me go through some of the most important motivations that led to the discovery of the AdS/CFT correspondence.

2.1.1 Geometrizing the renormalization group flow

During the 1960s Kadanoff, Wilson and others developed a new way of understanding quantum field theories. They found that it was very useful to study a system in terms of its energy (or length) scale. The idea is that if you are interested in the properties of a system at a given length scale u it is not convenient to use a theory that is defined at a length scale $u' \ll u$. What they propose is to integrate-out all the short-distance (i.e., high energy) degrees of freedom to obtain an effective theory that describes your system at the u scale that you are interested in. This procedure is known as renormalization group (RG) flow and it allows us to define a family of theories at a continuum of different scales (or energies). It is conceivable, then, to assume our quantum field theory in d dimensions to have an extra dimension u which represents the RG scale of the theory.

Let me consider a non-gravitational lattice system like the one Kadanoff firstly used in 1966 [130]: the Ising model. The Hamiltonian of such model is

$$H = -\sum_{\{i,j\rangle} J_{ij} S_i S_j - \mu \sum_j h_j S_j \tag{2.1}$$

where S_i is the spin value at each lattice site i, J_{ij} the interaction terms between sites, μ the magnetic moment and h_i the external magnetic field interacting with the lattice site. The interesting thing that he did is to consider multiple sites by a single site and averaging the value of the lattice variables. This process does not vary the form of the Hamiltonian but it changes the values of the couplings, i.e. J_{ij} and h_j. We can do this repeatedly, including more sites in each step defining some sort of RG flow by coarse graining our lattice, as can be pictured in Fig. 2.1.

Therefore, we can define the evolution of a given coupling of a theory, g, which is usually defined as a function of the energy scale

$$\beta_g(\mu) = \frac{\partial}{\partial \log \mu} g(\mu) \tag{2.2}$$

where β_g is the so-called *beta function* of the coupling g. These beta functions can be easily computed when the couplings are small by perturbation theory, but it is not the case for strong coupled systems, where AdS/CFT methods will be very helpful. All in all, it seems that we can parametrize our theory as a function of a scale that can play the role of a new dimension where the dynamics of the couplings will be governed by some action, this is why we can think of the AdS/CFT correspondence as a geometrization of the quantum dynamics by the RG.

Sometimes the dynamics of our theory can take our beta function to be $\beta_g = 0$. This special points are named fixed points and they describe a system that is invariant

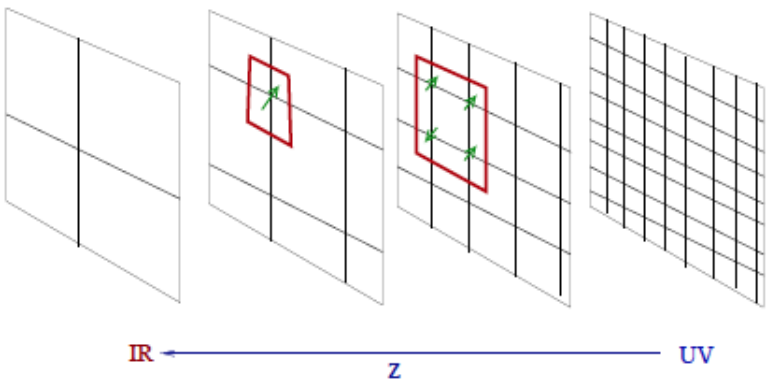

Figure 2.1: Representation of the RG flow of a lattice spin system. Figure from [149].

under scale transformation, sometimes also called self-similar. Scale invariance is a necessary condition to have conformal invariance (although it is not always sufficient) which is an important feature of conformal field theories that appear in the AdS/CFT correspondence.

2.1.2 Holographic principle

The holographic principle was first proposed by Gerard 't Hooft [204] and a couple of years later Leonard Susskind gave a precise string theory interpretation of it [202]. Here we are mainly going to follow Bousso's review of this principle [48].

The holographic principle claims, in essence, that the information stored in a volume $\mathcal{V}_{d+1}$ is encoded in its boundary area $\mathcal{A}_d$. The origin of this claim comes, surprisingly, from black hole thermodynamics.

Let us first take a look at the concept of black hole entropy, whose prediction has its origin in a couple of general relativity results.

Area theorem: this theorem [102] affirms that the area of a black hole never decreases with time, i.e. $d\mathcal{A} > 0$. This also applies to the merge of two black holes: the total area of the new black holes must exceed the sum of the two original ones. This theorem resembles the second law of thermodynamics, that claims that the entropy of an isolated system never decreases with time, giving a first glance on the relation between entropy and the area of the black hole.

No-hair theorem: A stationary black hole is only characterized by three quantities: charge, angular momentum and mass. The first version of this theorems comes from Israel [121, 122] and was then thoroughly studied by Hawking, Carter and others [56, 102, 103]. This theorem suggest that all the information (the "hair", as Bekenstein decided to call it metaphorically) carried by the matter that falls into the black hole disappears behind the black hole event horizon, inaccessible to an external observer. From the point of view of this observer, this process seems to violate the second law of thermodynamics as the entropy would seem to decrease over time.

These two theorems led Bekenstein to the idea that a black hole does carry an entropy [39–41] which should be proportional to its area $S_{BH} = \alpha\mathcal{A}$, where α should be of order unity. It was Hawking [104] who ultimately proved that $\alpha = 1/4$ leading to the famous result

$$S_{BH} = \frac{k_B\,\mathcal{A}}{4\,\ell_p^2} \tag{2.3}$$

where k_B is the Boltzmann's constant and ℓ_p the Planck length, which we restore here just to show that the entropy is given by the area in Planck units.

Moreover, using this result, Bekenstein proposed a generalized second law of thermodynamics (GLS)[1], which states that the sum of black hole entropy, S_{BH}, and the ordinary entropy of matter and radiation in the exterior of the black hole, S_m, cannot decrease

$$\Delta(S_{BH} + S_m) \geq 0. \tag{2.4}$$

Now, if we want to claim that this S_{BH} is actually the black hole entropy then it must also respect some basic thermodynamics. The first law of thermodynamics states that a black hole of mass M needs to have some temperature T

$$dM = T\,dS_{BH}. \tag{2.5}$$

It was Hawking [105] who resolved this mystery by proving that black holes do have a temperature given by

$$T = \frac{\kappa}{2\,\pi} \tag{2.6}$$

where κ is the surface gravity of the black hole.

With all these ingredients at hand we can arrive to the conclusion that the maximum entropy contained in a volume $\mathcal{V}$ is given by the area that encloses it $S_{max} = \mathcal{A}/4$, which is known as the Bekenstein bound. We can arrive to this conclusion by a thought

[1] As a funny anecdote, it is said that this discovery began with a cup of tea between Professor Wheeler and his student Bekenstein, who wanted to understand what would happen with the second law of thermodynamics if he threw his cup down to a black hole [110].

experiment. Let us consider an isolated matter system of mass M and entropy S_m. This system is confined inside a spherical area $\mathcal{A}$, which will be the smallest sphere that can fit around it. The system's mass cannot exceed the mass of a black hole of the same area, otherwise it would have already formed a black hole. Now we start throwing matter inside this area until the system collapses to a black hole. The initial entropy is

$$S_i = S_m + S_{thrown} \tag{2.7}$$

And as the final entropy will be that of a black hole and using the GSL

$$S_f = S_{BH} = \frac{\mathcal{A}}{4} \geq S_i = S_m + S_{thrown} \geq S_m \,. \tag{2.8}$$

We can deduce from here that the maximum entropy of this system is indeed given by S_{BH}. This result seems to be in contradiction with what we find in field theories in the absence of gravity. In such cases we find that the number of degrees of freedom of a system scales with the volume as $\mathcal{N} \sim \exp(V)$. This leads us to the conclusion that the entropy is an extensive property of the system using the Boltzmann's entropy formula $S \sim \log \mathcal{N} \sim V$. It can be shown that the field theory analysis overcounts the available degrees of freedom as it fails to include properly the effects of gravity [48], solving the apparent contradiction.

Finally, we can conclude that in a gravity theory in $(d+1)$-dimensions there are the same degrees of freedom that in a QFT with no gravity in d-dimensions. This is an essential point for the AdS/CFT correspondence which explains why we may refer to it as an holographic theory.

2.1.3 Weinberg-Witten no-go theorem

The Weinberg-Witten (WW) no-go theorem, as originally proposed [217] states:
All theories with a Lorentz-covariant energy-momentum tensor, such as all known renormalizable QFTs, composite as well as elementary massless particles with $j > 1$ are forbidden. Also, in all theories with a Lorentz-covariant conserved current, such as renormalizable theories with a symmetry that commutes with all local symmetries, there cannot exist composite or elementary particles with non-vanishing values of the corresponding charge and $j > 1/2$.

The first part of this theorem will place a great restriction to quantum gravities (QG). By QG here we mean quantum theories with a dynamical metric. In these kind of theories we find that the propagating mode of the metric is some spin-2 massless particle, which is usually called "graviton". Thus, the WW no-go theorem seems to invalidate the possibility of having a QG. Fortunately there are ways to go around this

theorem: it might be possible that the graviton, which has $j > 1$, is not living in the same space as the QFT. This is yet another indication to the AdS/CFT duality.

2.2 About Anti de Sitter space-time and Conformal Field Theory

After motivating the correspondence between gravity theories in anti de Sitter (AdS) space-time and Conformal Field Theories (CFT) here we give a quick introduction to both topics without going into much detail.

In the case of AdS space-time it is sufficient to follow the reviews cited about the AdS/CFT correspondence.

For the case of CFTs, apart from the reviews mentioned, more specific introductions are useful for this section [180, 185, 188].

2.2.1 Anti de Sitter space-time

The space-time that we are going to define here will be $(d+1)$-dimensional so it can ultimately be dual to a d-dimensional field theory.

What should we demand to our space time?

First, we must demand that the space-time is invariant under Poincaré transformations in d dimensions. The most general metric in $d+1$ dimensions that fulfils this is

$$ds^2 = \Omega^2(z)(-dt^2 + d\vec{x}^2 + dz^2) \tag{2.9}$$

where Ω can only depend on the spatial coordinate z if we want to demand translational symmetry in $(t, \vec{x})$. Poincaré symmetry is a necessary condition to construct a relativistic quantum field theory, but is not sufficient when describing a CFT. A conformally invariant theory must also be invariant under scale transformations

$$(t, \vec{x}) \to \lambda\,(t, \vec{x}) \quad ; \quad z \to \lambda\, z \tag{2.10}$$

where λ is a constant. This condition forces the function in front of the metric to respect

$$\Omega(z) \to \lambda^{-1}\,\Omega(z)\,. \tag{2.11}$$

This leaves us with a unique solution

$$\Omega(z) = \frac{L}{z} \tag{2.12}$$

where L is a constant that determines the curvature radius of the space. Thus, the metric 2.9 has to be

$$ds^2 = \frac{L^2}{z^2}(-dt^2 + d\vec{x}^2 + dz^2)\,. \tag{2.13}$$

This metric describes a $(d+1)$-dimensional anti de Sitter space time or AdS_{d+1}. We have reached this conclusion by just asking the space-time to be scale-invariant and invariant under Poincaré transformations. Moreover, this metric is also invariant under special conformal transformations, as it also happens in a CFT.

Properties of an anti de Sitter space-time

The AdS metric (2.13) is a solution of the equations of motion of a gravity action

$$S = \frac{1}{16\,\pi\,G_N}\int d^{d+1}x\sqrt{-g}\,(\mathcal{R} - 2\Lambda) \tag{2.14}$$

where G_N is the Newton constant, $g = \det g_{\mu\nu}$, $\mathcal{R}$ is the Ricci scalar and Λ is a cosmological constant.

The anti de Sitter metric is a maximally symmetric space-time. That means that our space-time has the maximal number of independent Killing vectors (or in other words, the maximum number of isometries). In d dimensions the maximum number of isometries a space-time can have is $d(d+1)/2$. There are only three possible space-time metrics that are maximally symmetric and they depend on the sign of Λ: for $\Lambda > 0$ we have a de Sitter space-time, $\Lambda = 0$ a flat (Minkowski) metric and $\Lambda < 0$ corresponds to an anti de Sitter metric. This cosmological constant determines the curvature of the space-time and manipulating the equations of motion from (2.14) we can find that for an AdS space-time

$$\Lambda = -\frac{d(d-1)}{2\,L^2} = \frac{d-1}{2(d+1)}\mathcal{R}\,. \tag{2.15}$$

A $(d+1)$-dimensional AdS space may be embedded into $(d+2)$-dimensional Minkowski metric with coordinates $(X^0, \ldots, X^{d+1}) \in \mathbb{R}^{2,d}$, with a metric $\eta = (-,+,\ldots,+,-)$, so

$$ds^2 = -(dX^0)^2 + \sum_{i=1}^{d}(dX^i)^2 - (dX^{d+1})^2\,. \tag{2.16}$$

The AdS_{d+1} will be defined by the hypersurface

$$\eta_{AB}X^A X^B = -L^2 \tag{2.17}$$

where $A, B \in (0, \ldots, d+1)$ and L is the radius of curvature of the AdS space. Notice that the hypersurface (2.17) is invariant under $O(2,d)$ transformations acting on $\mathbb{R}^{2,d}$,

thus the isometry group of AdS_{d+1} is $O(2,d)$, which is the same as the conformal group in d dimensions.
We can define a set of coordinates to parametrize the AdS_{d+1}

$$X^0 = L\,\cosh\rho\,\cos\tau, \tag{2.18}$$

$$X^{d+1} = L\,\cosh\rho\,\sin\tau, \tag{2.19}$$

$$X^i = L\,\Omega_i\,\sinh\rho, \quad \text{for}\, i = 1,\ldots,d \tag{2.20}$$

where Ω_i represent the angular coordinates and fulfill $\sum_i \Omega_i^2 = 1$. The other two coordinates take the range $\rho \in \mathbb{R}_+$ and $\tau \in [0, 2\pi)$. These coordinates are the so-called global coordinates of AdS_{d+1}, this is because all points of the hypersurface (2.17) are taken into account exactly once. This set of coordinates leads us to the next metric

$$ds^2 = L^2(-\cosh^2\rho\,d\tau^2 + d\rho^2 + \sinh^2\rho\,d\Omega_{d-1}^2) \tag{2.21}$$

In Fig. 2.2 we can see a representation of how an AdS_2 would look like when embedded into $\mathbb{R}^{2,1}$.
There is another set of coordinates that also parametrizes the hypersurface (2.17)

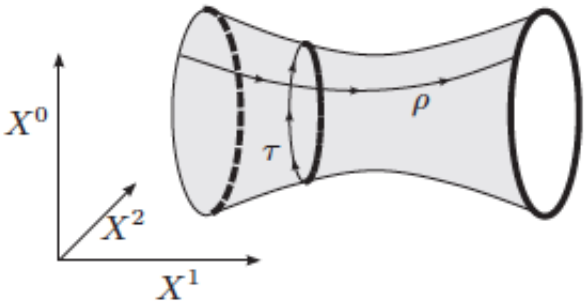

Figure 2.2: Representation of the embedding of an AdS_2 into $\mathbb{R}^{2,1}$. Figure from [13].

$$X^0 = \frac{L^2}{2r}\left(1 + \frac{r^2}{L^4}(\vec{x}^2 - t^2 + L^2)\right), \tag{2.22}$$

$$X^i = \frac{r\,x^i}{L}, \quad \text{for} \quad i = 1,\ldots,d-1, \tag{2.23}$$

$$X^d = \frac{L^2}{2\,r}\left(1 + \frac{r^2}{L^4}(\vec{x}^2 - t^2 - L^2)\right), \tag{2.24}$$

$$X^{d+1} = \frac{r\,t}{L}. \tag{2.25}$$

where $t \in \mathbb{R}$, $\vec{x} \in \mathbb{R}^{d-1}$ and $r \in \mathbb{R}_+$. Due to the restriction $r > 0$ we are only covering half of the AdS_{d+1}. This coordinates are the Poincaré patch coordinates and its metric reads

$$ds^2 = \frac{L^2}{r^2}\, dr^2 + \frac{r^2}{L^2}\left(-dt^2 + d\vec{x}^2\right) \equiv \frac{L^2}{r^2}\, dr^2 + \frac{r^2}{L^2}\eta_{\mu\nu} dx^\mu dx^\nu \tag{2.26}$$

where $\mu, \nu = 0, \ldots, d$ and $x^0 \equiv t$. Notice that by defining $z = L^2/r$ we recover exactly the metric in (2.13).

In the metric (2.26) we can see that there is a Minkowski metric multiplied by a factor r^2, this means that at every point r there is a Minkowski space whose lengths are re-scaled by this extra dimension. When this factor goes to infinity, $r \to \infty$, the space metric g_{ii} diverges quadratically with r. In general, any asymptotic AdS space will always have this quadratic divergence at a particular value r_*. The slice of space-time at $r = r_*$ is the conformal boundary. On the other hand, at $r = 0$ we have a degenerate Killing horizon (or Poincaré horizon). A Killing horizon is a null hypersurface defined by $k_\mu k^\mu = 0$, where k_μ is a Killing vector. A simple representation of an AdS space is displayed at Fig. 2.3.

The Poincaré patch metric can be defined by other possible definition of coordinates

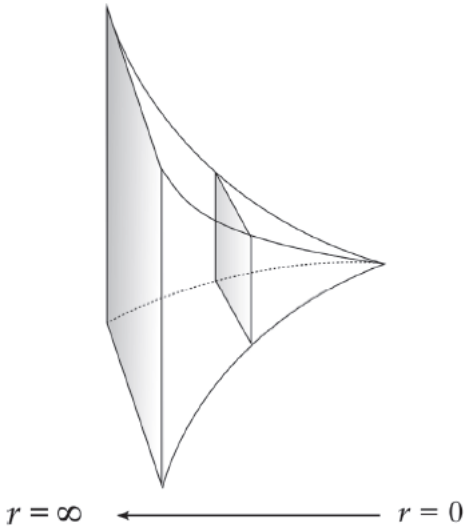

Figure 2.3: A schematic representation of an AdS space. Figure from [13].

as we saw. If we used the coordinate z the boundary would be located at $z = 0$ whereas the horizon would be located at $z \to \infty$. Another typical possibility is $z = e^{-r/L}$, where

we would have

$$ds^2 = dr^2 + L^2 e^{2r/L} \eta_{\mu\nu} dx^\mu dx^\nu. \tag{2.27}$$

In summary, the most remarkable point that we should highlight about anti de Sitter spaces is that the isometry group of (2.13) is $SO(2,d)$, which as we will see below coincides with the d-dimensional conformal group, giving more strength to the idea that a CFT could have a string theory description in AdS spacetime.

2.2.2 Conformal Field Theory

Generally we demand to our QFT to be Poincaré invariant. The Poincaré group can be extended to a more general group: the conformal group. This group consists of transformations that preserve angles but not lengths. In a Minkoswki space-time the conformal group defines the most general transformations that preserve local causality, i.e. spacelike (or timelike/lightlike) separated points remain spacelike separated points under a conformal transformation.

In a more practical sense, if we have a non-trivial line element $ds^2 = g_{\mu\nu} dx^\mu dx^\nu$, a conformal transformation will be that which leaves the metric $g_{\mu\nu}$ invariant up to an overall positive factor, i.e. under a conformal transformation $x \to x'$ we would get

$$g_{\mu\nu} \to \Lambda(x)^{-2} g_{\mu\nu} \equiv e^{2\sigma(x)} g_{\mu\nu}. \tag{2.28}$$

This transformation would then leave the angles constant but would re-scale the line element at every point x, i.e. $ds'^2 = \Lambda(x)^{-2} ds^2$. The special case where $\Lambda(x)$ is a constant corresponds to a scale transformation.

From now on, we will take the metric to be Minkowskian, i.e. $g_{\mu\nu} = \eta_{\mu\nu}$. For an infinitesimal transformation $x^\mu \to x'^\mu = x^\mu + \epsilon^\mu$ the metric would change as

$$\eta_{\mu\nu} \to \eta_{\mu\nu} + \partial_\mu \epsilon_\nu + \partial_\nu \epsilon_\mu. \tag{2.29}$$

We demand this transformation to fulfill

$$\partial_\mu \epsilon_\nu + \partial_\nu \epsilon_\mu = \left(\Lambda(x)^{-2} - 1\right) \eta_{\mu\nu} = 2\,\sigma(x)\,\eta_{\mu\nu} \tag{2.30}$$

where we use $\Lambda(x) = 1 - \sigma(x) + \mathcal{O}(\sigma^2)$. Taking the trace of (2.30) we get $\partial \cdot \epsilon = d\,\sigma(x)$, where d are the space-time dimensions. Using this condition we can re-write equation (2.30) as

$$\left(\eta_{\mu\nu}\partial^2 + (d-2)\,\partial_\mu \partial_\nu\right) \partial \cdot \epsilon = 0. \tag{2.31}$$

Notice that the equation simplifies a lot when considering $d = 2$. This particularity has great consequences and conformal theories are usually decomposed between those

with $d = 2$ and those with $d > 2$. Here we will focus on the second case. There are reviews on CFTs that focus primarily on two dimensional ones [82].

For the case $d > 2$, the solution to equation (2.31) is given by

$$\epsilon^\mu(x) = a^\mu + \omega^\mu_\nu x^\nu + \lambda\, x^\mu + b^\mu\, x^2 - 2\,(b\cdot x)\, x^\mu. \tag{2.32}$$

The trace of ϵ determines σ to be $\sigma = \lambda - 2\, b\cdot x$. Notice that the parameters a^μ, ω^μ_ν, λ and b^μ are determined by a finite number of components. Therefore the conformal algebra has a finite dimension. This would not be the case if we were working in $d = 2$, where the solutions would be infinite. This parameters determine the different transformations of the group, which I summarize below along with the generators of these transformations

	$\epsilon^\mu(x)$	Operator
Translation	a^μ	$P_\mu = \partial_\mu$
Lorentz transformation	$\omega^\mu_\nu x^\nu$	$J_{\mu\nu} = (x_\mu\partial_\nu - x_\nu\partial_\mu)/2$
Dilatation	$\lambda\, x^\mu$	$D = x^\mu\partial_\mu$
Special conformal transformation	$b^\mu x^2 - 2\,(b\cdot x)\, x^\mu$	$K_\mu = x^2\partial_\mu - 2x_\mu x^\nu\partial_\nu$

where $\omega_{\mu\nu} = -\omega_{\nu\mu}$. We have considered here just infinitesimal transformations, but this can be extended to finite transformations. We have a particular interest in scale transformations and special conformal transformations, which would transform as

$$x^\mu \to \lambda\, x^\mu\,, \tag{2.33}$$

$$x^\mu \to \frac{x^\mu + b^\mu x^2}{1 + 2\, b\cdot x + b^2 x^2}\,. \tag{2.34}$$

In order to define the special conformal transformation it is useful to introduce the inversion

$$x^\mu \to x'^\mu = \frac{x^\mu}{x^2}\,. \tag{2.35}$$

Thus, we can construct (2.34) by the composition of an inversion, a translation (of a factor b^μ) and another inversion.
The current of this special conformal transformation is given by

$$J^{(K)}_{\mu\nu} = x^2\, T_{\mu\nu} - 2x_\nu\, x^\rho\, T_{\mu\rho}\,. \tag{2.36}$$

By demanding that his current must be conserved we find a very remarkable property of CFTs, which is the tracelessness of the stress energy

$$\partial^\mu J^{(K)}_{\mu\nu} = 0 \Rightarrow T^\mu_\mu = 0\,. \tag{2.37}$$

This property is commonly assumed to be also correct in scale invariant theories, and although it is generically true it is not a necessary condition for scale invariant theories[2].

In a CFT we have a unitary action of the conformal group on the Hilbert space. The generators P^μ, $J_{\mu\nu}$, D and K^μ are represented by operators, as we can see above. These generators close the following algebra

$$[J_{\mu\nu}, J_{\rho\sigma}] = i\ (\eta_{\mu\rho}J_{\nu\sigma} + \eta_{\nu\sigma}J_{\mu\rho} - \eta_{\nu\rho}J_{\mu\sigma} - \eta_{\mu\sigma}J_{\nu\rho}) \tag{2.38}$$

$$[J_{\mu\nu}, P_\rho] = i\ (\eta_{\mu\rho}P_\nu - \eta_{\nu\rho}P_\mu) \tag{2.39}$$

$$[J_{\mu\nu}, K_\rho] = i\,(\eta_{\mu\rho}K_\nu - \eta_{\nu\rho}K_\mu) \tag{2.40}$$

$$[K_\mu, P_\nu] = -2\,i\,(\eta_{\mu\nu}D - J_{\mu\nu}) \tag{2.41}$$

$$[D, P_\mu] = i\,P_\mu \tag{2.42}$$

$$[D, K_\mu] = -i\,K_\mu \tag{2.43}$$

where the rest of commutations vanish. The first line determines the algebra of the Lorentz group $SO(1, d-1)$ with the generator $J^{\mu\nu}$ and the P^μ generator extends the Lorentz algebra to the Poincaré algebra. Moreover, we can assemble the rest of the generators in

$$J_{AB} = \begin{pmatrix} J_{\mu\nu} & \frac{K_\mu - P_\mu}{2} & -\frac{K_\mu + P_\mu}{2} \\ -\frac{K_\mu - P_\mu}{2} & 0 & D \\ \frac{K_\mu + P_\mu}{2} & -D & 0 \end{pmatrix} \quad A, B = 1, \ldots, d+2 \tag{2.44}$$

and notice that J_{AB} are the generators of the group $SO(2, d)$. We can summarize the relations through

$$[J_{AB}, J_{CD}] = i\,(\overline{\eta}_{AC}J_{BD} + \overline{\eta}_{BD}J_{AC} - \overline{\eta}_{BC}J_{AD} - \overline{\eta}_{AD}J_{BC})\,, \tag{2.45}$$

where the metric is $\overline{\eta}_{AB} = \mathrm{diag}(-1, 1, \ldots, 1, -1)$.

We generally identify a particle by its mass and by Lorentz quantum numbers, which correspond to the Casimirs of the Poincaré group. In a conformal invariant theory the mass operator $P_\mu P^\mu$ does not commute anymore with other generators, such as D. This means that mass and energy can be actually re-scaled. Thus if a representation of the conformal group contains a state with some energy, it will contain states with arbitrary energy, from zero to infinity, as we are free to apply dilatations to our theory. It is because of this that an S matrix formalism does not makes sense for CFT and there are no well-defined particles. We are going to need different ways to label

[2]This will be more deeply discussed in Chapter 5. For the interested reader there are many references that cover this issue such as [62, 124, 159, 173, 185].

the states of our theory.

A simple example of a classically[3] scale invariant scalar field theory is a massless field with only quartic interaction in $d = 4$

$$S = \int dx^4 \left((\partial\phi)^2 + \frac{\lambda}{4!}\,\phi^4 \right) . \tag{2.46}$$

The action remains invariant if we make a dilatation in the space-time coordinates (i.e. $x \to x' = \Lambda x$) and in the field with a specific weight

$$\phi(x) \to \phi'(x') = \Lambda^{-\Delta}\,\phi(x) \tag{2.47}$$

where Δ is called the scaling dimension of the field and here coincides with the canonical dimension $\Delta = 1$. This scale invariance can be broken by just adding a mass $m^2\,\phi^2$ term to the action. It is generally assumed that a scale invariant theory is inevitably conformal invariant as well, and usually this assumption leads us to the correct answer.

In a CFT we consider fields with good transformation properties under dilatation. The quantum version of (2.47) in a CFT is given by

$$[D, \phi(x)] = -i\,\Delta\,\phi(0). \tag{2.48}$$

This implies that the field ϕ has a scaling dimension Δ, which shall be an important label for the field. Moreover, we can restrict to fields that are annihilated by the operator K_μ at $x = 0$, i.e.

$$[K_\mu, \phi(0)] = 0. \tag{2.49}$$

The fields that satisfy this condition are called *primary fields*. We can take a look at equations (2.42)-(2.43) and realize that P_μ increases the scaling dimension of the field while K_μ decreases it, therefore the fields annihilated by K_μ at $x = 0$ are the ones with the lowest scaling dimension[4]. The rest of the fields are commonly called *descendant fields*, and they are obtained by repeatedly acting on them with $P_\mu = \partial_\mu$. We can restrict our analysis to primary fields, which are classified according to the scaling dimension Δ and the Lorentz quantum numbers.

[3]Scale invariance here is broken by quantum corrections when the theory is quantized, so let us keep the discussion at the classical level.

[4]This scaling dimension has actually a minimum value that is restricted by the unitarity bound (i.e. by demanding the positivity of the norm of a state in a given representation) and particularly for a scalar in d dimensions we can fin that $\Delta \geq \frac{d-2}{2}$. The proof of this can be found in [13]

Conformal symmetry facilitates also the treatment of two and three-point correlation functions by imposing some restrictions. For instance, if we use the invariance under scale transformations we find that

$$\langle \phi_1(x_1)\phi_2(x_2)\rangle = \Lambda^{\Delta_1+\Delta_2}\langle \phi_1(\Lambda x_1)\phi_2(\Lambda x_2)\rangle\,, \tag{2.50}$$

where the ϕs are scalar conformal primary operators. Since the correlator can only depend on $(x_1 - x_2)$ due to Poincaré invariance we are restricted to

$$\langle \phi_1(x_1)\phi_2(x_2)\rangle = \frac{C_{12}}{(x_1-x_2)^{\Delta_1+\Delta_2}}. \tag{2.51}$$

A similar result is obtained for the three-point function.

In this small introduction to the CFT in d dimensions we have seen that the isometry group of these theories is $SO(2,d)$, which coincides exactly with what we find in a gravity theory in an AdS space-time in $d+1$ dimensions. Other properties and details explained here shall be considered when comparing both sides of the AdS/CFT correspondence.

2.2.3 Comparing degrees of freedom

Now that we have discussed both sides of the AdS/CFT correspondence we can go back to the argument of section 2.1.2 to match the number of degrees of freedom of both sides of the duality.

Let us start with the CFT side. First of all we need to regularize the theory by putting a UV and IR regulator. Consider that the system is inside a box of side R (which will restrict long-distance modes and thus will be an IR cutoff) and let us introduce a lattice spacing δ that will play the role of a UV regulator. In d space-time dimensions the system will have R^{d-1}/δ^{d-1} cells. In each cell there will be c_{CFT} degrees of freedom, which we will refer to as the central charge. Therefore, the total number of degrees of freedom is

$$N_{CFT} = \left(\frac{R}{\delta}\right)^{d-1} c_{CFT}\,. \tag{2.52}$$

If the CFT we are studying is a $SU(N)$ gauge field theory (like the one we will discuss in the next section) the fields are going to be $N\times N$ matrices in the adjoint representation, which for large N will contain N^2 independent components. We can then say that the central charge of a $SU(N)$ CFT should scale as $c_{CFT}\sim N^2$.

On the other hand, the number of degrees of freedom of the AdS_{d+1} gravity theory can be deduced from the Bekenstein-Hawking formula (2.3). This formula tells us that

the degrees of freedom contained in a certain region is given by

$$N_{AdS} = \frac{\mathcal{A}}{4\,\ell_P^{d-1}}\,, \tag{2.53}$$

where $\mathcal{A}$ is the area of the region at the boundary of AdS_{d+1}, i.e. $z \to 0$, and we have taken $k_B = 1$. Let us evaluate the area of the space defined by the metric (2.13) at $z = \delta \to 0$

$$\mathcal{A} = \int_{\mathbb{R}^{d-1}, z=\delta} dx^{d-1}\,\sqrt{g} = \left(\frac{L}{\delta}\right)^{d-1} \int_{\mathbb{R}^{d-1}} dx^{d-1} \tag{2.54}$$

The integral of the right hand side is the volume of $\mathbb{R}^{d-1}$ and is infinite, so let us do as we did with the CFT: we put the system inside a box of size R which will act as an IR regulator

$$\int_{\mathbb{R}^{d-1}} dx^{d-1} = R^{d-1}\,. \tag{2.55}$$

With this we can already evaluate the number of degrees of freedom of the AdS space-time gravity

$$N_{AdS} = \frac{1}{4}\left(\frac{R}{\delta}\right)^{d-1}\left(\frac{L}{\ell_P}\right)^{d-1}\,. \tag{2.56}$$

Comparing this with the result we obtained for the CFT we can identify, considering that the UV and IR cutoffs are the same,

$$\frac{1}{4}\left(\frac{L}{\ell_P}\right)^{d-1} = c_{CFT} \tag{2.57}$$

The gravity theory we are considering has to be at least semiclassical, which demands that the AdS_{d+1} radius L has to be large compared to the Planck length, i.e.

$$\left(\frac{L}{\ell_P}\right) \gg 1\,. \tag{2.58}$$

The conclusion we get from this is that a CFT will have a classical gravity dual only if c_{CFT} is large, i.e. if there is a large number of degrees of freedom per unit volume or a large number of species (in a $SU(N)$ gauge theory this would mean taking a large N limit).

2.3 AdS/CFT correspondence: required tools and conjecture

We have seen in the last sections that the AdS/CFT correspondence relates gravity theories in asymptotically Anti-de Sitter spacetimes in $d+1$ dimensions to conformal field theories in d dimensions. There are various examples[5], but we will restrict our discussion to the most prominent example which relates $\mathcal{N}=4$ Super Yang-Mills theory in $3+1$ dimensions and type IIB superstring theory on $AdS_4 \times S^5$. This correspondence was originally developed in the context of string theory, which we will very briefly review here so we can have an understanding of this duality. Moreover, we will take a look at the large N gauge theories mentioned before, which will have an important role in the story.

We will not fully study string theory in all its details, just give a glimpse of its properties, a more exhaustive review of it can be found in [90, 174, 228].

2.3.1 Large N expansion in gauge theories

A $U(N)$ Yang-Mills gauge theory can be simplified in the limit where the number of colors, N, is large. This was first discovered by 't Hooft in the 1970s [203] and has interesting consequences for the AdS/CFT duality.
We are going to consider a $U(N)$ Yang-Mills theory, whose Lagrangian is

$$\mathcal{L} = -\frac{1}{g_{\mathrm{YM}}^2}\,\mathrm{Tr}[F_{\mu\nu}F^{\mu\nu}]\,, \tag{2.59}$$

where the non-abelian gauge field strength is given by

$$F_{\mu\nu} = \partial_\mu A_\nu - \partial_\nu A_\mu + i\,[A_\mu, A_\nu]\,. \tag{2.60}$$

The gauge field A_μ is an $N \times N$ matrix whose elements are written as $A^a_{\mu,b}$ where $a, b = 1, \ldots, N$. We can re-express our Lagrangian as

$$\mathcal{L} = -\frac{N}{\lambda}\,\mathrm{Tr}[F_{\mu\nu}F^{\mu\nu}]\,, \tag{2.61}$$

where $\lambda \equiv g_{\mathrm{YM}}^2 N$ is the so-called 't Hooft coupling. It is a well known result that for these theories the beta function scales as $\beta(g) \sim -g_{\mathrm{YM}}^3 N$, so in the large N limit the β

[5] E.g. other realizations of the correspondence are the one that states that M-theory in $AdS_7 \times S^4$ is equivalent to the so-called $(2,0)$-theory in six dimensions [145] or the one that claims that M-theory on $AdS_4 \times S^7$ is equivalent to the ABJM superconformal field theory in three dimensions [4].

function would diverge and $g_{\rm YM}$ would go to zero. However, if we take the limit where N goes to infinity while keeping λ constant we can then find that the renormalization group equation of λ has finite coefficients

$$\beta(\lambda) \sim -\lambda^2 \,. \tag{2.62}$$

This type of expansion is called 't Hooft expansion and in this limit it will be λ who acts as the effective coupling constant and not $g_{\rm YM}$, which goes to zero.

We adopt a double line notation (see Fig. 2.4) for the gauge propagator that will

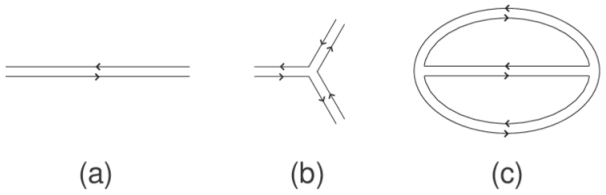

Figure 2.4: Double line representation of a diagram: (a) A gauge field propagator, which scales as $\sim \frac{\lambda}{N}$ (b) A vertex, which scales as $\sim \frac{N}{\lambda}$ (c) A planar diagram with two loops, which scales as $\sim N^2\lambda$. Figure from [3].

simplify the discussion of this non-abelian gauge theory. Feynmann diagrams will then become networks of double lines where vertices will scale as $g_{\rm YM}^{-2} = \frac{N}{\lambda}$ and propagators as $g_{\rm YM}^2 = \frac{\lambda}{N}$. Moreover, every loop contributes an N factor coming from the trace. Therefore, it is easy to estimate how a given diagram $\mathcal{D}$ with no external lines will scale. If there are P propagators, V vertices and L number of loops we conclude that the diagram will scale as

$$\mathcal{D}(P, L, V) \sim \left(\frac{\lambda}{N}\right)^P \left(\frac{N}{\lambda}\right)^V N^L = N^{L-P+V}\, \lambda^{P-V} \tag{2.63}$$

The power of the expansion parameter N is precisely the Euler characteristic

$$\chi \equiv L - P + V = 2 - 2\,g \tag{2.64}$$

related to a surface with the number of handles g (the genus) of a surface (see Fig. 2.5).

It is evident from equation (2.64) that in the large N limit the major contribution will come from the terms with $g = 0$, which correspond to the planar diagrams: those that can be drawn on a piece of paper without self-crossing. It is because of this that the large N limit can also be found under the name of planar limit of the gauge theory.

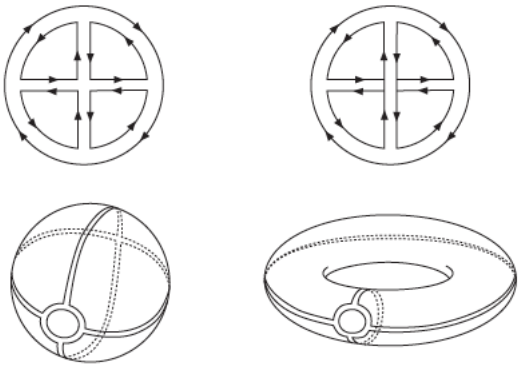

Figure 2.5: Two different vacuum amplitudes. The left one has genus $g = 0$ (it is a planar diagaram) and scales as $\sim N^2$ for large N, the right one has genus $g = 1$ and scales as $\sim N^0$. The planar diagram can be drawn on a sphere (no handles) whereas the non-planar has to be drawn on a torus (one handle). Figure from [181].

Any physical quantity of this theory may be expressed as an expansion of N and g. For instance, the partition function Z and the generating functional W for connected Green functions have the structure

$$i\,W = \log Z = \sum_{g=0}^{\infty} N^{2-2g} \sum_{i=0}^{\infty} c_{i,g}\lambda^i = \sum_{g=0}^{\infty} N^{2-2g} f_g(\lambda) \tag{2.65}$$

with $f_g(\lambda)$ a polynomial in the 't Hooft coupling. This result will be important when we want to compare the large N limit of gauge theories with string theory.

2.3.2 String theory and D-branes

The historical origin of string theory begins in the 1960s as an attempt to describe the hadronic resonances of high spin observed in experiments. The squared mass of these kind of particles was known to be linearly related to its spin J

$$M^2 \sim J\,. \tag{2.66}$$

These hadrons are then distributed along Regge trajectories, as can be seen in Fig. 2.6. Geoffrey Chew and Steven Frautschi were the first ones to conjecture that strong

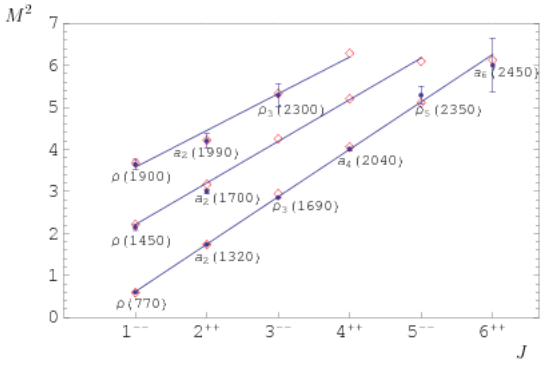

Figure 2.6: Mass and spin of hadrons, following a Regge trajectory, where squared mass and spin are linearly related. Figure from [76].

interacting particles had this linear relation between mass and spin [60]. String theory is then introduced to reproduce this relation of hadron properties. It is not very difficult to verify (at least qualitatively) that a particle described as a string can exhibit the relation shown in (2.66). Let us suppose that we have an open string of length L and tension T that is rotating around its center of mass. The mass of this string would be $M \sim T\,L$, and its angular momentum would be $J \sim P\,L$, where P is the angular momentum. In a relativistic theory we have $P \sim M$, thus $J \sim M\,L \sim M^2\,T^{-1}$. This reproduces exactly the Regge behaviour (2.66) with a slope proportional to the string tension T.

The most basic difference between string theory and quantum field theory is what kind of object is the responsible of describing the most fundamental particles. In string theory these are, as the name already announces, one dimensional extended strings with a characteristic length ℓ_s and a tension T which are related by

$$T = \frac{1}{2\pi\alpha'} \quad ; \quad \alpha' \equiv \ell_s^2 \tag{2.67}$$

where α' is actually the Regge slope we discussed above.
In order to construct the action that will control the dynamics of these strings we can take a look at the special relativistic description of a point particle of mass m moving in a flat space with a Minkowskian metric. The curve in space-time that describes the trajectory of this particle (the worldline) can be represented by a function $x^\mu(\tau)$, where x^μ is the coordinate in the space where is moving and τ is the coordinate that parametrizes the path of the particle. The action of this particle is proportional to the

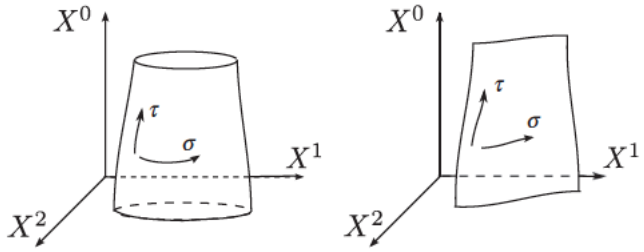

Figure 2.7: Strings can be either open or closed (strings with no boundaries). Here we show worldsheets of a closed and open string in a 3-dimensional target space. Figure from [13].

integral of the line element of the curve

$$S = -m \int ds = -m \int d\tau \sqrt{-\eta_{\mu\nu} \dot{x}^\mu \dot{x}^\nu}\,, \tag{2.68}$$

where $\dot{x}^\mu = \frac{dx^\mu}{d\tau}$.
On the other hand, a string moving will not describe a one-dimensional trajectory but some sort of surface (the worldsheet). Therefore, the action we postulate is then something proportional to the integral of such area, the so-called Nambu-Goto action:

$$S_{NG} = -T \int dA\,. \tag{2.69}$$

In this case there will be two coordinates, $\sigma^\alpha = (\sigma^0, \sigma^1) \equiv (\tau, \sigma)$, that will describe the worldsheet Σ (see Fig. 2.7) and then, if we assume that the worldsheet is embedded in a flat space, there will be a mapping to the target space-time given by some function $X^\mu(\sigma^\alpha)$. Therefore the worldsheet will have an induced metric on Σ given by

$$g_{\alpha\beta} \equiv \eta_{\mu\nu} \partial_\alpha X^\mu \partial_\beta X^\nu\,. \tag{2.70}$$

Finally we can write the action as

$$S_{NG} = -T \int d^2\sigma \sqrt{-\det g_{\alpha\beta}} \tag{2.71}$$

Until now we have just worked with a classical theory, if we want to describe quantum states we need to quantize the theory. The simplest way is through canonical quantization, *i.e.* by considering that the functions X^μ are in fact operators and imposing

canonical commutation relations between X^μ and its conjugate momenta. Doing so we find that there is an infinite tower of particles of different masses and spins (organized in Regge trajectories) whose mass gap is of order $1/\ell_s$. This quantization also leads us to many non-trivial properties of this theory. First of all, we find that there are tachyon particles in the spectrum (*i.e.* particles with $m^2 < 0$), which is a signal of instability. This can be solved by considering fermionic strings, to do that we need to require that the theory is supersymetric, *i.e.* that there is a symmetry between bosonic and fermionic degrees of freedom. This generalization of string theory is the so-called superstring theory. There are different types of superstring theories depending on the supersymmetries that we consider, whether strings are orientable or not, etc. In particular, the type of superstring theory that will be of our interest goes under the name of type IIB superstring theory, which only contains orientable closed strings and has the maximum amount of supersymmetries in 10 dimensions. More details about the different types of superstring theories go beyond the scope of this text, but a nice description of them can be found in [172]. Other remarkable issues regarding the (bosonic) string theory are related to the dimension of the target space D. In summary, we find that in order to describe Lorentz invariant massless modes we need to impose that this dimension is $D = 26$ in the bosonic description[6].
In the spectrum of open string we find massless spin-one particles which are identified with gauge bosons (photons, gluons,etc.) and scalars modes such as the dilaton Φ, but one of the most astonishing results we find it when analysing the spectrum of closed strings in superstring theory: the appearance of a massless spin-two string, which is identified as the graviton. Moreover, when we go to the limit of low energies, *i.e.* $E \ll m_s = \ell_s^{-1}$, we can integrate out the massive modes and obtain an effective low energy theory for the massless particles and, lo and behold, we find that this effective theory has the form of Einstein gravity coupled to other massless fields

$$S = \frac{1}{16\pi G} \int d^D X \sqrt{-g}\, \mathcal{R} + \dots \,. \tag{2.72}$$

Einstein equations appear naturally in string theory! Therefore we get to the conclusion that string theory is actually a quantum gravity theory and not a hadronic theory as was originally intended. This is why sometimes this superstring theories go under the name of supergravity theories.

To conclude, we need to discuss how strings interact with each other. In general, these interactions between strings will be controlled by a small coupling constant g_s which will allow us to construct a perturbative expansion in terms of Feynmann diagrams, similar

[6] In the case of the type IIB superstring theory we find that $D = 10$ but in this case the condition comes from demanding that there are no tachyonic states.

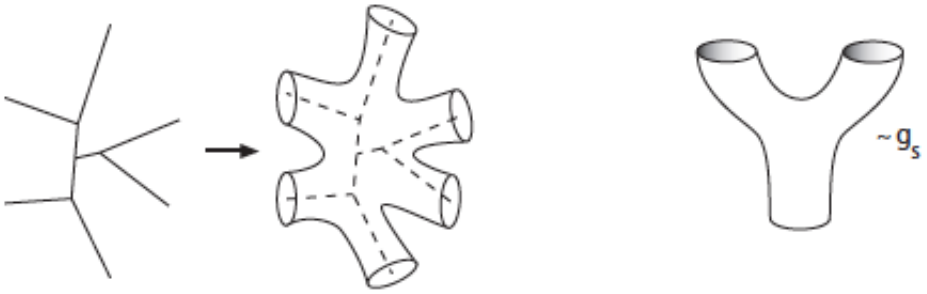

Figure 2.8: We can think of diagrams in string theory as thickened versions of Feynmann diagrams in quantum field theory. A three-(closed)-string vertex would look like a slingshot and will be proportional to g_s. Figure from [181].

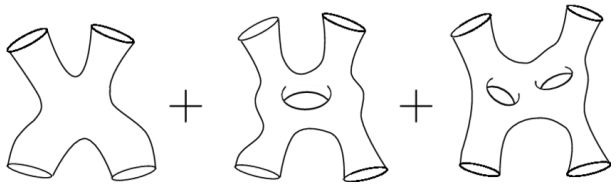

Figure 2.9: Perturvative expansion for closed strings. For each loop we have a hole in the worldsheet. Figure from [201].

to what is done in quantum field theory (see Fig. 2.8). When these strings interact by splitting or joining with other strings we can represent it by a two dimensional surface with holes and boundaries. Take as an example a closed string splitting into two strings (whose diagram would look like a slingshot) and then rejoining. This would produce a worldsheet that would be a surface with a hole in it. Thus, in general we can represent higher order terms in perturbation theory as surfaces with more and more holes. This means that perturbative expansion in string theory can be understood as a topological expansion. Now, if the reader is feeling a *deja vu* is because we have seen something very similar in the large N expansion above. In particular, the perturbative expansion of these interactions would be of the type

$$\mathcal{A} = \sum_{g=0}^{\infty} g_s^{2g-2} f_g(\alpha') \tag{2.73}$$

where $\mathcal{A}$ is the amplitude. Comparing this with (2.65) clearly suggests that there is probably a relation with the expansion in large N if we identify g_s to

$$g_s \sim \frac{1}{N} \tag{2.74}$$

The AdS/CFT correspondence is an explicit realization of this connection in the limit $(N, \lambda) \to \infty$ (the planar limit in the strongly coupled regime).

Up until now we have commented (without going into much detail) the quantization of open and closed strings, their spectrum and its effective theory of closed strings at low energies. However, in string theory there are objects that lie in the non-perturbative sector which are of great importance for the AdS/CFT correspondence. In this sector we have a variety of higher-dimensional solitonic objects and D-branes (short for Dirichlet membrane) are a particularly important class of solitons that were discovered by Dai, Leigh and Polchinski, [69] and independently by Hořava [111], in 1989. We have two different ways of looking at a D-brane.
On one hand we can define them as hypersurfaces where open strings can end and are fixed to. These open strings might deform this hypersurface and lead to non-trivial excitations on the D-brane. Thus, the D-brane is not only a geometric construction but a dynamical object.
On the other hand we can study D-branes as very massive objects which distort the surrounding space-time. Both points of view will be reviewed in the next two sections. We can see in Figure 2.12 when either of the perspectives are reliable.

D-branes: Open string perspective

Let us consider a Dp-brane that extends in the x^μ ($\mu = 0, \ldots, p$) directions, with y^i ($i = p+1, \ldots, 9$ if we consider that $D = 10$) transverse directions, that specify the (Dirichlet) boundary conditions of open strings, *i.e.* open strings are fixed to this hypersurface. Dp-branes have a finite number of massless excitations. In particular, the massless spectrum consists of a gauge field A_μ and $9-p$ scalars ϕ^i (and their superpartners). These scalar modes can be identified as the fluctuations in the transverse directions y^i of the Dp-brane, *i.e.* they describe the rigid body motion and the deformation of its shape. On the other hand, since string endpoints are charged they are coupled to a gauge field A_μ that lives in the Dp-brane, this gauge field will describe the internal excitations of the Dp-brane. The action that describes Dp-branes and takes

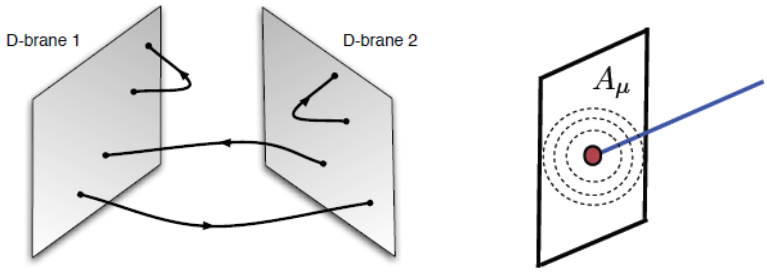

Figure 2.10: **Left:** Two D-branes with open strings attached to them. Figure from [57]. **Right:** Open strings source a gauge field on the D-brane worldvolume. Figure from [181]

into account these kind of excitations is the so-called Dirac-Born-Infeld (DBI) action:

$$S_{DBI} = -T_{D_p} \int dx^{p+1} \sqrt{-\det(g_{\mu\nu} + 2\pi\ell_s^2 F_{\mu\nu})}\,, \tag{2.75}$$

where $g_{\mu\nu}$ is the induced metric on the worldvolume, $F_{\mu\nu}$ is the field strength of the gauge field A_μ and T_{D_P} is given by

$$T_{D_p} = \frac{1}{(2\pi)^p g_s \ell_s^{p+1}} \tag{2.76}$$

and is the tension of the Dp-brane, *i.e.* its mass per unit spatial volume, which its dependence scaling with the coupling constant $\sim 1/g_s$ makes evident the non-perturbative nature of Dp-branes.

Notice that in the absence of a field strength ($F_{\mu\nu} = 0$) this is just a generalization of the Nambu-Goto action (2.71) for an objected extended in p directions instead of two. Scalar excitations seem to be absent in (2.75) but they are actually encoded inside the induced metric. If we consider a Dp-brane in a flat space the induced metric would take the form of

$$g_{\mu\nu} = \eta_{\mu\nu} + (2\pi\ell_s^2)(g_{i\mu}\partial_\nu\phi^i + g_{j\nu}\partial_\mu\phi^j) + (2\pi\ell_s^2)^2\partial_\mu\phi^i\partial_\nu\phi^i\,, \tag{2.77}$$

where the scalars ϕ^i parametrize the embedding of the brane. Finally, we can expand the DBI action in the limit $\ell_s \to 0$

$$S_{DBI} = -\frac{1}{g_{YM}^2}\left(\frac{1}{4}F_{\mu\nu}\,F^{\mu\nu} + \frac{1}{2}\partial_\mu\phi^i\partial^\mu\phi^i + \dots\right). \tag{2.78}$$

This expansion describes the system at its low energy limit ($\ell_s \to 0$) as juts an ordinary gauge field action and $9-p$ free scalar fields. Moreover we identify the Yang-Mills coupling in (2.78) as a function of ℓ_s and g_s

$$g^2_{\rm YM} = 2\,(2\pi)^{p-2}\,\ell_s^{p-3} g_s \tag{2.79}$$

Another astonishing feature of Dp-branes is the appearance of a non-abelian gauge field when we set branes close to each other. Let us take as an example just two branes (see Fig. 2.78): in this case we would have two massless gauge field in each brane, $(A_\mu)^1_1$ and $(A_\mu)^2_2$, and two massive gauge fields that are attached to both branes, $(A_\mu)^1_2$ and $(A_\mu)^2_1$, with a mass proportional to the distance between branes, *i.e.* $m = r/2\pi\ell_s^2$. If we go to the limit where branes are on top of each other, $r \to 0$, these fields would become massless and we would represent these fields as $(A_\mu)^a_b$ with $a, b = 1, 2$ corresponding precisely to a $U(2)$ non-abelian gauge field[7]. In general, for N branes, this gauge group would be a $U(N)$ group.

Now that we have seen some of the properties of Dp-branes, let us consider a $(9+1)$ type IIB supergravity theory where we embed N coincident D3-branes in the limit of low energies, *i.e.* $E \ll \ell_s^{-1}$, and for a small effective coupling constant $g_s\, N \ll 1$, which is the limit where this perspective is reliable. Perturbative string theory in this background consists of two kinds of strings: open strings that begin and end on the branes and closed strings. As we have seen, open string may be viewed as excitations of a $(3+1)$-dimensional hyper plane, whereas closed string are the excitations of the $(9+1)$-dimensional flat spacetime. At low energies only massless modes are taken into account, so we may write the effective action for these massless string modes as

$$S = S_{closed} + S_{open} + S_{int} \tag{2.80}$$

which we can summarize as

- S_{open} defines a non-abelian gauge field as we have seen above, in particular it contains the action of a $\mathcal{N} = 4$ Super Yang-Mills theory with a gauge group $SU(N)$ and a constant $g_{YM} = 4\pi g_s$.
- S_{closed} corresponds to the action of a ten dimensional type IIB supergravity.
- S_{int} contains the interaction between open and closed strings and is proportional to $\alpha'^2 g_s$ and so it vanishes in the low energy limit $\alpha' \to 0$ if we keep g_s finite. This means that at low energies open and closed string are decoupled.

[7] A similar thing would happen to scalars, which would organize as 2×2 matrices $(\phi^i)^a_b$ transforming in the adjoint representation of the $U(2)$ gauge group.

In conclusion, from the open string perspective we find two decoupled theories in the low-energy limit: $\mathcal{N} = 4$ Super Yang-Mills theory in four dimensions and type IIB supergravity on $\mathbb{R}^{9,1}$.

D-branes: Closed string perspective

In a theory that contains gravity any form of matter affects the space-time metric and D-branes are no exeption. Therefore, D-branes are massive dynamical objects that will be a source of supergravity fields. In this case we are going to consider that $L/\ell_s \ll 1$ which will ensure that there is weak curvature, this means that this closed string perspective is reliable only in the limit $g_s N \gg N$. Let us take again N D3-branes in a ten dimensional type IIB supergravity theory. It can be shown by solving the supergravity equations of motion ([83, 86, 112]) that the metric sourced by these branes is given by[8]

$$ds^2 = H^{-1/2} dx^\mu dx_\mu + H^{1/2} dy^i dy_i \quad ; \quad H(r) = 1 + \left(\frac{R}{r}\right)^4 \tag{2.81}$$

$$R^4 = 4\pi g_s N \ell_s^4 \tag{2.82}$$

where the D3-branes extends over the x^μ coordinates and the y^i coordinates are the transverse ones. There are two clear limits that correspond to different regions of the space-time

- $r \gg R$: In this limit we find $H \simeq 1$ and the metric reduces to a flat ten dimensional space.
- $r \ll R$: This is so-called *near-horizon* or *throat*. In this limit we find that the space-time metric goes to

  $$ds^2 = \frac{r^2}{R^2} dx^\mu dx_\mu + \frac{R^2}{r^2} dr^2 + R^2 d\Omega_5^2 \tag{2.83}$$

  which is the geometry of an $AdS_5 \times S_5$ spacetime.

It can be shown that closed strings propagating in these two regions are decoupled in the low-energy limit. Notice that the from the point of view of an observer at infinity

[8] To be complete: there is also a field strength tensor $F_{(5)}$ living in the worldvolume which we can omit as it will not affect the discussion.

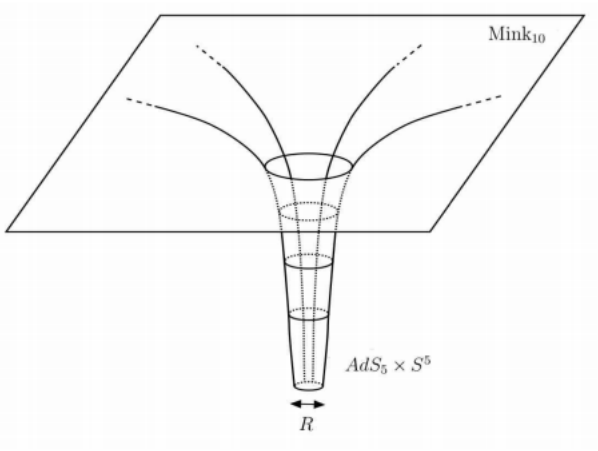

Figure 2.11: Space-time deformed by the N D3-branes. At $r \ll R$ we are in the throat, *i.e.* in a $AdS_5 \times S^5$ space-time, while in $r \gg R$ we are in a flat ten-dimensional space-time. Figure from [147].

the energy of a closed string, E_s, gets redshifted by the time metric component g_{tt} as $E_\infty = \sqrt{-g_{tt}} E_s$. In the limit where $r \ll R$ we would have

$$E_\infty \sim \frac{r}{R} E_s \,. \tag{2.84}$$

Therefore an observer at infinity sees two different low-energy excitations:

- Supergravity modes propagating in a flat ten-dimensional space-time.
- String excitations in the near horizon region, which corresponds to an $AdS_5 \times S^5$ space-time.

In conclusion, from the closed string perspective we find two decoupled theories in the low-energy limit: type IIB supergravity on $AdS_5 \times S^5$ and type IIB supergravity on $\mathbb{R}^{9,1}$.

2.3.3 The conjecture

Finally, we have all the motivation, tools and physical descriptions necessary to cope with the so-called AdS/CFT correspondence. The strongest form of the AdS_5/CFT_4 correspondence can be summarized as

$\mathcal{N} = 4$ Super Yang-Mills (SYM) theory
with gauge group $SU(N)$ and coupling $g_{\rm YM}$
is dynamically equivalent to
Type IIB superstring theory
with string length ℓ_s and coupling constant g_s
on $AdS_5 \times S^5$ with curvature radius R (and N units of $F_{(5)}$ flux on S^5).

There are two free parameters at each side of the equivalence: in the field theory side we have g_{YM} and N while in the string theory case we have g_s and the dimensionless ratio R/ℓ_s. The first identification can be found in (2.79) which in our case is

$$g^2_{\rm YM} = 4\pi g_s \,. \tag{2.85}$$

Moreover, using (2.82) we may derive the second identification between the free parameters of both theories

$$2\lambda = (R/\ell_s)^4 \tag{2.86}$$

where $\lambda \equiv g^2_{\rm YM} N$ is the 't Hooft coupling.

As mentioned above, the open and closed perspective depend on the effective coupling $g_s N$. In the limit $g_s N \ll 1$ we have that $R \ll \ell_s$, thus the throat geometry effect is smaller than the characteristic length of strings. In such limit the open and closed strings are decoupled and the open string perspective is reliable, while the closed string description is innaplicable since we would need to know the effects of gravity at scales smaller than ℓ_s. On the other hand if we consider the limit $g_s N \gg 1$ the backreaction of branes over the background is large enough to consider the closed string perspective. However the the open string perspective would not be reasonable as we would have to deal with a strongly coupled gauge theory.

The AdS/CFT conjecture is no less than conjecturing that both perspectives in the low energy limit should be equivalent. In this particular limit we find a mapping between a strongly coupled field theory and a weakly curved supergravity theory. This special limit is referred to as the weak form of the AdS/CFT conjecture.

The AdS/CFT correspondence stated above says that both sides of the correspondence are *dinamically equivalent*. This means that the two theories are identical and therefore describe the same physics from two very different perspectives. Thus, if the AdS/CFT conjecture holds, the physics from one theory can be mapped to the other one. This identification is particularly curious due to we would be mapping a quantum gravity theory candidate, *i.e.* superstring theory, to a field theory that has no gravitational degrees of freedom. This correspondence is also a realisation of the holographic principle that we introduced at the beginning of this section once we do a dimensional

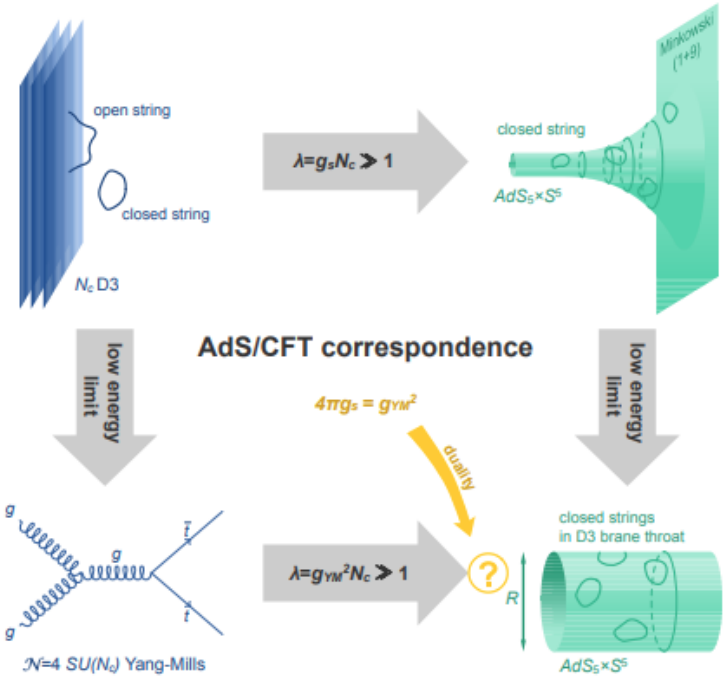

Figure 2.12: A sketch of the AdS/CFT correspondence. Figure from [131].

Kaluza-Klein reduction on the sphere S^5 and we map the five-dimensional superstring theory to the four-dimensional field theory[9].

2.4 User's guide

Previously we have focused on the motivation and mathematical basis of the AdS/CFT correspondence but we have not shown yet the most pragmatic aspect of it. Before diving into this we must be aware that throughout this thesis we will restrict ourselves to the so-called bottom-up holographic description. In general we can separate holographic models as *top-down* or *bottom-up* models.

In the former case we know exactly the two sides of the duality we are dealing with. On the field theory side we know the Lagrangian, which we may study in perturbation

[9]The reduction of the 5-sphere S^5 will be omitted here but can be found in any of the AdS/CFT reviews mentioned at the introduction of this section such as [181].

theory at weak coupling, while the dual gravity theory is treatable in the supergravity limit. This approach has the advantage that we can precisely identify operators on each side and rely on its correspondence.

The latter case, however, does not need to know what is the exact Lagrangian of the dual field theory, if it even exists. In this case we proceed as explained in [200]:

- Identify the minimal AdS gravity model with the desired features (symmetries, operator content).
- Determine the background solution by solving the equations of motion subject to the symmetries or other features asked.
- Perform the dual computations, such as correlation functions.

This approach has the advantages of not needing to know the two dual theories, we have easier computations to carry out or that we may obtain more universal results. Therefore, this will be the kind of holographic theories that we will consider throughout the text.

Field $\leftrightarrow$ operator correspondence

What we want to do now is to establish a mapping between the spectra of the two sides of the duality. In a CFT the important observables are the correlators of local observables $\mathcal{O}(x)$, whose generating functional is constructed out of sources. We can identify the sources of these operators as the boundary values of some field $\phi(x, z)$ of the gravity theory. To support this claim we make use of one of the most remarkable equations of AdS/CFT, known as the GPKW equation[10]

$$\mathcal{Z}_{\text{grav}}\left[\phi(x, z \to 0) = \phi_0(x)\right] = \left\langle e^{\int \phi_0(x)\mathcal{O}(x)} \right\rangle_{\text{CFT}} = \mathcal{Z}_{\text{CFT}}[\phi_0]\,. \tag{2.87}$$

On the left hand side we have the partition function of the gravity theory evaluated over all functions with the value ϕ_0 at the boundary. In the limit of weakly coupled gravity we can just approximate by the classical action

$$\mathcal{Z}_{\text{grav}} \simeq e^{S^{\text{sp}}_{\text{grav}}[\phi_0]} \tag{2.88}$$

where $S^{\text{sp}}_{\text{grav}}[\phi_0]$ is the action of the gravitational theory at the saddle point, *i.e.* the least action associated with the classical limit, evaluated at the boundary of AdS. On

[10] This equation was deduced by Witten [219] and independently by Gubser, Polyakov and Klebanov [95] around 1998.

the right hand side of (2.87) we have the generating functional of correlators in the CFT with some sources $\phi_0(x)$. This leads us to propose a correspondence between fields in the bulk theory and operators in the boundary field theory. This mapping can be determined based on the tensor structure, the dimension and some other quantum numbers, some examples of this mapping are

$$g_{\mu\nu} \quad \longleftrightarrow \quad T_{\mu\nu} \tag{2.89}$$
$$A_\mu \quad \longleftrightarrow \quad J_\mu \tag{2.90}$$
$$\phi \quad \longleftrightarrow \quad \mathcal{O} \tag{2.91}$$

where an example of operator $\mathcal{O}$ could be $\mathcal{O} = \mathrm{Tr}(F^{\mu\nu}F_{\mu\nu})$.

Let us now consider the most simple example: a scalar field theory with no interactions. We will consider an AdS_{d+1} space in Euclidean signature

$$ds^2 = \frac{R^2}{z^2}\left(\delta_{\mu\nu}dx^\mu dx^\nu + dz^2\right) \tag{2.92}$$

and an action given by

$$S = -\frac{1}{2}\int d^{d+1}x\sqrt{g}\left(\partial^M\phi\partial_M\phi + m^2\phi^2\right) \tag{2.93}$$

where $\mu,\nu = 0,\ldots,d-1$ and $M = 0,\ldots,d$. The equations of motion for this scalar field are

$$\frac{1}{\sqrt{g}}\partial_M\left(\sqrt{g}g^{MN}\partial_N\phi\right) - m^2\phi = 0\,. \tag{2.94}$$

By plugging the metric these equations reduce to

$$z^{d+1}\partial_z(z^{1-d}\,\partial_z\phi) + z^2\,\partial^\mu\partial_\mu\phi - m^2R^2\phi = 0\,. \tag{2.95}$$

We can now perform a Fourier transform of ϕ in the x^μ coordinates

$$\phi(z,x^\mu) = \int\frac{d^dk}{(2\pi)^d}e^{i\,k\cdot x}f_k(z) \tag{2.96}$$

and the equation then becomes

$$z^{d+1}\partial_z(z^{1-d}\partial_z f_k) + z^2k^2f_k - m^2R^2f_k = 0\,. \tag{2.97}$$

The exact solution of this equation is given by two Bessel functions whose asymptotic behaviour near the boundary go as a power of z, *i.e.* $f_k \sim z^\beta$. Thus, keeping the leading terms close to $z \sim 0$ we obtain the equation

$$\beta\,(\beta - d) - m^2 R^2 = 0 \tag{2.98}$$

which has two solutions[11]

$$\beta_\pm = \frac{d}{2} \pm \sqrt{\frac{d^2}{4} + m^2 R^2}\,. \tag{2.99}$$

Let us express the solution as a sum of these two powers of z, back into the coordinate space, as

$$\phi(x,z) \simeq \mathcal{A}(x)\, z^{\beta_-} + \mathcal{B}(x)\, z^{\beta_+} \quad \text{where } z \to 0\,. \tag{2.100}$$

We will only consider real exponents, thus we will impose $m^2\, R^2 \geq -d^2/4$[12]. The role that the functions $\mathcal{A}(x)$ and $\mathcal{B}(x)$ will have in the boundary theory can be determined by their normalizability with respect to the inner product, *i.e.* to

$$(\Psi_1, \Psi_2) = -i \int_{\Sigma_t} dz dx^{d-1} \sqrt{-g} g^{tt} (\Psi_1^* \partial_t \Psi_2 - \Psi_2 \partial_t \Psi_1^*)\,, \tag{2.101}$$

where Σ_t is a constant time slice of space-time.
There are two regions we must distinguish in order to assign the role to each function. On the one hand we have the region $m^2 R^2 \geq -d^2/4 + 1$, which corresponds to the so-called *standard quantization*. In this case we have that the function $\mathcal{B}(x)$ is normalizable whereas $\mathcal{A}(x)$ is not. Just as we have said above, the boundary value of the bulk field ϕ should correspond to the source of a boundary operator $\mathcal{O}$. Therefore, since the term that will be relevant at the boundary for the function $\phi(x,z)$ is $\mathcal{A}(x)$ we conclude that this non-normalizable mode should correspond to the source of the boundary operator and we will call it the *leading* mode. On the other hand, the normalizable modes are elements of the bulk Hilbert space. The equivalence between bulk and boundary theories must be applied to this Hilbert space as well, which leads us to conclude that normalizable modes should be identified with states of the boundary theory, and as we shall see below the mode $\mathcal{B}(x)$ determines the expectation value of

[11] This can be generalized for any p-form field of mass m, *i.e.* an antisymmetric tensor $A_{\mu_1,\ldots,\mu_p}$ with p indices, as: $\beta_\pm = \frac{d}{2} \pm \sqrt{\left(\frac{d-2p}{2}\right)^2 + m^2 R^2}$.

[12] Particles in AdS spaces might have negative mass squared particles and be stable, provided the mass is not *too negative*. This bound is called Breitenlohner-Freedman bound, which tells us that we need to respect $R^2\, m^2 \geq -d^2/4$. This result was first derived in [49, 51].

the dual operator $\mathcal{O}$. This will be the so-called *sub-leading* mode.

The second region corresponds to $-d^2/4 \leq m^2R^2 \leq -d^2/4+1$. Here both modes are normalizable, thus we may consider both modes to be identified with states of the boundary [50, 52], and an *alternative* quantization where $\mathcal{B}(x)$ gets to be the source might be considered, giving rise to two different possible CFTs [133]. Even a more general quantization where both modes are used to build the physical states can be considered [42, 107, 109, 220]. For the moment we will just stick to the standard quantization.

Let us now come back to the solution found in (2.100): it is trivial to notice that near the boundary the power that will dominate is β_-. Thus we need to impose boundary conditions on the dominant solutions at some $z=\epsilon$, which we will then send to $\epsilon \to 0$, so the solution does not diverge at the boundary

$$\phi(x,z)|_{z=\epsilon} = \epsilon^{\beta_-}\Phi(x)\,. \tag{2.102}$$

With this definition we have a scalar field $\Phi(x)$ which is finite and will be controlled by $\mathcal{A}(x)$ near the boundary. These powers $\beta_\pm$ are of great importance for the CFT operator $\mathcal{O}$ that the field $\phi(x,z)$ is sourcing. At the boundary action we can find

$$S_{\text{bdy}} \sim \int d^dx\sqrt{\gamma_\epsilon}\,\phi(x,\epsilon)\,\mathcal{O}(x,\epsilon) \tag{2.103}$$

where $\gamma_\epsilon = \left(\frac{R}{\epsilon}\right)^{2d}$ is the induced metric at the $z=\epsilon$ boundary. By using (2.102) we get

$$S_{\text{bdy}} \sim R^d \int d^dx\,\epsilon^{-d}\Phi(x)\,\epsilon^{\beta_-}\,\mathcal{O}(x,\epsilon)\,. \tag{2.104}$$

We want S_{bdy} to be finite and independent of ϵ, thus the operator must have the next form close to the boundary

$$\mathcal{O}(x,\epsilon) = \epsilon^{d-\beta_-}\mathcal{O}(x) = \epsilon^{\beta_+}\,\mathcal{O}(x) \equiv \epsilon^{\Delta}\,\mathcal{O}(x)\,. \tag{2.105}$$

The interpretation of this power Δ is that it acts as the mass scaling dimension of the operator $\mathcal{O}$ and similarly, for the field $\phi(x,z)$, we deduce that $\beta_- = d-\Delta$ is the mass scaling dimension of the source $\Phi(x)$. These parameters tell us how the source and the operator transform under scale transformations, *i.e.*

$$x \to \lambda\,x\,, z \to z/\lambda \quad \Longrightarrow \quad \Phi \to \lambda^{d-\Delta}\,\Phi\,, \mathcal{O} \to \lambda^{\Delta}\mathcal{O} \tag{2.106}$$

Thus the parameter Δ defines exactly the conformal dimension of the operator $\mathcal{O}$. We can divide the mass scaling dimensions in three categories depending on their values

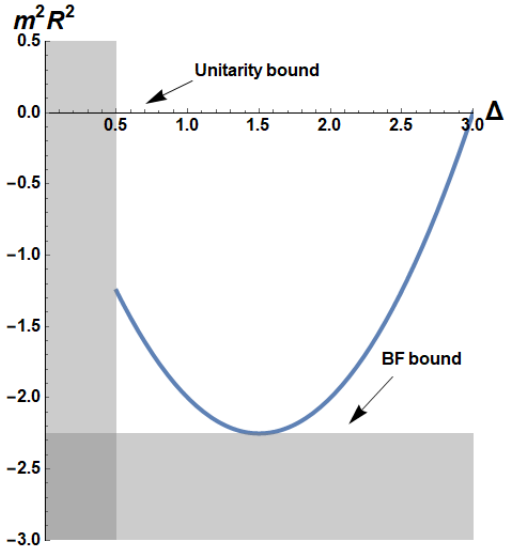

Figure 2.13: Relation between the conformal dimension Δ and m^2R^2 in $d = 3$ with unitarity and Breitenlohner-Freedman bounds represented in the graphic. Alternative quantization belongs to the region $1/2 < \Delta < 3/2$.

- *Relevant operator:* for $\Delta < d$. In this case the operator's effect is going to be significant for RG flows into the IR region. Relevant operators may be turned on without spoiling the AdS boundary, as the bulk field ϕ will go to a constant or zero at $z \to 0$, or in other words, these operators will not spoil the UV fixed point of the field theory. Here we have $-(d/2R)^2 < m^2 < 0$.
- *Marginal operators:* for $\Delta = d$. Here we have $m^2 = 0$. In this case the corrections would be, at most, logarithmic with energy.
- *Irrelevant operators:* for $\Delta > d$. These operators will not be important in the IR regime but might change the UV structure of the field theory. Here we will have $m^2 > 0$.

Finally we can consider a bound to this conformal dimension coming from the so-called unitarity bound. This bound comes from demanding that all states in a representation of a quantum field theory have positive norm. In the case of scalars in d dimensions one can find [151] that $\Delta \geq \frac{d-2}{2}$[13] (see Fig. 2.13).

[13]See [16] for AdS/CFT examples beyond the unitarity bound

Correlation functions

As stated above, correlation functions are important in CFTs and we can derive them by using (2.87). In general we will need to take care of possible divergences and renormalize the gravitational action by a holographic renormalization [197], thus we will now consider the renormalized action $S^{\rm sp}_{\rm grav} \to S^{\rm ren}_{\rm grav}$. Using this identification it is easy to derive that for a n-point correlation function we get

$$\langle \mathcal{O}(x_1) \dots \mathcal{O}(x_n) \rangle = \frac{1}{\mathcal{Z}_{\rm CFT}} \left. \frac{\delta^n \mathcal{Z}_{\rm CFT}}{\delta\Phi(x_1)\dots\Phi(x_n)} \right|_{\Phi=0} = \left. \frac{\delta^n S^{\rm ren}_{\rm grav}}{\delta\Phi(x_1)\dots\Phi(x_n)} \right|_{\Phi=0} . \quad (2.107)$$

Notice that we are taking the derivative with respect to Φ, if we want to compute a one point correlation function in terms of the field ϕ we would need to re-scale the expression using the relation (2.102), *i.e.*

$$\langle \mathcal{O}(x) \rangle = \lim_{z\to 0} z^{d-\Delta} \left. \frac{\delta S^{\rm ren}_{\rm grav}}{\delta\phi} \right|_{\phi=0} , \quad (2.108)$$

where Δ is the conformal dimension of the operator $\mathcal{O}$.
This functional expression can be fairly simplified. Consider that the gravity action is given by

$$S_{\rm grav} = \int dz\, d^d x\, \mathcal{L}[\phi, \partial\phi] , \quad (2.109)$$

with a boundary located at $z = \epsilon$. By performing an infinitesimal change $\phi \to \phi + \delta\phi$, integrating by parts and using the equations of motion we obtain

$$\delta S^{\rm sp}_{\rm grav} = - \int d^d x \left. \frac{\partial\mathcal{L}}{\partial(\partial_z\phi)} \delta\phi \right|_{z=\epsilon} . \quad (2.110)$$

Let us now define

$$\Pi(x,z) = -\frac{\partial\mathcal{L}}{\partial(\partial_z\phi)} \quad (2.111)$$

which is the canonical momentum when z plays the role of the time coordinate.
Using this we can rewrite (2.110) as

$$\delta S^{\rm sp}_{\rm grav} = \int d^d x\, \Pi(x,\epsilon)\, \delta\phi(x,\epsilon) . \quad (2.112)$$

Generally the full renormalized action is a combination of this on-shell action and the counterterms, which are defined in the boundary. Therefore

$$\Pi^{\rm ren}(x,z) = -\frac{\delta S^{\rm ren}_{\rm grav}}{\delta\phi(x,z)} . \quad (2.113)$$

This expression in the boundary must be

$$\Pi^{\text{ren}}(x,\epsilon) = -\frac{\partial \mathcal{L}}{\partial(\partial_z \phi)} + \frac{\delta S^{\text{ct}}_{\text{grav}}}{\delta \phi(x,z)} \tag{2.114}$$

which using (2.108) leads us to a nice expression for the one-point correlation function

$$\langle \mathcal{O}(x) \rangle = \lim_{z\to 0} z^{d-\Delta} \Pi^{\text{ren}}(x,z)\,. \tag{2.115}$$

Linear response theory

Finally we can comment the use of these correlation functions for the so-called linear response theory (see [108]). Let us write the one-point function as it is defined in a QFT

$$\langle \mathcal{O}(x) \rangle = \int d\Psi\, \mathcal{O}(x)\, e^{S_E[\Psi] + \int d^d y\, \Phi(y)\mathcal{O}(y)} \tag{2.116}$$

where Ψ are the different fields in the QFT. We may expand this expression as a power series of the source Φ up to linear order

$$\langle \mathcal{O}(x) \rangle = \langle \mathcal{O}(x) \rangle_{\Phi=0} + \int d^d y\, \langle \mathcal{O}(x)\mathcal{O}(y) \rangle\, \Phi(y) + \dots\,. \tag{2.117}$$

The two-point correlation function can be defined as the Euclidean two-point function $G_E(x-y)$ as

$$G_E(x-y) = \langle \mathcal{O}(x)\mathcal{O}(y) \rangle\ . \tag{2.118}$$

Moreover, let us consider $\langle \mathcal{O}(x) \rangle_{\Phi=0} = 0$. This can always be achieved as long as we subtract to $\mathcal{O}$ its vacuum expectation value with no source. Using this parametrization we can consider $\langle \mathcal{O}(x) \rangle$ as the fluctuation away from the vacuum, so the linear response of the system to an external source is

$$\langle \mathcal{O}(x) \rangle = \int d^d y\, G_E(x-y)\, \Phi(y)\,, \tag{2.119}$$

by Fourier transforming this expression we can express it as

$$\langle \mathcal{O}(k) \rangle = G_E(k)\, \Phi(k)\,. \tag{2.120}$$

Finally, using (2.108) and (2.115), we arrive to the expression

$$G_E(k) = \lim_{z\to 0} z^{2(d-\Delta)}\, \frac{\Pi^{\text{ren}}}{\phi}\,. \tag{2.121}$$

Let us use these results in the example presented in (2.93), which under partial integration and using the equations of motion we can obtain the on-shell action

$$S^{\rm sp} = -\frac{\zeta}{2}\int dz d^d x \partial_M \left[\sqrt{g}\phi g^{MN}\partial_N \phi\right] , \tag{2.122}$$

where ζ is some normalization constant. The boundary of this space corresponds to $z = \epsilon$ and we can then express the action as

$$S^{\rm sp} = -\frac{\zeta}{2}\int d^d x \ \sqrt{g}\phi g^{zz}\partial_z \phi|_{z=\epsilon} . \tag{2.123}$$

Using (2.111) we compute the conjugate momentum

$$\Pi = \zeta\sqrt{g}\, g^{zz}\, \partial_z\, \phi. \tag{2.124}$$

and re-write the action as

$$S^{\rm sp} = \frac{1}{2}\int_{z=\epsilon} d^d x\, \Pi(x,z)\, \phi(x,z)\,. \tag{2.125}$$

Let us now perform a Fourier transformation like we did in (2.96) on both ϕ and Π and express the action as

$$S^{\rm sp} = \frac{1}{2}\int \frac{d^d k}{(2\pi)^d}\Pi_{-k}(z=\epsilon) f_k(z=\epsilon)\,. \tag{2.126}$$

The results from (2.100) and (2.124), expressed on terms of Δ, allow us to compute the on-shell action in the limit $\epsilon \to 0$

$$S^{\rm sp} \approx \frac{R^{d-1}}{2}\int \frac{d^d k}{(2\pi)^d}\left(\epsilon^{d-2\Delta}(d-\Delta)\mathcal{A}(-k)\,\mathcal{A}(k) + d\mathcal{A}(-k)\mathcal{B}(k)\right) , \tag{2.127}$$

The first term $\epsilon^{d-2\Delta}$ is clearly divergent and one can find that an appropriate counterterm to the action in order to cancel this divergence is

$$S_{ct} = -\frac{d-\Delta}{2\,R}\int d^d x\sqrt{\gamma}\phi^2\,. \tag{2.128}$$

Performing again a Fourier transformation and adding the counterterm to the action we derive the renormalized action

$$S^{ren} = R^{d-1}\,\frac{2\Delta - d}{2}\int \frac{d^d k}{(2\pi)^d}\mathcal{A}(-k)\,\mathcal{B}(k)\,. \tag{2.129}$$

We would like to use the formulas we have derived to compute the one-point function from this renormalized actions. To do that we need to take the functional derivative with respect to the source $\Phi(x) = \mathcal{A}(x)$. Due to the coefficient $\mathcal{B}(x)$ also depends functionally on $\mathcal{A}(x)$ we will need to define the ratio $\mathcal{B}/\mathcal{A}$, which, as we will see below, is uniquely determined in the deep IR ($z \to \infty$), as $\chi \equiv \mathcal{B}/\mathcal{A}$. Therefore the renormalized action in terms of $\Phi(x)$ is

$$S^{ren} = R^{d-1}\,\frac{2\Delta - d}{2}\int \frac{d^d k}{(2\pi)^d}\Phi(-k)\,\chi(k)\,\Phi(k)\,. \tag{2.130}$$

From this we can finally obtain the one-point function

$$\langle \mathcal{O}(k)\rangle_\Phi = R^{d-1}\,(2\Delta - d)\chi(k)\Phi(k) = (2\Delta - d)\mathcal{B}(k)\,. \tag{2.131}$$

This is a very important result: we have found that the subleading term of the field ϕ is the one that determines the vev of the operator on the boundary! Moreover, using (2.120) we can also compute the two-point function

$$G_E(k) = R^{d-1}\,(2\Delta - d)\frac{\mathcal{B}(k)}{\mathcal{A}(k)}\,. \tag{2.132}$$

It is an interesting exercise to compute explicitly the ratio of the functions $\mathcal{A}$ and $\mathcal{B}$. We first need to define a new function g_k through the relation $f_k = z^{d/2}\,g_k$, which solving equation (2.97) lead us to two independent solutions

$$g_k(z) \sim I_{\pm\nu}(k\,z), \quad \nu \equiv \Delta - \frac{d}{2}\,. \tag{2.133}$$

where $I_{\pm\nu}$ are modified Bessel functions. Taking the limit $z \to 0$ these modified Bessel functions go as

$$I_{\pm\nu} \sim z^{\pm\nu}\,. \tag{2.134}$$

Thus, the functions in (2.100) can be identified with these solutions, so we finally get that $f_k(z)$ is

$$f_k(z) = z^{d/2}\left(\Gamma(1-\nu)\,\left(\frac{k}{2}\right)^{\nu}\mathcal{A}(k)\,I_{-\nu}(kz) + \Gamma(1+\nu)\,\left(\frac{k}{2}\right)^{-\nu}\mathcal{B}(k)\,I_\nu(kz)\right)\,. \tag{2.135}$$

The Bessel function, in the limit $z \to \infty$, goes as

$$I_{\pm\nu} \sim \frac{e^z}{\sqrt{2\pi z}}\,. \tag{2.136}$$

We want to impose that the function $f_k(z)$ is finite in this limit, which will force us to impose some condition on the functions $\mathcal{A}$ and $\mathcal{B}$. Looking at the limit $z \to \infty$ of $f_k(z)$

$$f_k(z) = \frac{z^{d/2}\, e^{kz}}{\sqrt{2\pi k z}} \left(\Gamma(1-\nu) \left(\frac{k}{2}\right)^{\nu} \mathcal{A}(k) + \Gamma(1+\nu) \left(\frac{k}{2}\right)^{-\nu} \mathcal{B}(k) \right) . \tag{2.137}$$

This function will diverge in the IR unless we demand that

$$\frac{\mathcal{A}(k)}{\mathcal{B}(k)} = -\frac{\Gamma(1-\nu)}{\Gamma(1+\nu)} \left(\frac{k}{2}\right)^{2\nu} = \frac{\Gamma(-\nu)}{\Gamma(\nu)} \left(\frac{k}{2}\right)^{2\nu} . \tag{2.138}$$

which fixes the ratio of $\mathcal{A}$ and $\mathcal{B}$. With this result we find that the Green function scales with k as

$$G_E(k) \sim k^{2\Delta - d} . \tag{2.139}$$

Expressing this result in the coordinate space by an inverse Fourier transformation we finally obtain[14]

$$G_E(x) = \langle \mathcal{O}(x) \mathcal{O}(0) \rangle \sim \frac{1}{|x|^{2\Delta}} . \tag{2.140}$$

And this result is also of great importance, as it confirms that Δ is actually the conformal dimension of the boundary operator $\mathcal{O}(x)$.

Holographic temperature

Let us now consider that our field theory is in a thermal bath at temperature T. The correspondence to this property in the gravity theory is given by a bulk geometry with an event horizon (*i.e.* a black hole or black brane) and the Hawking temperature we discussed in Section 2.1.2 will be identified as the temperature of this thermal bath[15]. This field theory that we are trying to identify to a gravity theory has now a scale, T, and thus is not completely conformal invariant. The temperature of the system will represent an IR deformation of the theory due to at energies much higher than T, in

[14] Tip: to compute this Fourier transformation we need that

$$\int \frac{d^d k}{(2\pi)^d} e^{ikx} k^n \sim \frac{1}{|x|^{d+n}}$$

[15] A finite temperature system in AdS may also be described by a solution with no horizon, the so-called "thermal AdS". Hawking and Page studied the transition between black hole and thermal AdS in [106]. Here we will omit this discussion.

the UV, this temperature will be negligible and the theory could be considered again to be conformal.

Let us discuss the most simple example: the Schwarzschild black brane in AdS. In this case the pure AdS space will be generalized to the next metric

$$ds^2 = \frac{R^2}{z^2}\left(-f(z)dt^2 + \frac{dz^2}{f(z)} + d\vec{x}^2\right) \tag{2.141}$$

where $f(z)$ is called the emblackening factor and goes as

$$f(z) = 1 - \left(\frac{z}{z_h}\right)^d \tag{2.142}$$

where z_h is the position of the event horizon, where the metric component g_{tt} will vanish. Notice that in the limit $z \to 0$ we will asymptotically go towards an AdS space. This behaviour is already telling us something about the dual field theory. As we discussed in Section 2.1.1 moving through the holographic coordinate z can be considered as moving through an RG flow. In this case we have that in the limit $z \to 0$ we are going to the UV limit of the field theory, where we recover the conformal symmetry. Inversely, when we move towards the black hole we leave this AdS space and pointing out that there is a notion of IR deformation in the dual field theory.

We will use the definition of the Hawking temperature (see (2.6)) as the holographic temperature

$$T = \frac{\kappa}{2\pi} \tag{2.143}$$

where κ is the surface gravity. There is a simple argument by Gibbons and Hawking [85] that helps us understand this formula. First of all we need to Wick rotate our time coordinate to $\tau = i\,t$. Then, in order to avoid (conical) singularities at z_h we must demand that this new time coordinates periodically identifies as

$$\tau \sim \tau + \frac{4\pi}{|f'(z_h)|}\,. \tag{2.144}$$

When studying a field theory with a periodically identified Euclidean time we know the temperature is the inverse of this period. Since τ corresponds precisely to the Euclidean time coordinate in the boundary theory we can safely say that the temperature is given by the inverse of this period. Therefore in this case

$$T = \frac{|f'(z_h)|}{4\pi} \tag{2.145}$$

which can be proved to be exactly (2.143)[16]. The temperature in the case of (2.142) is then

$$T = \frac{d}{4\pi\, z_h}\,. \tag{2.146}$$

From this expression it seems we have a continuum of temperatures for different values of z_h, but notice that we can always perform a scale transformation of the space-time coordinates of (2.141) as $(x^\mu, t, z) \to z_h(x^\mu, t, z)$, which fixes the temperature to be $T = d/4\pi$. In more general metrics the temperature can be obtained by

$$T = \frac{\kappa}{2\pi} = \frac{1}{2\pi}\sqrt{-\frac{\nabla_\mu n_\nu \nabla^\mu n^\nu}{2}} \tag{2.147}$$

where n_μ is the timelike Killing vector at the horizon.
In the same spirit we may also define what is the entropy of the field theory by taking a look at Section 2.1.2. There we see that the entropy of the black hole is related to its area. The Bekenstein-Hawking formula says then

$$S = \frac{A_H}{4G_N} \tag{2.148}$$

where G_N is the Newton's constant and A_H is the area of the horizon. This will determine the entropy of the dual field theory.

Finite charges

Another feature that we would like to incorporate to our models is a $U(1)$ charge, such as the electromagnetic charge. We are going to consider field theories that have a global $U(1)$ symmetry, instead of a gauged one. What this means for an electromagnetic $U(1)$ symmetry is that we will neglect the effect of photons in our theory. This assumption seems to be sensible as generally the coupling of the $U(1)$ symmetry is small[17] and the electromagnetic interaction is screened in a charged medium.

Thus, the question now is how do we translate this global symmetry of the field theory into our gravity theory. In order to incorporate a global symmetry in our field theory we must impose this symmetry to be a gauge symmetry in the gravity side [57],

[16]The surface gravity κ of a static Killing horizon is defined through the next equation $k^\mu \nabla_\mu k^\nu = \kappa k^\nu$ evaluated at the horizon, where k^μ is a normalized Killing vector.

[17]There are examples where this assumption might fail and photons are mediating a strong effective coupling, such as [198].

therefore let us consider an Einstein-Maxwell action, which respects this $U(1)$ gauge symmetry

$$S = \int d^{d+1}x\sqrt{-g}\left[\frac{1}{2}\left(R + \frac{d(d-1)}{R^2}\right) - \frac{1}{4g^2}F^2\right], \tag{2.149}$$

where $F = dA$ is the field strength.
We can introduce two new scales in this theory without breaking the rotational symmetry of our field theory. The first one is a chemical potential $\mu = A_t^{(0)}$ and the other possible scale we can introduce that preserves rotational symmetry, at least in a $2+1$ dimensional field theory, is a background magnetic field $B = F_{xy}^{(0)}$. Just like in the case of finite temperature presented before, here we are introducing new scales which will deform our space away from a pure AdS spacetime as we get closer to into the IR region.
Here we will study only the case with a chemical potential and no magnetic field for simplicity. In this case the Einstein equations of motion are

$$R_{\mu\nu} - \frac{R}{2}\,g_{\mu\nu} - \frac{d(d-1)}{2R^2}g_{\mu\nu} = \frac{1}{2g^2}\left(2F_{\mu\sigma}F_\nu^\sigma - \frac{1}{2}g_{\mu\nu}F_{\sigma\rho}F^{\sigma\rho}\right) \tag{2.150}$$

to which we need to add also the Maxwell equations

$$\nabla_\mu F^{\mu\nu} = 0\,. \tag{2.151}$$

The solutions to these equations of motion lead us to a Reissner-Nordstrom (RN) black hole in AdS

$$ds^2 = \frac{R^2}{r^2}\left(-f(r)dt^2 + \frac{dr^2}{f(r)} + d\vec{x}^2\right), \tag{2.152}$$

$$f(r) = 1 - \left(1 + \frac{r_h^2\mu^2}{\gamma^2}\right)\left(\frac{r}{r_h}\right)^d + \frac{r_h^2\mu^2}{\gamma^2}\left(\frac{r}{r_h}\right)^{2(d-1)}, \tag{2.153}$$

$$\gamma^2 = \frac{(d-1)g^2R^2}{(d-2)} \tag{2.154}$$

where r_h is the position of the black hole horizon. The scalar potential is

$$A_t = \mu\left[1 - \left(\frac{r}{r_h}\right)^{d-2}\right]. \tag{2.155}$$

From this solution we can extract already some information about the dual field theory. Firstly, the background Maxwell potential of the field theory is read off from the boundary value of the bulk Maxwell potential

$$A_\mu(r) = A_\mu^{(0)} + \ldots \quad \text{as} \quad r \to 0\,. \tag{2.156}$$

From this we can see that the chemical potential is μ. Moreover, the chemical potential μ is the source of a charge response ρ which can be read off the subleading term of A_t. Just as it happened when we introduced the temperature, this chemical potential is deforming the IR physics of this theory, which will not be noticeable for high energies. The temperature can also be found here as, we discussed in the last section, and in this case we obtain

$$T = \frac{1}{4\pi r_h}\left(d - \frac{(d-2)r_h^2\mu^2}{\gamma^2}\right). \tag{2.157}$$

Notice a very remarkable feature of this temperature compared with the Schwarzschild black hole: here we can reduce the temperature continuously to zero without the horizon vanishing. In this space-time we can still scale out r_h but in this scale we still have the scale of the chemical potential and thus with the dimensionless ratio T/μ. Due to we only have these two scales, in a scale invariant theory all dimensionless quantities can only depend through the ratio of temperature to the chemical potential. The zero temperature case is quite interesting and we want to point out a couple of things about it:

- The zero temperature RN black hole has finite entropy. This seems to mean that the ground state of this theory is degenerate (see [155] for a real example of finite entropy at zero temperature system).

- In the limit of small temperature $T \ll \mu$ we find an example of a "holographic" renormalization group flow between fixed points. In this limit the space-time close to the horizon may be described by an $AdS_2 \times \mathbb{R}^{d-1}$ space, thus we have an interpolation between an AdS_{d+1} space close to the boundary to this new $AdS_2 \times \mathbb{R}^{d-1}$ space in the horizon. The presence of this AdS space close to the horizon seems to indicate that at low temperature and low energies an emergent scale invariant symmetry appears in our theory, which was originally broken by both temperature and chemical potential. For more details see [80], where this holographic flow was first discussed.

The holographic dictionary

There are many aspects of gauge/gravity dualities that have been omitted which can be consulted in the references provided at the beginning of this section. To conclude, let us summarize what we have learnt in this introduction about the AdS/CFT correspondence as what is commonly known as a "holographic dictionary".

Anti de Sitter gravity theory	Conformal field theory
$d+1$ dimensions	d dimensions
$g_{\mu\nu}$ metric	$T^{\mu\nu}$ stress-energy tensor
gauge field A_μ	$U(1)$ current J^μ
scalar field ϕ	scalar operator $\mathcal{O}$
gauged symmetry	global symmetry
Hawking temperature	QFT temperature
AdS scale r	RG energy scale μ
mass m^2	conformal dimension Δ
...	...

2.4.1 Hydrodynamics and transport coefficients

Let us end this chapter by discussing the hydrodynamic description of strongly coupled CFTs using the AdS/CFT correspondence. It has been known for a very long time that finite temperature systems may be well described by an effective theory called hydrodynamics. The main idea of hydrodynamics is to consider only perturbations around the equilibrium whose wave-length is much larger than the mean free path, which is the characteristic length in an interacting system,

$$\lambda_{hydro} \gg \ell_{mfp}\,. \tag{2.158}$$

We can consider that the hydrodynamic description of a system is some effective theory where high energy modes have been integrated out.
In particular, the hydrodynamic equations of a fluid are determined by the conservation of the stress-energy tensor $T_{\mu\nu}$ (for an uncharged system)

$$\nabla^\mu T_{\mu\nu} = 0 \tag{2.159}$$

where the stress tensor, up to first order in derivative expansion, with a fluid velocity u^μ is given by

$$T_{\mu\nu} = p\,(g_{\mu\nu} + u_\mu u_\nu) + \rho\, u_\mu u_\nu - \sigma_{\mu\nu} \tag{2.160}$$

where the first two terms describe an ideal or perfect fluid and the third, $\sigma_{\mu\nu}$, introduces dissipative effects on the fluid. This dissipative term is

$$\sigma^{\mu\nu} = P^{\mu\alpha}P^{\nu\beta}\left(\eta\nabla_{(\alpha}u_{\beta)} + \left(\zeta + \frac{2}{3}\eta\right)g_{\alpha\beta}\,\theta\right). \tag{2.161}$$

The coefficients η and ζ are the shear and bulk viscosities, while θ is the divergence of the fluid velocity, $\theta = \nabla_\mu u^\mu$.

In [44] (see also [115, 182]) it was found that the gravitational equations of black holes in AdS space-time provided the exact same equations of a dissipative/viscous fluid. Therefore, this black-hole is acting as some finite temperature fluid with some viscosity that, through the AdS/CFT correspondence, might help us understand strongly correlated viscous systems. This is the so-called fluid-gravity correspondence.

What we are interested in now is whether we are able to compute properties of this fluid, such as η, by the holographic methods that we have introduced above.

First, we are going to consider the local rest frame, where the spatial part is going to be zero $u^\mu = (1, 0, 0, 0)$. This particular frame forces the stress tensor to have $T^{\mu 0} = 0$. Notice also that taking a constant velocity does not lead us to a vanishing $T_{\mu\nu}$, as we will have non-zero terms due to the covariant derivative of u^μ. Let us take the next space-time metric

$$g_{00}(t, x^i) = -1, \quad g_{0i}(t, x^i) = 0, \quad g_{ij}(t, x^i) = \delta_{ij} + h_{ij}(t) \tag{2.162}$$

where h is a perturbative element $h_{ij} \ll 1$ and is a traceless tensor $h^i_i = 0$. This perturbative term only depends on time and it will vary very slowly, as we expect in the hydrodynamic limit.
It is a trivial excercise to compute the different Christoffel symbols which leads us to the next covariant derivatives

$$\nabla_0 u_i = \nabla_0 u_0 = 0, \quad \nabla_i u_j = \frac{1}{2}\,\partial_0 h_{ij}, \quad \nabla \cdot u = 0\,. \tag{2.163}$$

With this result we can already find the off-diagonal term of the stress-energy tensor as

$$T^{ij}(t) = \eta\,\partial_0 h_{ij}(t), \quad i \neq j \tag{2.164}$$

which in the momentum space is

$$T^{ij}(\omega) = -i\eta\,\omega\,h_{ij}(\omega)\,. \tag{2.165}$$

The source for this component of the stress-energy tensor is, then, h_{ij}. Therefore, the one-point function of this element is given by[18]

$$\langle T_{ij}(x)\rangle = -\int G_R(x-y)\,h_{ij}(y)dy\,, \tag{2.166}$$

[18]Here we use the real time coordinate, as opposed to the Euclidean one-point function expressed in (2.116).

where here $G_R(x-y)$ is the retarded Green's function

$$i\,G_R(x-y) \equiv \theta(x^0-y^0)\,(\langle[T_{ij}(x),T_{ij}(y)]\rangle\ . \tag{2.167}$$

It is due to causality that the vev of the operator T_{ij} is given by this retarded Green function as it would not be possible to influence the system until the source has been active. Now, going into the momentum space

$$\left\langle T_{ij}(\omega,\vec{k})\right\rangle = -G_R(\omega,\vec{k})\,h_{ij}(\omega,\vec{k})\,. \tag{2.168}$$

Comparing equations (2.165) and (2.168) we can the so-called Kubo formula

$$\eta = -\lim_{\omega\to 0}\lim_{\vec{k}\to 0}\frac{1}{\omega}\,\mathrm{Im}G_R(\omega,\vec{k})\,. \tag{2.169}$$

We would like to compute this shear viscosity in the case stated above, i.e. for an AdS black hole. For a 4-dimensional space-time the metric is going to be

$$ds^2 = \frac{R^2}{z^2}\left[-f(z)\,dt^2+\frac{dz^2}{f(z)}+d\vec{x}^2\right],\quad f(z)=1-\left(\frac{z}{z_h}\right)^3 \tag{2.170}$$

where the boundary is at $z=0$ and the horizon at $z=z_h$. We are going to perturb the off-diagonal term of the metric, $g_{xy}=h_{xy}\equiv h\ll 1$, and obtain the Einstein equation at linear order which is, after a Fourier transformation,

$$h''+h'\left(\frac{2}{z}+\frac{f'}{f}\right)+h\left(\frac{\omega^2}{f^2}-\frac{2}{z^2}+\frac{2\,f'}{z\,f}\right)=0 \tag{2.171}$$

where the prime denotes derivatives with respect to z. Now a nice trick is to define a new variable such that $H\equiv h\,z^2$, which will lead us to

$$H''+H'\left(\frac{f'}{f}-\frac{2}{z}\right)+H\,\frac{\omega^2}{f^2}=0\,. \tag{2.172}$$

The interesting thing about this equation is that is exactly the one you obtain from the action of a massless scalar field

$$S=\zeta\,\frac{1}{2}\int d^dx\sqrt{-g}\,\partial^\mu H\,\partial_\mu H \tag{2.173}$$

in the limit where $\vec{k}\to 0$. Luckily, this allows us to use the results derived in (2.115) and (2.124) with $\Delta=d$, obtaining

$$\langle T_{xy}\rangle = \Pi = \zeta\,\sqrt{-g}\,g^{zz}\,H' = \zeta\,\frac{f}{z^2}\,H' \tag{2.174}$$

and because $\Delta = d$ the source for this vev is exactly H, thus

$$G_R(\omega, \vec{k}) = - \left. \frac{\Pi}{H} \right|_{z=0} . \tag{2.175}$$

In principle we need to compute this term at the boundary, but it is trivial to check that

$$\partial_z \Pi = -\zeta \, \frac{H}{z^2 f} \, \omega^2 \tag{2.176}$$

thus, in the limit where $\omega \to 0$ this quantity is going to be conserved (up to order ω^2), i.e. we can evaluate the momentum Π anywhere we want to. To find a solution for the field H we are going to propose an ansatz which, close the the horizon, goes like

$$H \sim H_0 \, (z_h - z)^\beta \tag{2.177}$$

which will be a solution when

$$\beta = \pm \frac{i \, \omega \, z_h}{3} . \tag{2.178}$$

Only one of these solutions is going to respect causality and it is important to decide which one we should choose. To do this let us define a new variable $e^r \equiv (z_h - z)$, where the horizon will be located at $r \to -\infty$, and re-inserting the time dependence we will have that

$$H \sim e^{-i \, \omega \, t \pm \beta r} . \tag{2.179}$$

If we consider a small time displacement $t \to t + \delta t$ we are going to need a positive (negative) δr if we take the positive (negative) solution of β to keep the solution constant. What this means is that the positive (negative) solution is the outgoing (infalling) wave at the horizon. The infalling boundary conditions are the ones that are naturally associated with the retarded Green's function, as in order to influence the horizon with a source at the boundary we need to locate this source in the past (see [176, 199] for more details).

Finally, we can compute the shear viscosity

$$\eta = - \lim_{\omega \to 0} \lim_{\vec{k} \to 0} \mathrm{Im} \left. \frac{\Pi}{\omega \, H} \right|_{z=z_h} = \frac{\zeta}{z_h^2} . \tag{2.180}$$

This result is very useful to derive the famous Kovtun-Son-Starinets (KSS) bound, which states that the ratio of the shear viscosity to entropy density is bounded by below as $\eta/s \geq 1/4\pi$ [175]. In our case the entropy density, which is given by the area of the horizon (2.148), is

$$s = \frac{S}{\mathcal{V}} = \frac{1}{4 \, G_N} \frac{1}{z_h^2} \tag{2.181}$$

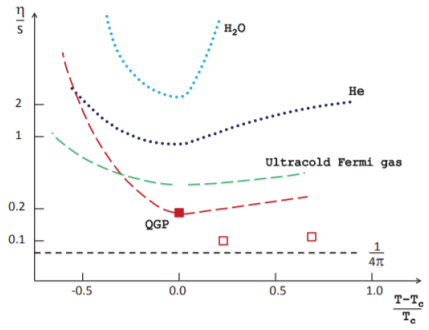

Figure 2.14: Different experimental results for the η/s ratio. All systems considered respect the bound $\eta/s \geq 1/4\pi$. Figure from [67].

where $\mathcal{V}$ is the two dimensional spatial volume at the horizon. All in all, taking the normalization constant $\zeta = 16\pi\, G_N$ as the gravitational one, we arrive to

$$\frac{\eta}{s} = \frac{1}{4\pi}\,, \tag{2.182}$$

which saturates the KSS bound.
In [175] they conjectured that this bound should be always respected by all systems and it indicates how strongly coupled a system is. So far this bound has been always been proved to be respected in all experiments [65, 142, 158, 192, 196], as can be seen in Fig.2.14. However, considering more complicated theories of gravity this bound is certainly violated, such as in the Gauss-Bonnet theory [53] or in massive gravity theories [9], among other examples (see [65] for a review). It is because of this that other bounds, related to the diffusion constants of the systems might be more general than the η/s ratio [27, 101, 224].

Chapter 3

Condensed matter and solid physics aspects

As we have pointed out in Chapter 2, one of the fields in which AdS/CFT correspondence has been remarkably prominent is in the study of condensed matter physics. This branch of physics is the one that deals with macroscopic and microscopic properties of matter. Its main concern is the "condensed" phase of matter that appears when the number of constituents is large and the interactions among them are strong. One of the most familiar cases are solids (which will play a major role in this manuscript) and liquids which emerge from electromagnetic interactions among atoms.

In this section we will focus on solid physics and more particularly on its elastic properties. This will be a good way to introduce what we mainly studied in [7, 23, 24], where we examine the physical properties of solids, either scale invariant or not, which we will analyze in Chapters 4 and 5. Furthermore, we will introduce the Coset construction that will allow us to build up the EFT for a solid system from its symmetry breaking pattern. Some references that have been useful for this chapter are [132, 138, 144, 152, 193].

3.1 Elasticity theory

When we apply a finite stress to a solid body this will exhibit a deformation, either in its shape or its volume. The elastic response describes necessary stress in a material to produce a mechanical deformation, i.e. the strain. Let us define the position of any point in the body by some vector $\Phi^i = x^i$, which can be used as the mapping of any

mechanical deformation as

$$\Phi^i = x^i + \phi^i(t, x) \tag{3.1}$$

giving the positions of every given solid element. The deviations from equilibrium from this solid (which we will take as isotropic and homogeneous) is then encoded in $\phi^i(t, x)$. These ϕ^i are the displacement vectors (i.e. $\phi^i = x'^i - x^i$, where x'^i is the new position of a particular element) and can be considered like a set of dynamic scalar fields. There is a very useful way to parametrize deformations through these scalars and it is through an object called the strain tensor

$$\epsilon_{ij} = \frac{1}{2}\left(\partial_i\phi_j + \partial_j\phi_i\right) , \tag{3.2}$$

that is symmetric by construction, i.e. $\epsilon_{ij} = \epsilon_{ji}$.

We are going to consider two particular types of deformation: bulk and shear deformations. Bulk deformations physically correspond to an expansion/contraction of a body, i.e. a change of the volume of the system. The bulk strain is defined by the trace of the strain tensor

$$\kappa \equiv \epsilon_{ii} = \vec{\partial} \cdot \vec{\phi} \tag{3.3}$$

and can be either positive (contraction) or negative (expansion). On the other hand, a deformation that only affects the shape of the body but does not affect its volume are called pure shear deformations and are given by

$$\epsilon \equiv \epsilon_{ik} - \frac{1}{d}\,\delta_{ik}\epsilon_{jj} \tag{3.4}$$

with d spatial dimensions and $i \neq k$. Notice that the trace of this shear strain is exactly zero. In general any mechanical deformation is a combination of shear and bulk deformations.

We can now describe what response do these solid system exhibit under mechanical deformations. At a linear level (for small external strains) we can find two elastic moduli. In this linear response approximation the deviation of the stress tensor from its equilibrium value is

$$\sigma_{ij} \equiv T_{ij} - p\,\delta_{ij} \tag{3.5}$$

where p is the pressure at equilibrium. Then at linear level we can define it as

$$\sigma_{ij} = \mathcal{K}\,\delta_{ij}\,\epsilon_{kk} + 2\,\mathcal{G}\,\left(\epsilon_{ij} - \frac{1}{d}\,\delta_{ij}\,\epsilon_{kk}\right) \tag{3.6}$$

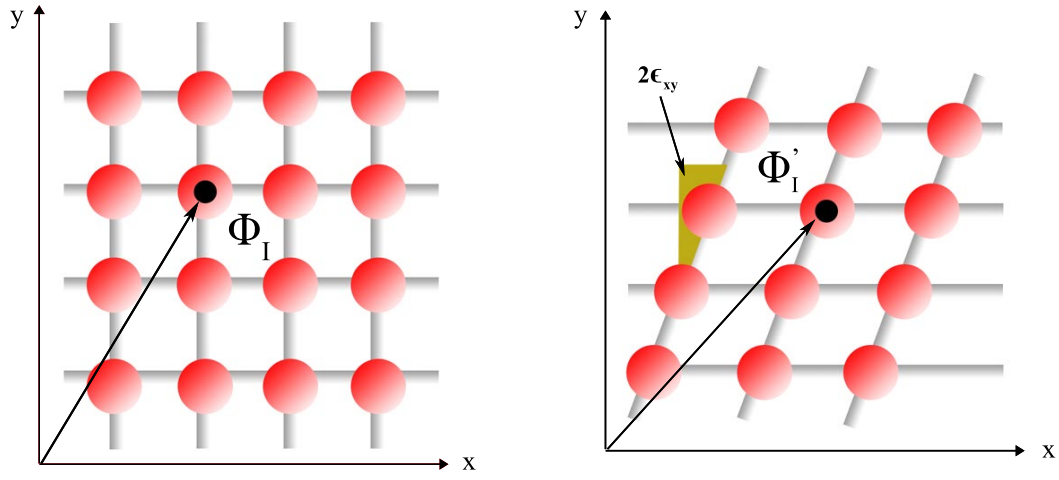

Figure 3.1: The description of the mechanical deformations in terms of the displacement vector $\Phi^i = x^i + \phi^i$. **Left:** The equilibrium configuration for the solid system is simply $\Phi^I_{eq} = x^I$. **Right:** An example of a shear deformation and the geometrical interpretation of the strain tensor ε_{ij}. The configuration changes from Φ^i_{eq} to Φ^i such that $\Phi^i - \Phi^i_{eq} = (\varepsilon_{xx}\, dx + \varepsilon_{xy}\, dy, \varepsilon_{yy}\, dy + \varepsilon_{xy}\, dx)$.

where $\mathcal{G}$ and $\mathcal{K}$ are referred to as the linear shear and bulk elastic moduli respectively. We can define the elastic bulk modulus also as the inverse of the compressibility β, which will be a useful definition, as

$$\mathcal{K} = \frac{1}{\beta} = -\mathcal{V}\,\frac{\partial T_{ii}}{\partial \mathcal{V}} \tag{3.7}$$

where $\mathcal{V}$ is the volume of the system.

Another simple and important parameter that allow us to characterize different kind of materials (at small deformations) is the so-called Poisson's ratio. It parametrizes how much a material compresses (or dilates) in the transverse direction when under an applied axial tensile strain,

$$\mathcal{R} \equiv -\frac{\epsilon_{\text{trans}}}{\epsilon_{\text{axial}}}\,. \tag{3.8}$$

We can express this ratio in terms of elastic moduli, by re-writing the elastic strain as

$$\epsilon_{ij} = \frac{\sigma_{kk}}{d^2\mathcal{K}}\,\delta_{ij} + \left(\sigma_{ij} - \frac{1}{d}\delta_{ij}\,\sigma_{kk}\right)\frac{1}{2\,\mathcal{G}}\,. \tag{3.9}$$

This may also be expressed differently, according to [208],

$$\epsilon_{ij} = \frac{1}{E}\left[(1+\mathcal{R})\,\sigma_{ij} - \mathcal{R}\sigma_{kk}\delta_{ij}\right] \tag{3.10}$$

where E is the Young modulus (the linear moduli for an uniaxial deformation). Thus, the Poisson's ratio can be defined as a function of the shear and bulk moduli

$$\mathcal{R} = \frac{d\,\mathcal{K} - 2\,\mathcal{G}}{d\,(d-1)\,\mathcal{K} - 2\,\mathcal{G}}\,. \tag{3.11}$$

This parameter allows us to classify models accordingly to their elastic properties. By construction, in two spatial dimensions the Poisson's ratio is bounded as $-1 < \mathcal{R} < 1$.

Notice that this ratio can be negative, giving a rather exotic type of response where the material actually dilates in the transverse directions. Materials of this type are called "auxetic" and have a number of applications[1].

3.1.1 Non-linear elastic response

The study of elasticity in solid materials must be extended beyond the linear regime, where the Hooke's law still holds, if we want to investigate their properties at finite deformations. This is studied by the finite or nonlinear elasticity [81], whose theoretical developments were initiated particularly in the rubber industry because of the importance of (natural) rubber in many engineering elements.

To introduce these finite deformations (either in the bulk or shear sectors) we consider a new configuration for the set of scalar fields $\Phi^i(t,x)$, where now its deformations $\phi^i(t,x)$ are not going to be infinitesimal. If we are dealing with a two dimensional solid we will take as the strained configuration

$$\Phi^i_{\text{str}} = O^i_j\,x^j\ ,\ O^i_j = \alpha\begin{pmatrix} \sqrt{1+\frac{\epsilon^2}{4}} & \frac{\epsilon}{2} \\ \frac{\epsilon}{2} & \sqrt{1+\frac{\epsilon^2}{4}} \end{pmatrix}\,. \tag{3.12}$$

From the definition of the shear and bulk strain in (3.4) and (3.3) we find that ϵ plays the role of the shear strain, whereas the bulk strain is defined through α as

$$\kappa = 2\,(\alpha - 1)\,. \tag{3.13}$$

[1] An example of a "real world" auxetic material is the sole material of some types of footwear, which allows it to expand in size while walking or running, increasing its flexibility.

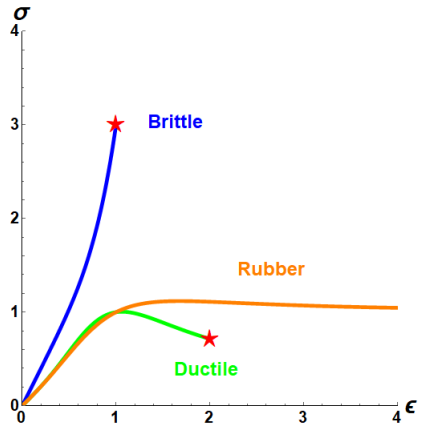

Figure 3.2: A sketch of the non-linear stress-strain curve $\sigma(\epsilon)$ for different type of materials: rubber (orange), brittle (blue) and ductile (green). All curves start with a linear regime. The red star is the breaking point at which the fracture of the material happens.

One of the physical observables that we are going to be interested in are the stress-strain curves that will be produced when this strain is introduced in the solid material. We will read the stress from the off-diagonal and diagonal terms of the stress tensor for the shear and bulk strains respectively.

Experimentally, this curve is obtained by gradually applying load to the solid and measuring the deformation produced, from which the stress and the strain can be determined. We show a schematic classification of the type of material we are dealing with depending on their stress-strain curve in Figure 3.2. Therefore, from that figure let us classify the materials into: rubber (or elastomers), brittle and ductile.

Rubber materials can sustain very large deformations until reaching the breaking point while also being able to go back to its equilibrium position once the stress is no longer applied. In figure 3.2 the scaling is "softening", meaning that the scaling is smaller than linear, but this is not always the case and "stiffening" scaling may also show up.

Brittle materials (e.g. a piece of chalk or a thin layer of glass) are materials that cannot sustain large amounts of deformation. In these materials the breaking point is found at small values of ϵ while the stress needed to get there can be large.

Ductile materials (e.g. steel and many other alloy of metals), on the other hand, start with a linear relation between strain and stress but at some point they display plastic deformations, which cannot be reversed back as elastic deformations do.

The type of materials that we are going to describe with our EFT and AdS/CFT methods are elastic, with no plastic effects, and we aim to find whether rubber-like materials are achievable. As we will see in Chapter 4 and 5 there will be a clear relation between the fact that materials are hyper-elastic and the strain scaling ν, both in the shear and bulk sectors.

3.2 Phonons

The study of phonons plays a major role in condensed matter physics. Phonons are defined as the collective excitations of the particles that form a solid (and even some liquids [47, 143]). Solids materials consist of atoms arranged in a lattice that interact among each other that allow to generate mechanical waves that carry heat and sound through the system. From the point of view of quantum mechanics a phonon can be described as a quasiparticle which represents an excited state of the mode of vibration of the elastic structures of these interacting particles. Phonons are useful to determine the thermal properties of a solid, which are related to its phonon structure, in particular the phonon density state determines the heat capacity and thermal conductivity of a crystal [71]. Even more interestingly, the phonon-electron interaction was of major importance in the BCS (Bardeen–Cooper–Schrieffer) theory that describe certain types of superconductors [33, 34].

These elastic excitations can be decomposed in different modes, depending on how they oscillate. In particular, there is a mode that oscillates in the same direction of propagation, called longitudinal mode, and modes that oscillate in the perpendicular directions of propagation, called transverse modes. The dispersion relation for these waves in the long wave-length limit

$$\omega = c_i k \tag{3.14}$$

where c_i can be either refer to the transverse or the longitudinal mode. The fact that for low values of k (i.e. long wavelength) this dispersion relation is almost linear means that the speed of propagation for phonons with different wavelength propagate large distances across the lattice without breaking apart. This is why the sound propagates through solids without much distortion. Moreover, these speeds can be related to the elastic moduli presented above

$$c_T^2 = \frac{\mathcal{G}}{\rho + p} \quad , \quad c_L^2 = \frac{\mathcal{K} + 2\,\frac{d-1}{d}\,\mathcal{G}}{\rho + p} \tag{3.15}$$

where ρ is the energy density of the system.
For more details about phonon physics and its applications, such as in the Debye model that estimates the contribution of phonons to the specific heat in a solid, we refer to [152].

An interesting way of approaching phonon physics is by realizing that these quasiparticles can be understood as the Goldstone bosons of some spontanously broken symmetry, in particular of translations. This was first realized in [139] where the author studies the implications of these hidden symmetries for the properties of the sound waves of solids. As a consequence of this symmetry phonons necessarily contain nonlinear terms, which describe phonon-phonon scattering.

This is the same mechanism that we use to study $\pi\,\pi$-scattering from the point of view of an effective field theory at low energies. In that case we have that the Lagrangian is invariant under $SU(2) \times SU(2)$ which is broken down to the diagonal subgroup $SU(2)$. The spontaneous breaking of the $SU(2) \times SU(2)$ symmetry leads to a triplet of massless pions, which can be studied through a nonlinear sigma model. This determines the form the Lagrangian must have, allowing us to know all possible $\pi\,\pi$ interactions without having to deal with QCD theory[2].

As we will see below we can build up a theory for solids by coset construction just like it is done for pions. In this case we will assume that fluctuations around the equilibrium value $\left\langle \Phi^I \right\rangle = x^I$ are the so-called phonons.

3.2.1 Coset construction

Firstly, let us state in which QFT sense we can treat elasticity theory as an EFT. The first property that we must have is a clear separation of scales, as opposed to what we have in a CFT, i.e. a continuum of states. In this case we will have that the low energy modes are going to be phonons, and any other mode above this will be integrated-out and will not participate in the EFT. This condition allows us to exploit the fact that phonons can be considered as Goldstone bosons of translational symmetry breaking.

[2]This was pioneered in [54, 61]. See [193] for a more recent discussion.

When we have a symmetry broken spontaneously we can make use of the coset construction that allows us to define a non-linear description of our theory just by knowing the breaking symmetry pattern.

Consider a continuous global symmetry $\mathcal{G}$ that spontaneously breaks down to a subgroup $\mathcal{H}$. This means that the vacuum will be invariant under this subgroup $\mathcal{H}$ but not under the rest of $\mathcal{G}$, which in group theory is known as the coset and is labeled as $\mathcal{G}/\mathcal{H}$. The Goldstone bosons of this symmetry breaking will transform linearly under the unbroken subgroup $\mathcal{H}$ but non-linearly under the coset $\mathcal{G}/\mathcal{H}$.

As we have already commented, the iconic example of these type of theories is the EFT of pions and we will summarize it here following [193]. Let us start by writing the QCD Lagrangian (including only up and down quarks)

$$\mathcal{L} = -\frac{1}{4}(F^a_{\mu\nu})^2 + i\bar{u}\not{D}u + i\bar{d}\not{D}d - m_u\bar{u}u - m_d\bar{d}d \tag{3.16}$$

where we use the notation $\not{D} = D_\mu\gamma^\mu$ where γ^μ are the Dirac matrices. This Lagrangian is symmetric under a global $SU(2)$ transformation that rotates up and down quarks into each other only if the masses of these quarks are the same. These masses are actually not equal, but they are very small compared to the QCD scale Λ_{QCD}, so let us take the limit $m_u = m_d = 0$. In this case we have actually two independent $SU(2)$ symmetries, since left-handed and right-handed quarks are completely decoupled. We can see this by writing the Lagrangian as a function of left and right handed spinors, i.e. $\Psi_q^{R/L} = \frac{1}{2}(1 \pm \gamma_5)\Psi_q$

$$\mathcal{L} = -\frac{1}{4}(F^a_{\mu\nu})^2 + i\bar{u}^R\not{D}u^R + i\bar{u}^L\not{D}u^L + i\bar{d}^R\not{D}d^R + i\bar{d}^L\not{D}d^L \tag{3.17}$$

This will be invariant under

$$\begin{pmatrix} u^L \\ d^L \end{pmatrix} \to g_L \begin{pmatrix} u^L \\ d^L \end{pmatrix}, \quad \begin{pmatrix} u^R \\ d^R \end{pmatrix} \to g_R \begin{pmatrix} u^R \\ d^R \end{pmatrix} \tag{3.18}$$

where $g_L \in SU(2)_L$ and $g_R \in SU(2)_R$.

At some point this $SU(2) \times SU(2)$ symmetry spontaneously breaks. Presumably this happened around 14 billion years ago, when the temperature of the universe cooled below some critical temperature $T_C \sim \Lambda_{QCD}$. Below this scale the thermal energy of quarks was smaller than their binding energy, leading to the appearance of hadrons. The ground states would be now quark bilinears

$$\langle\bar{u}u\rangle = \langle\bar{d}d\rangle = V^3\,. \tag{3.19}$$

This cannot be proven by QCD itself, but the strength spontaneous symmetry breaking is that we do not need to understand exactly how this works in QCD to be able to describe an effective theory for the pions. This vacuum expectation value breaks the symmetry $SU(2) \times SU(2)$ down to the diagonal subgroup, i.e. the unbroken symmetry is now rotating simultaneously left and right-handed spinors the same way.

The idea now is to forget that pions are actually composite particles of quarks and just focus on the symmetry breaking pattern.

We will model this breaking with a set of scalars $\Sigma_{ij}(x)$ that will transform under $SU(2) \times SU(2)$ as[3]

$$\Sigma \to g_L \Sigma g_R^\dagger, \quad \Sigma^\dagger \to g_R \Sigma^\dagger g_L^\dagger \,. \tag{3.20}$$

Thus, an effective Lagrangian for this field is

$$\mathcal{L} = |\partial_\mu \Sigma|^2 + m^2 |\Sigma|^2 - \frac{\lambda}{4} |\Sigma|^4 \tag{3.21}$$

where $|\Sigma|^2 \equiv \Sigma_{ij}\Sigma_{ij}^\dagger$. This Lagrangian is commonly named linear sigma model and is invariant under $SU(2) \times SU(2)$ transformations.

The potential in (3.21) is usually named "Mexican hat" potential and the interesting point is that depending on the signature of the quadratic term the minimum of the potential is either at $\Sigma = 0$ or at a finite value as can be seen in Fig. 3.3, which spontaneously breaks the symmetry of the Lagrangian. Specifically, in this case the potential is minimized for

$$\langle \Sigma_{ij} \rangle = \frac{v}{\sqrt{2}} \begin{pmatrix} 1 & 0 \\ 0 & 1 \end{pmatrix}, \quad v = \frac{2\,m}{\sqrt{\lambda}} \tag{3.22}$$

which breaks the $SU(2) \times SU(2)$ symmetry down to the diagonal subgroup $SU(2)$.

What we need to do now is expand our field around this vacuum expectation value in terms of a modulus field $\sigma(x)$ and some angular fields $\pi(x)$ as

$$\Sigma(x) = \frac{v + \sigma(x)}{\sqrt{2}} \exp\left(2\,i\, \frac{\pi^a(x)\tau^a(x)}{F_\pi} \right) \tag{3.23}$$

where τ^a are the Pauli matrices, which are the basis of the Lie algebra $\mathfrak{su}(2)$, and used $F_\pi = \frac{2\,m}{\sqrt{\lambda}}$ so the kinetic terms are normalized. If we transform our field as in (3.20) with $g_{L,R} = \exp(i\,\theta^a_{L,R}\tau^a)$ in the infinitesimal limit we get that σ does not change whereas

$$\pi^a \to \pi^a + \frac{F_\pi}{2}(\theta^a_L - \theta^a_R) - \frac{1}{2} f^{abc}(\theta^b_L + \theta^b_R)\pi^c + \ldots \tag{3.24}$$

[3]Notation: the superscript † means that we take the conjugate transpose of the matrix.

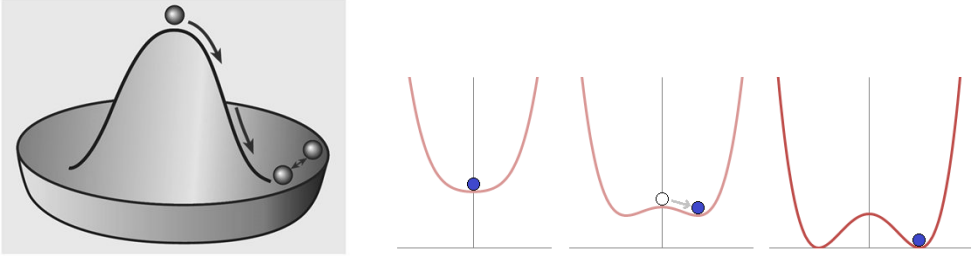

Figure 3.3: **Left:** "Mexican hat" potential. The center point is an unstable point and the equilibrium position is now away from it, sponteaneously breaking the symmetry. Figure from [215]. **Right:** The quadratic term changes its signature and a new vacuum expectation value arises. Figure from [64].

where $f^{abc} = \epsilon^{abc}$ is the structure constant, which in the case of $SU(2)$ is the Levi-Civita symbol. Notice that for transformations with $\theta_R^a = \theta_L^a$, which are the transformations of the unbroken diagonal subgroup $SU(2)_V$, the π field transforms linearly at leading order but non-linearly for transformations with $\theta_R^a = -\theta_L^a$, which form the axial transformations.

Due to the field σ does not transform under these symmetries we can consider it irrelevant for this discussion, therefore we may take the limits $m \to \infty$, $\lambda \to \infty$ and keep F_π fixed in order to decouple the field σ. Thus, let us change our initial field as

$$\frac{\sqrt{2}}{v}\Sigma(x) \to \Pi(x) \equiv \exp\left[2\,i\,\frac{\pi^a\tau^a}{F_\pi}\right] = \exp\left[\frac{i}{F_\pi}\begin{pmatrix} \pi^0 & \sqrt{2}\,\pi^- \\ \sqrt{2}\,\pi^+ & -\pi^0 \end{pmatrix}\right], \tag{3.25}$$

where we have used $\pi^\pm \equiv \frac{1}{\sqrt{2}}(\pi^1 \pm i\pi^2)$ and $\pi^0 \equiv \pi^3$. The field $\Pi(x)$ transforms as $\Sigma(x)$ in (3.20) and fulfills $\Pi\,\Pi^\dagger = 1$.

The idea now is to construct the most general Lagrangian invariant under a $SU(2)\times SU(2)$ transformation. This is usually called a non-linear sigma model, and particularly in this case a chiral Lagrangian, which is

$$\begin{aligned}\mathcal{L}_\Pi =& \frac{F_\pi^2}{4}\mathrm{Tr}\left[(D_\mu\Pi)(D^\mu\Pi)^\dagger\right] + \alpha_1\mathrm{Tr}\left[(D_\mu\Pi)(D^\mu\Pi)^\dagger\right]^2 \\ &+ \alpha_2\mathrm{Tr}\left[(D_\mu\Pi)(D_\nu\Pi)^\dagger\right]\mathrm{Tr}\left[(D^\nu\Pi)^\dagger(D^\mu\Pi)\right] \\ &+ \alpha_3\mathrm{Tr}\left[(D_\mu\Pi)(D^\mu\Pi)^\dagger(D_\nu\Pi)(D^\nu\Pi)^\dagger\right] + \ldots\end{aligned} \tag{3.26}$$

Due to the field Π fulfills $\Pi\,\Pi^\dagger = 1$ only derivative terms appear on the Lagrangian, which forbids π to acquire mass. We may expand the leading term in (3.26) to obtain

the Lagrangian for the π^a fields

$$\frac{F_\pi^2}{4}\mathrm{Tr}\left[(D_\mu\Pi)(D^\mu\Pi)^\dagger\right] = \frac{1}{2}(\partial_\mu\pi^0)(\partial^\mu\pi^0) + (D_\mu\pi^+)(D_\mu\pi^-)^\dagger + \frac{1}{F_\pi^2}\left[-\frac{1}{3}\,\pi^0\pi^0 D_\mu\pi^+ D^\mu\pi^- + \dots\right] + \frac{1}{F_\pi^4}\left[\frac{1}{18}(\pi^-\pi^+)^2\, D_\mu\pi^0 D^\mu\pi^0 + \dots\right] + \dots \tag{3.27}$$

We have chosen the appropriate normalization so that the kinetic terms are canonically normalized while the interactions will be suppressed by powers of $\frac{1}{F_\pi^2}$. On the other hand, interaction terms of the field Π have four or more derivatives, and thus at low energies are suppressed by powers of $\frac{E}{F_\pi}$. Then, at low energies, interactions among π^a fields are completely fixed from the leading term expansion, and we have determined these interactions by knowing the symmetry breaking pattern!

To construct the EFT of a solid system we are going to need a similar approach to what we have shown for the pion Lagrangian, which is precisely what is done in [163,164]. There, they exploit the fact that phonons can be considered as the Goldstone bosons of translational symmetry breaking and build up a Lagrangian by using the coset construction. The dynamical degrees of freedom that will be responsible for the spontaneous breaking of translations that take place in solids are the ones we already introduced in (3.1). These fields acquire a vacuum expectation value given by

$$\langle\Phi^i\rangle = x^i\,, \tag{3.28}$$

in the equilibrium configuration, while the phonons are identified as the perturbations around this background.

We can formalize the EFT more sharply if we define these scalar fields with an 'internal' index, i.e. by defining them as $\Phi^I(x)$. If we are working in d space-time dimensions we will need $d-1$ scalars, thus the internal index runs over $I = 1, \dots, d-1$. By introducing this index we can consider that there is an internal symmetry group given by an Euclidean group, $ISO(d-1)$, acting on Φ^I like standard translations and rotations in the internal space. With this new definition let us re-write the vev from (3.28) as

$$\langle\Phi^I\rangle = x^i\,\delta_i^I\,, \tag{3.29}$$

this vev breaks the symmetry group[4] $ISO(d-1)\times ISO(d-1,1)$ down to the diagonal subgroup, i.e. by transformations on both Φ^I and x^i which leave (3.29) invariant, i.e.

[4]The group $ISO(d-1,1)$ is the d dimensional Poincaré group.

$$ISO(d-1,1) \times ISO(d-1) \Rightarrow \mathbb{R}_t \times ISO(d-1)\,. \tag{3.30}$$

What we find is that the action describing this EFT of solids must be constructed out of the matrix $B^{IJ} = \partial_\mu \Phi^I \partial^\mu \Phi^J$, which in $d+1$ dimensions can only build up a limited amount of independent terms. If we define $[B^n] \equiv \mathrm{Tr}((B^{IJ})^n)$, then for we can obtain the next d independent terms

$$X_1 = [B]\ ,\ X_2 = [B^2]\ ,\ \ldots\ ,\ X_d = [B^d]\,, \tag{3.31}$$

then the action must be

$$S = \int d^{d+1}x\, F(X_i)\ ,\ i = 1, \ldots, d\,. \tag{3.32}$$

It is also interesting to note that this method can also be applied for a perfect fluid system. For a perfect fluid we demand that the action for the scalars is invariant under internal volume preserving diffeomorphisms, i.e.

$$\Phi^I \to \chi^I(\Phi^J) \quad \text{where} \quad \det\left(\frac{\partial \chi^I}{\partial \Phi^J}\right) = 1\,. \tag{3.33}$$

In this case we are restricted to an action that depends on the determinant of the matrix B_{IJ}, thus

$$S = \int d^{d+1}x\, F(Z)\,, \tag{3.34}$$

where $Z = \det(B_{IJ})$. Notice that this is a subset of actions that can be considered for solids, as the determinant can be expressed as a function of the different X_i traces, e.g. for $d = 2$ and $d = 3$ we find that

$$\det(B) = \frac{1}{2}\,(X_1^2 - X_2) \tag{3.35}$$

$$\det(B) = \frac{1}{6}\,(X_1^3 - 3X_2\,X_1 + X_3)\,. \tag{3.36}$$

In conclusion, in order to describe the low energy dynamics of a solid system we will be able to do it by using the action (3.32), which may also be constructed with the determinant Z and the set of traces X_i where $i = 1, \ldots, d-1$, i.e.

$$S = \int d^{d+1}x\, F(Z, X_i) + \ldots\ ,\ i = 1, \ldots, d-1\,. \tag{3.37}$$

The function F will depend on the physical properties of the solid, such as the equation of state, while the dots indicate that there could be higher derivative terms which are negligible at low energies.

This will be the kind of action that we are going to consider throughout Chapter 4.

3.3 Quantum criticality

A quantum phase transition is a phase transition between different matter states at zero temperature [186]. Classically phase transitions are driven by temperature, but in this case the transitions occur due to the variation of other physical parameters, such as pressure or magnetic fields. The point between these phases is called a quantum critical point and it is of major importance in condensed matter physics and its relation with AdS/CFT.

Due to we this phase transition occurs at zero temperature the fluctuations that will dominate are going to be quantum fluctuations rather than thermal ones. As in classical phase transitions the correlation length of the system ζ diverges when approaching to the point, so we can say there is a long range quantum entanglement in the system. Moreover, as the continuous quantum critical point is approached, the energy of the first excited state (the so-called mass gap) vanishes. Therefore, a quantum critical theory is a scale invariant theory that needs to be treated with a CFT. Typically the quantum critical theory is strongly coupled which makes it a very interesting candidate to be treated by AdS/CFT methods.

Experimentally we cannot obtain an absolute zero temperature system, but this is

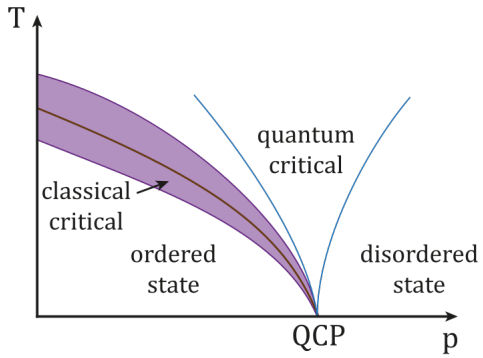

Figure 3.4: Typical phase transition diagram controlled by pressure and temperature. Above the quantum critical point (QCP) there is a region where there is still a notion of criticality and, thus, scale-invariance. Figure from [218].

not important as the effects of this critical points are still present at finite temperature $T > 0$. As long as we are in a region where quantum fluctuations, $\mathcal{Q}$, are bigger than thermal fluctuations $\mathcal{Q} > T$ we are still in a "critical region" where the effects of the quantum critical point are still noticeable (see Fig. 3.4).

There are a variety of metallic (anti-)ferromagnetic materials that develop a quantum critical behavior at very small temperature controlled by pressure, chemical doping or magnetic fields. Their metallic properties change abruptly by the critical fluctuations, departing from the Fermi liquid behavior to a state called non-Fermi liquid or strange metal. These kind of materials have been studied deeply because they are believed to exhibit superconducting properties. In particular, these strange metals could be related to high temperature superconductors as is pointed out in [194] and holographic examples have already been proposed [80].

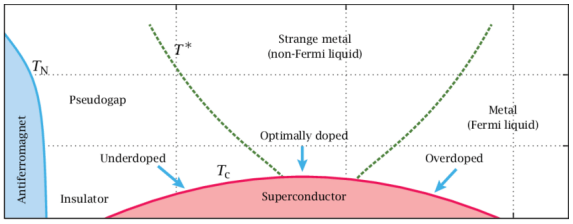

Figure 3.5: Phase diagram for a cuprate superconductor controlled by a doping parameter and temperature. Notice that the quantum critical region above the superconducting phase is described by the non-Fermi liquid/strange metal state. Figure from [183].

Chapter 4

Effective field theory of solids

In this chapter we will introduce and study a description of a solid system applying Effective Field Theory (EFT) methods with the action presented in Section 3.2.1. The theory of elasticity is an outstanding and early example of an EFT, providing us a continuum limit description of a solid's mechanical response, including its sound wave excitations, the so-called phonons we introduced in Section 3.2 (see [59,138]). The EFT for this solids will be expressed as a derivative expansion of the displacement vector of the solid elements with respect to its equilibrium position.

We prove the predictive power of these methods applying them on a particular case of solid materials, i.e. those solids that display a power-law scaling in the stress-strain relation $\sigma \sim \epsilon^{\nu}$.

The results that will be shown here are based on [7] and [23].

4.1 Elastic response

With the EFT action in our hands we can already start looking at the physical properties that these kind of systems have, in particular with the linear elasticity which has been introduced already in Section 3.1.

In order to study the mechanical response we must compute the stress-energy tensor of the action which has a rather simple form[1]

$$T_{\mu\nu} = -\frac{2}{\sqrt{-g}}\frac{\delta S}{\delta g^{\mu\nu}} = -\eta_{\mu\nu}\, V + 2\,\frac{\partial V}{\partial B^{IJ}}\,\partial_\mu \Phi^I \partial_\nu \Phi^J\,. \tag{4.1}$$

[1]Many computations presented in this Chapter are explained with more detail in Appendix B

If we consider a potential that is a function of the determinant Z and the traces $x_n \equiv X_n/Z^{n/2}$ (which will simplify the expressions) we will get that the second term can be expressed as

$$\frac{\partial V}{\partial B^{IJ}} = \frac{\partial Z}{\partial B^{IJ}} \frac{\partial V}{\partial Z} + \sum_{n=1}^{d-2} \left(\frac{\partial \mathrm{Tr}(B^n)}{\partial B^{IJ}} \frac{1}{Z^{n/d-1}} - \frac{\partial Z}{\partial B^{IJ}} \frac{n}{d-1} \frac{x_n}{Z} \right) \frac{\partial V}{\partial x_n} \,. \tag{4.2}$$

The first thing we can extract from the stress-tensor are the elastic moduli of the material, which tell us how the system responds to small deformations. For a pure shear strain our background changes to

$$\Phi^I = (\delta^I_i + \epsilon^I_i)\, x^i \tag{4.3}$$

where the tensor ϵ^I_i can be taken to be symmetric. Taking a look at equation (3.6) we see that we must look at the component T_{ij}, with $i \neq j$, at first order in the deformation ϵ^I_j. The term $\partial Z/\partial B^{IJ}$ that appears twice vanishes when is contracted with $\partial_i \Phi^I \partial_j \Phi^J$, thus we are left with

$$T_{ij} = 4\, \epsilon_{ij} \sum_{n=1}^{d-2} n^2 \frac{\partial V}{\partial x_n} \,. \tag{4.4}$$

Therefore the shear modulus is

$$\mathcal{G} = 2 \sum_{n=1}^{d-2} n^2 \frac{\partial V}{\partial x_n} \,. \tag{4.5}$$

On the other hand, for a bulk deformation we will use

$$\Phi^I = \alpha\, \delta^I_i\, x^i \tag{4.6}$$

and thus, the bulk strain is

$$\kappa = (d-1)(\alpha - 1) \,. \tag{4.7}$$

Looking at the diagonal component of the stress-tensor, T_{ii}, we can arrive to a simple form

$$T_{ii} = -V + 2\, Z\, V_Z \,. \tag{4.8}$$

Finally, we obtain the bulk modulus through either of the definitions given in (3.6) or (3.7)[2] , thus we arrive to

$$\mathcal{K} \equiv -\mathcal{V} \frac{dT_{ii}}{d\mathcal{V}} = \frac{dT_{ii}}{d\kappa} = 4 Z^{3/2}\, \partial_Z \left(\sqrt{Z}\, V_Z \right) \,. \tag{4.9}$$

[2]For the second definition we use the fact that the volume scales as $\mathcal{V} \propto \alpha^{1-d}$.

Therefore, we see that the potential that we choose to define our EFT already defines the elastic moduli of the system. These moduli are related to the speed of the phonon modes as we have seen in (3.15), which must be confirmed in this EFT.

We can, indeed, derive the speeds of the phonon modes from the action we have considered assuming that the phonons are the perturbations around the background configuration of the fields Φ^I, i.e. $\Phi^I = \Phi^I_b + \pi^I$ where π^I play the role of the phonons. We must take a look at the action at quadratic order in π^I, which is given by

$$\delta S^{(2)} = -\int d^d x \left(-N\,\dot{\pi}^2 + c_1^2(\partial_i \pi_i^L)^2 + c_2^2(\partial_i \pi_j^T)^2\right) \tag{4.10}$$

where we have split the perturbation into transverse and longitudinal modes $\pi^I = \pi^I_T + \pi^I_L$, i.e. modes that satisfy

$$\partial_i \pi_i^T = 0\ ,\ \partial_{[i}\pi^L_{j]} = 0\,. \tag{4.11}$$

What we found in Appendix B is that

$$N = Z\,V_Z\,, \tag{4.12}$$

$$c_L^2 = \frac{c_1^2}{N} = 1 + \frac{2\,V_{ZZ}\,Z}{V_Z} + \frac{2\,(d-2)}{d-1}\,c_T^2\,, \tag{4.13}$$

$$c_T^2 = \frac{c_2^2}{N} = \sum_{n=1}^{d-2} \frac{n^2\,V_{x_n}}{Z\,V_Z}\,. \tag{4.14}$$

Thus from here it is easy to check that the speeds of these phonon modes fulfill the relation introduced in (3.15).

Up until now we have restricted ourselves to the infinitesimal limit of the deformations, but we can go beyond this regime and explore what happens to the elastic response at finite deformations. At this level of deformation we want to find what is the stress-strain relations of both the shear and bulk channels which encode several response parameters such as the proportional limit or the failure point (see [170] for definitions) which are properties of materials that define their behavior deep into the nonlinear response regime. These parameters are not easily derived from a microscopic theory but from the EFT methods we can better understand these elastic phenomena.

In order to determine what potential characterizes the material that we want to study we should look at the shape of the stress-strain function, taking into account that

the materials that we can describe with these EFT methods are restricted to materials without dissipative or plastic effects[3] such as the so-called Cauchy hyperelastic solids [169]. Ideally one could construct the potential describing a solid just from the shape of the stress-strain function.

Another property that is inherent to real world solids is the fact that they can get deformed up to a point of fracture or elastic failure of the material. One should then wonder how is this breaking apparent in the EFT of the solid. Maybe the potential becomes singular for some finite deformation? Or does the breaking show up in the EFT as some dynamical process (e.g., an instability) that can be found in a regular potential? As we shall see the latter possibility arises, allowing us to extract information between the parameters of the potential that control the large deformation regime and the point of fracture of this solid.

What we are going to do is analyze the stability properties of the strained configuration, similar to what we did in (4.10) but this time allowing the strain to be finite. Thus we would set our scalar fields to be

$$\Phi^I = \Phi^I_{\rm str} + \pi^I \tag{4.15}$$

and expand the action for small perturbations π^I, where $\Phi^I_{\rm str}$ is defined at (3.12). What we find is that the speeds of the phonon modes, c_L and c_T, depend on the deformation of the solid. This dependence is long known and it is the so-called acoustoelastic effect (see [1, 99, 116, 157, 205, 209]). From the relation between these speeds and the deformation of the solid we can find that eventually the action undergoes some kind of instability. When increasing the deformation we usually find that the speeds either become imaginary or greater than the speed of light. The value of $\epsilon_{\rm max}$ shall be understood as an upper bound on the maximal strain that the material can support, since other effects not included here can enter before, thus lowering the actual maximum deformation. For instance, typically in solid materials we expect plastic/dissipative effect to enter at some point. This would only alter our results if $\epsilon_{\rm plastic} < \epsilon_{\rm max}$.

In the case where $\epsilon_{\rm max}$ is determined by gradient instability one expects that, like in any instability, it is physically resolved by a transition to another ground state, most likely described by a different EFT. The nature of this transition is hidden to the low energy EFT presented here.

Regarding superluminality, we must emphasize that in constrat to ghost and gradient instabilities the issue of superluminal propagation relates to the possibility of a Lorentz invariant UV completion, not to the stability of propagation [2]. In order to apprehend the physical picture, it is instructive to recall a classic in field theory:

[3]There have been attempts to incorporate such effects to EFT-like models as can be seen in [18, 37, 38, 68, 70, 88, 92, 96–98, 126, 127, 210, 211].

the example given by high spin fields where the problem of superluminality is known to arise [214]. As discussed in [177, 178], there are two ways to resolve the problem, which require to augment the EFT either by higher order operators or with additional light degrees of freedom. Any of the two resolutions makes it manifest that the naive EFT truncation breaks down. The possibility that higher order operators (with more derivatives) can fix the superluminality problem while keeping the rest of the elastic response properties is nontrivial and we leave it for future research. On the other hand, the possibility that one needs to supplement the benchmark model with other light degrees of freedom seems quite reasonable – after all in real world materials phonons do couple to many other modes. If this is the resolution, then the physical interpretation of the bound given by superluminality is that $\epsilon_{\max}$ can be understood as an upper limit on when these light degrees of freedom have to be taken into account.

4.2 Benchmark potentials

From symmetry conditions we cannot restrict the action of the solid much further that what we have in (3.32), so in principal any potential that we want to choose should be conceivable. However, in order to obtain results we are going to need to specify what potential, or family of potentials, do we want to study. Therefore, we will consider a particular class of materials, which are those whose stress-strain functions have a power-law scaling at large deformations

$$\sigma \sim \epsilon^{\nu} \text{ for } \epsilon \gg 1 \,, \tag{4.16}$$

where the exponent ν is what we are going to call *strain exponent*.

An example of elastic materials that display this type of stress-strain relation are elastomers which are polymers that have very weak intermolecular forces and a high failure strain (e.g. [114, 134]). The classical example of synthetic material that is made of elastomers is rubber. The shape of the stress-strain function of these types of materials is very characteristic and constraint the type of potentials that we might employ. Our goal is to test whether by imposing this constraint to our solid system we might be able to derive non-trivial results such as the possible relation between the elasticity bounds and the strain exponents.

We will restrict ourselves to two different types of potentials whose stress-strain function achieves something similar to what we have in (4.16). For simplicity we are going to consider only theories with two spatial dimensions so the potentials that we

can consider can only depend either on (X_1, X_2) or, equivalently, (X_1, Z). We are going to choose the latter variables and the two type of potentials studied are the same ones considered in [7]:

- **Monomial potentials:** These are potentials consist only of a single monomial term, i.e.
$$V(X, Z) = \rho_0 \, X^A Z^{\frac{B-A}{2}} \tag{4.17}$$
where we have $X \equiv X_1/2$ and ρ_0 is the dimensionful energy density set by the equilibrium configuration. This potential displays a stress-strain curve of the same nature of (4.16) and there are many phenomenological models [21, 84, 119, 128, 153, 167, 168, 212] that reduce to this particular kind of potentials at large deformations. Notice that there are two particular limits of this potential that must be mentioned: when $A = 0$ we are dealing with a perfect fluid [74, 163, 164], as we saw in (3.34), and for $A = B = 1$ the model reduces to two free scalar fields.

- **Non-relativistic potentials:** One caveat of the monomial potentials is that, as we will see below, for generic values of A and B the speeds of the phonon modes are of order of the speed of light. However, the typical speed of phonons is, at most, of order 10^{-4} the speed of light (e.g. see [63]). The potential that we call *non-relativistic* is of the form of
$$V(X, Z) = \rho_0 \left(\sqrt{Z} + v^2 \, X^A \, Z^{\frac{B-A}{2}} \right) \tag{4.18}$$
where $v^2 \ll 1$ in order to obtain a small phonon speed. This potential ensures that the stress-strain curve is still of the form (4.16) while keeping a small phonon speed, due to the term $\sqrt{Z}$ does not contribute to the spatial components of the stress tensor T_{ij}.

4.2.1 Monomial potential

The first physical properties that we can compute now that we have chosen the form of the potential are the elastic moduli, which have been found in (4.5) and (4.9), where we need to take into account that now the potential is not a function of $x_1 = X_1/\sqrt{Z}$ but X, which brings us to
$$\mathcal{G} = V_X = \rho_0 \, A \,, \tag{4.19}$$

$$\mathcal{K} = 2 \, Z \, V_Z + 4 Z^2 V_{ZZ} + 4 X \, Z \, V_{XZ} + X^2 \, V_{XX} = \rho_0 \, B \, (B - 1) \,, \tag{4.20}$$

where we have evaluated these quantities in the equilibrium configuration, i.e. at $X = 1$ and $Z = 1$. We can observe that, indeed, for $A = 0$ the shear modulus is zero, which is consistent with the interpretation of $V(Z)$ being the potential of a fluid system rather than a solid one.

Another elastic parameter that allows us to determine what kind of material we are dealing with is the so-called Poisson's ratio, that we defined in (3.11), which in $d = 2$ (spatial dimensions) takes the simple form of

$$\mathcal{R} = \frac{\mathcal{K} - \mathcal{G}}{\mathcal{K} + \mathcal{G}} = \frac{B(B-1) - A}{B(B-1) + A}\,. \tag{4.21}$$

From this expression we can see that for large values of B the system resembles to that of a perfect incompressible elastic material. However, when A is larger than $B\,(B-1)$ then the Poisson's ratio $\mathcal{R}$ becomes negative, which is typical of exotic systems ("auxetic") as we have commented in Section 3.1. In Figure 4.1 we can see that in general the allowed values in this model are around $-0.5 < \mathcal{R} < 0.5$, which is a common Poisson's ratio in steels and rigid polymers.

The monomial potential has only three free parameters that we can vary: A, B and ρ_0. However, due to this potential is a monomial the parameter ρ_0 is only useful to specify the dimensions, so it will only act as a re-scaling parameter. Therefore, we want to know what constraints the values of A and B, which will come from demanding some consistency and stability conditions: (i) no negative kinetic energy (i.e. no ghosts) (ii) no imaginary sound speed (i.e. gradient instability) and (iii) no superluminal propagation (i.e. modes that propagate faster than light).

Let us then evaluate the speeds and the kinetic term coefficient (see (4.12)-(4.14)) for the monomial potential, which take this simple form

$$N = \frac{B}{2}\,V(X,Z), \tag{4.22}$$

$$c_T^2 = \frac{A}{B}, \tag{4.23}$$

$$c_L^2 = \frac{A}{B} + B - 1\,. \tag{4.24}$$

With these expressions we can impose stability and consistency conditions to our theory

(i) *No ghosts:* This condition requires the sign of the kinetic term (4.22) to be positive. Thus, demanding $N > 0$ gives us the condition of no ghosts, which is fulfilled whenever $B > 0$.

(ii) and (iii) *No gradient instability and subluminality:* For these two conditions we must take a look at the speeds of the phonon modes. These two speeds are given by $c_T^2 = \frac{A}{B}$ and $c_L^2 = B-1+\frac{A}{B}$. The gradient condition requires these speeds to obey $c_{T,L}^2 \geq 0$, thus this leads us to $A \geq 0$ and $B - 1 \geq -\frac{A}{B}$. On the other hand the condition that requires no superluminal modes leads us to $A \leq B$ and $A \geq B(B-2)$.

(*) There is an extra condition that we will impose which is not strictly necessary for the stability of the model, which is the positivity of both elastic moduli. The positivity of the bulk modulus requires that $B \geq 1$ while the shear modulus needs $A \geq 0$ (which is already fulfilled if there are no gradient instabilities). Notice that there is a region where we could have negative bulk modulus while being perfectly consistent from the EFT perspective: as long as $\mathcal{K} > -\mathcal{G}$ we will have $c_L^2 > 0$. The negativity of the bulk modulus has been studied in four dimensional models [137,216] and observed experimentally [154], however we will be conservative here and require $\mathcal{K}$ to be positive.

In summary we find that the parameters A and B are only allowed in the region

$$0 \leq A \leq 1 \ , \ 1 \leq B \leq 1 + \sqrt{1-A} \, . \tag{4.25}$$

as can be seen in Fig. 4.1.

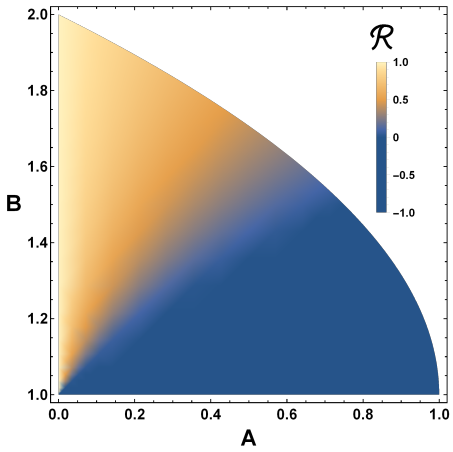

Figure 4.1: Poisson's ratio $\mathcal{R}$ values within the allowed parameter region. The values range between $\mathcal{R} = -1$ (at $B = 1$) and $\mathcal{R} = 1$ (at $A = 0$).

We can go beyond the linear limit and explore what happens for large deformations. In order to do so we can use the configuration presented in (3.12) for a system under

strain, which we repeat here for clearness

$$\Phi^I_{\rm str} = O^I_J\, x^J \ , \ O^I_J = \alpha \begin{pmatrix} \sqrt{1+\frac{\epsilon^2}{4}} & \frac{\epsilon}{2} \\ \frac{\epsilon}{2} & \sqrt{1+\frac{\epsilon^2}{4}} \end{pmatrix} \tag{4.26}$$

When the shear deformation is large enough the quadratic action (4.10) gets more cumbersome as interaction terms such as $N_{T,L}\dot{\pi}_L\,\dot{\pi}_T$ and $\lambda_{T,L}\partial_i\pi_T\partial_i\pi_L$ will appear, so we will not show the full expression here (see [7] for the full expressions). Nonetheless we are able to find something remarkable, which is that for some finite value of ϵ we eventually will encounter either a gradient instability or a superluminal mode, giving us an upper bound to the maximum deformation the system can sustain, i.e. an $\epsilon_{\rm max}$. This is indeed what we see in Fig. 4.2, where we observe the upper bounds to the maximum shear deformation as a function of the parameters A and B. Notice that we are not considering a maximum bulk deformation κ, just the shear one. This is because the potential is a monomial and performing a bulk deformation can be interpreted just as a re-scaling of the potential, i.e. if we take the configuration to change as $\Phi^i = x^i \to \Phi^i = \alpha\, x^i$ then the potential just changes as $V(X,Z) \to \alpha^{2B}\, V(X,Z)$.

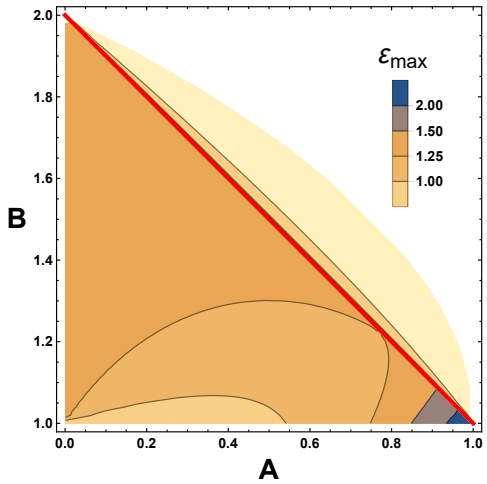

Figure 4.2: Maximum shear deformation within the allowed parameter region. The red line separates the regions where $\epsilon_{\rm max}$ (maximum shear deformation) is determined by gradient instability (below the red line) and by subluminality condition (above the red line).

Let us explore now the full non-linear response in both the bulk and shear channels. We are going to study the shear response through the off-diagonal term of the stress-

energy tensor, T_{ij}, which we have computed in (4.4). In the case of our potential this reduces to

$$\sigma_S(\epsilon) \equiv T_{ij} = \epsilon \sqrt{1+\frac{\epsilon^2}{4}}\, V_X\left(1+\frac{\epsilon^2}{2}, 1\right) \tag{4.27}$$

$$= \rho_0\, A\, \epsilon \sqrt{1+\frac{\epsilon^2}{4}} \left(1+\frac{\epsilon^2}{2}\right)^{A-1} . \tag{4.28}$$

From here it is trivial to realize that for small deformations the shear response starts

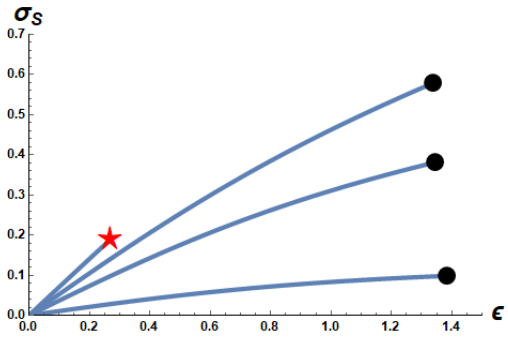

Figure 4.3: Stress-strain curve $\sigma_S(\epsilon)$ for the benchmark model (4.17) for $B = 1.6$ and $A = 0.05, 0.2, 0.35, 0.5, 0.61$ (from bottom to top). The black dots represent the 'breaking' points of the material arising due to the onset of gradient instability. The red star indicates the onset of superluminality. A and B are related to the non-linear scalings as $(\nu_S, \nu_B) = (2\,A, 2\,B)$.

linear with ϵ. However, at large deformations the stress scales as

$$\sigma_S \sim A\, \epsilon^{2A} \tag{4.29}$$

so the shear exponent is $\nu_S = 2\,A$. The curves of the stress-strain relation that this potential can mimic includes a large diversity of materials such as fibers, glasses or elastomers [119]. The shear response that we have in (4.27) describes Neo-Hookean systems that follow Hooke's law at small strain (that is, it starts linearly) but at large deformations it exhibits a power-law scaling [170].

The allowed range of values of this shear exponent is bounded to be $0 \leq \nu_S \leq 2$ as can be seen in Fig. 4.2. Moreover, notice that the closer we are to the point $(A, B) = (1, 1)$ the larger is the deformation that can be performed on the system before it breaks down.

Demanding that there are no gradient instabilities we can actually find the analytic solution for $\epsilon_{\max}$, which has a different expression depending on what region of A and B we are considering. In particular we find that for a region that includes the limit $A = 0$ the expression is rather simple and it is given by

$$\varepsilon_{max} = \sqrt{2}\left(\frac{(B-1)\,B}{A\,(1-A)-B\,(1-B)}\right)^{1/4} = \sqrt{2}\left(\frac{(\nu_B-2)\,\nu_B}{\nu_S\,(2-\nu_S)-\nu_B\,(2-\nu_B)}\right)^{1/4} \tag{4.30}$$

where this expression only applies to certain values of A and B (see Figure 4.4). Surprisingly we find that in the fluid limit (in the limit in which the shear exponent goes to zero, $\nu_S = 2\,A = 0$) the maximum shear deformation has a universal value

$$\epsilon_{max} = \sqrt{2} \quad \text{for} \quad A \to 0 \;(\nu_S \to 0)\,. \tag{4.31}$$

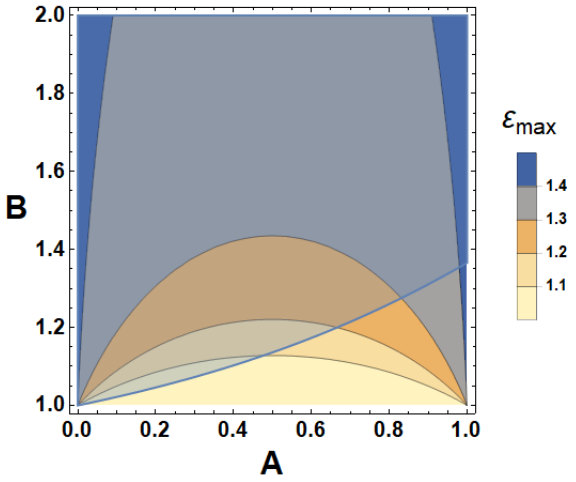

Figure 4.4: Analytic solution for ε_{max} without imposing subluminality constraints. The simple expression (4.30) applies in the shaded area above the blue line.

The expression outside the blue area from Figure 4.4 is too large to be expressed here, but it allows us to find that close to the point $(A, B) = (1, 1)$ the maximum shear deformation grows as

$$\epsilon_{max} \simeq \left(\frac{2}{1-A}\right)^{1/4} = \left(\frac{4}{2-\nu_S}\right)^{1/4} \quad \text{for} \quad A \lesssim 1\,. \tag{4.32}$$

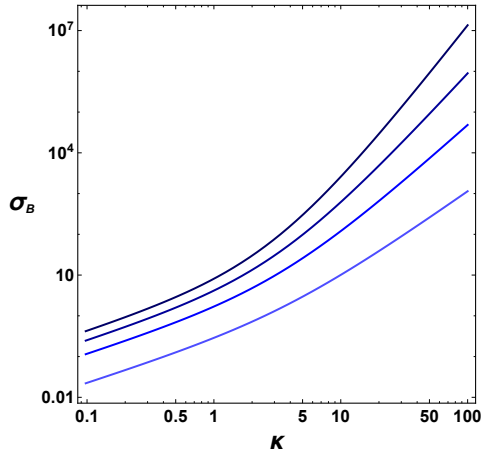

Figure 4.5: Bulk stress σ_B at large deformation for the monomial potential for $A = 1$ and $B = 1.1, 1.4, 1.7, 2.0$. The large deformation regime is determined by a power-law scaling $\nu_B = 2\,B$.

We may also explore the non-linear response due to a pure bulk deformation κ, which in this case we will read from the diagonal part of the stress-energy tensor. From the definition (3.5) we obtain

$$\sigma_B(\kappa) = \rho_0\,(B-1)\,\left[\left(1+\frac{\kappa}{2}\right)^{2B} - 1\right]\,. \tag{4.33}$$

Again we see that for small deformations (i.e. $\kappa \ll 1$) we obtain a linear dependence on the strain. On the contrary, when this bulk deformation is large the stress-strain dependence is a power-law dependence, just like in the case of the shear deformations. In particular we find that at large strain

$$\sigma_B \sim (B-1)\,\kappa^{2B}\,. \tag{4.34}$$

Notice that this scaling appears for compression processes, i.e. for positive bulk strains $\kappa > 0$, but not for expansion processes, i.e. negative bulk strains $\kappa < 0$. As we have mentioned, there is no limit in the bulk strain from consistency and stability conditions as it happens for the shear strain.

4.2.2 Non-relativistic potential

The monomial potential has an important downside if we want it to be a model for realistic solids, which is related to the speeds of the phonons. These speeds have been

computed in (4.23) and (4.24) but let us write them down here making explicit the dependence of this speed with the speed of light c, which we have set to $c = 1$ in most part of the text:

$$c_L^2 = \left(B - 1 + \frac{A}{B} \right) c^2 \,, \tag{4.35}$$

$$c_T^2 = \frac{A}{B} c^2 \,. \tag{4.36}$$

From these expressions we can readily notice that for generic values of A and B the speeds are of order of the speed of light. The only region that is safe from this issue is around $(A, B) \to (0, 1)$, which substantially restricts the values of the power-law scaling ν_B and ν_S due to realistic values of the speeds should be bounded by above as $c_{L,T}^2 \lesssim 10^{-8}\, c^2$ (needless to say, this concern does not affect relativistic solids such as neutron star interiors [35]), thus we would conclude that materials are restricted to have scaling of order $\nu_S \sim 10^{-8}$ for the shear deformations and $\nu_B \sim 2$ for bulk deformations. This does not seem to represent what we find in solids generically so we expect that the monomial potential is a very restricted one.

The first proposal that deviates from the monomial potential is the one introduced in (4.18). This potential has the nice property that speeds become much smaller than (4.23),(4.24) while keeping the stress-strain function unaffected.

What we do is we add a new term to the monomial potential which is $\delta V \propto \sqrt{Z}$ with a coefficient in front much larger than the one in front of the monomial. This potential has some very interesting properties that must be commented. First of all, the extra term can be understood as the mass density of the material [139]. This fact may explain why the coefficient in front of $\sqrt{Z}$ is much larger than the one in front of the monomial: the mass density contributes to the Lagrangian weighted by a c^2 factor and in principle it should be much larger than the typical stresses in solids.

Moreover, we can check in (4.4) and (4.8) that the extra term contributes neither to the shear response T_{ij} nor the bulk response T_{ii} so the stress-strain function is not altered at all. The only component where we will notice this term is in the energy density T_{00}. This is not surprising as this term contributes as some inertial mass and thus acts as a pressureless fluid (or "dust" in the cosmologist lingo).

Therefore we consider this potential to be a good candidate to mimic the response of a solid while still retaining some predictive and constricting power of the EFT while just including a new parameter to vary, i.e. v^2. At zero strain we find that the speed of propagation of the phonon modes are

$$c_L^2 = \frac{v^2 \, (A + B(B-1))}{1 + B\, v^2} \,, \tag{4.37}$$

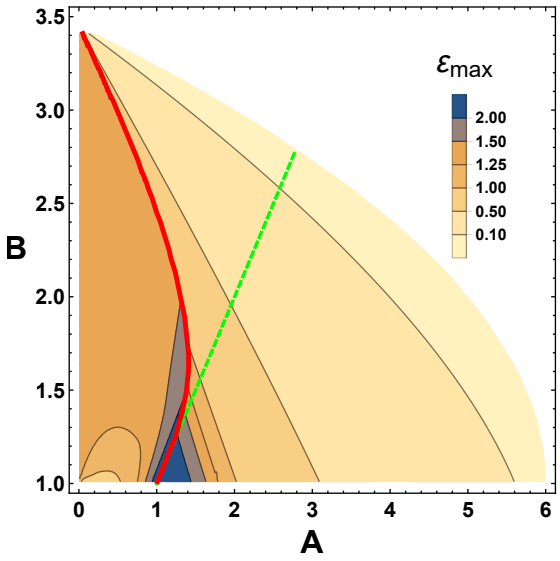

Figure 4.6: Allowed parameter region for the non-relativistic potential with $v^2 = 0.2$. Below the red line the maximum shear stress is restricted by gradient instabilities while above this line is constrained by subluminal conditions. The green dashed line shows $A = B$. Above this line the maximum shear stress is always determined by subluminality. A and B are related to the non-linear scalings as $(\nu_S, \nu_B) = (2\,A, 2\,B)$.

$$c_T^2 = \frac{v^2\,A}{1 + B\,v^2}\,. \tag{4.38}$$

Demanding that there are no gradient instabilities nor superluminal modes we find that the parameter region allowed for A, B and v^2 is given by

$$v^2\,(A + B(B-2)) < 1 \tag{4.39}$$

with $A > 0$ and $B > 1$. This region can be seen in Fig. 4.6 for a potential with $v^2 = 0.2$, where we can already see a significant difference with the monomial potential. This region is pushed away to maximum values of the parameters A and B of the order of $A \sim \sqrt{B} \sim v^2$, allowing materials to acquire very large exponents $\nu_S = 2A$ and $\nu_B = 2B$. In Fig. 4.7 this limit is way out of the scope of the graphic due to the smallness of v^2.

In Fig. 4.6 we can notice that for $A > B$ the maximum shear strain is always determined by subluminality conditions while for $A < B$ there are two separate regions

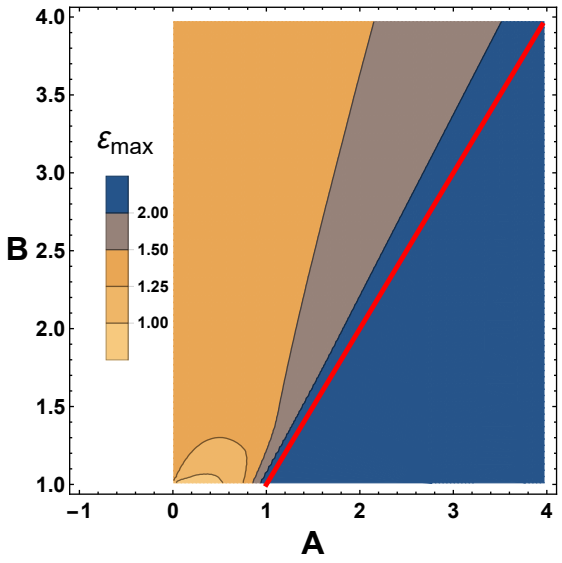

Figure 4.7: Allowed parameter region for the non-relativistic potential with $v^2 = 10^{-8}$. The limits on A and B are pushed away to maximum values of the order of $B \sim 10^4$ and $A \sim 10^8$. A and B are related to the non-linear scalings as $(\nu_S, \nu_B) = (2\,A, 2\,B)$.

governed by gradient instability and subluminality respectively. The most remarkable result about the maximum shear deformation is that we only find sectors with very large deformations close to the line $A = B$: a narrow line for $A < B$ (whose thickness is independent of the v^2 parameter, as it does not affect the gradient instability condition) and a larger region for $A > B$ which is larger the smaller the value of v^2 is. Thus, generically very elastic materials should display similar exponents both in the shear and bulk deformations, i.e. $\nu_S \simeq \nu_B$. Such maximum deformation is given by

$$\epsilon_{\max} \sim \left(\frac{2\,A}{B-A}\right)^{1/4} = \left(\frac{2\,\nu_S}{\nu_B - \nu_S}\right)^{1/4} \quad \text{for } \nu_S \lesssim \nu_B\,. \tag{4.40}$$

In equations (4.37) and (4.38) we see that phonon speeds are of order v^2 when the strain deformations are infinitesimal. In this way it makes sense to call the potential defined in (4.18) as "non-relativistic" whenever we are in the limit $v^2 \ll 1$. However the speeds of these phonon modes change substantially when we increase the strain ϵ and they might not be small for finite values of the deformation. In particular we can see in Figure 4.6 that there is a smooth transition between regions where ϵ_{max} is determined by gradient instability and regions where is determined by subluminality conditions. This must mean that while one of the velocities, let us call it c_-, decreases

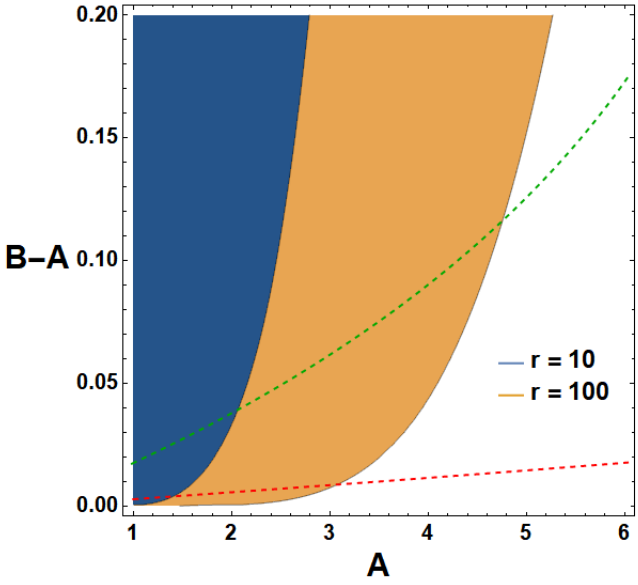

Figure 4.8: Speed ratio constraints for $r = 10, 10^2$. Dashed lines show where $\epsilon_{max} = 3, 5$ (Green, Red).

to small values (until reaching a gradient instability $c_-^2(\epsilon_{max}) = 0$) the other speed, c_+, is actually growing. Thus, we need to look at the value of the speed that is growing when we encounter this gradient instability so we can be sure that the speed can still be considered to be small, i.e. we want to know how big is $c_+^2(\epsilon_{max})$.

For this purpose let us define a parameter that will control how c_+ grows from $\epsilon = 0$ to ϵ_{max}, which is

$$r \equiv \frac{c_+(\epsilon_{max})}{c_+(\epsilon = 0)} \,. \tag{4.41}$$

Let us demand this ratio to be small, of order $r \sim 10 - 10^2$, in order to be considered realistic. This ratio only makes sense in $A < B$, as in $A > B$ the maximum deformation is not determined by gradient instabilities but from subluminal conditions.

We determine this ratio in the limit $v^2 \ll 1$ which close to the region $A = B$ scales as

$$r \sim (B - A)^{-A/4} \,. \tag{4.42}$$

This ratio r is shown as a function of A and $B - A$ in Figure 4.8. In this figure we can see a finite region of values A and B that overlaps with a region with large values of ϵ_{max}, which then can be considered to be a region that could define realistic hyperelastic materials.

Finally, we should note that because this potential is not a monomial, here the bulk strain does have a limit which can also be found by demanding consistency and stability conditions at finite κ. However, to keep the discussion simpler, we have only considered the maximum shear strain, ϵ_{max}.

4.3 Three-phonon interaction terms

To further illustrate the predictive power of the low energy methods, we show here another nontrivial powerful statement that follows from the EFT construction which, as explained above, applies when translations (and possibly scale invariance) are broken spontaneously.

The nontrivial statement contained in the EFTs (3.37) is simply that once the stress-strain relations are known then the full Lagrangian is fixed. Let us illustrate now how this impacts for instance in the determination of the cubic phonon interactions. Assuming that the stress-strain relations both for bulk and shear deformations are known, then one can reconstruct the full form of the function $V(X, Z)$, up to an irrelevant additive constant.

Then, the cubic phonon interactions (around the homogeneous, isotropic equilibrium configuration $\Phi^I = x^I$) are obtained by expanding our Lagrangian around the background solution, i.e. $\Phi^I = x^I + \pi^I$. At third order in π^I we obtain

$$\begin{aligned} V(X,Z) \Rightarrow\, & \mathcal{C}_1 \left(\partial_i \pi_L^i\right)^3 + \mathcal{C}_2 \left(\partial_i \pi_L^i\right) \left(\dot{\pi}_j\right)^2 + \mathcal{C}_3 \left(\partial_i \pi_L^i\right) \left(\partial_j \pi_k\right)^2 \\ & + \mathcal{C}_4 \, \dot{\pi}^i \, \dot{\pi}^j \, \partial_i \pi_j + \mathcal{C}_5 \left(\partial_i \pi_L^i\right) \left(\partial_j \pi_k\right) \left(\partial_k \pi_j\right) , \end{aligned} \tag{4.43}$$

where $\pi^I = \pi_L^I + \pi_T^I$. The terms we find are

$$\mathcal{C}_1 = \frac{1}{6} \left(8\, V_{ZZZ} + 12\, V_{XZZ} + 6\, V_{XXZ} + V_{XXX}\right) + 4\, V_{ZZ} + 2\, V_{XZ} + V_Z \,, \tag{4.44}$$

$$\mathcal{C}_2 = -2\, V_{ZZ} - \frac{1}{2}\, V_{XX} - 4\, V_Z - 2\, V_{XZ} \,, \tag{4.45}$$

$$\mathcal{C}_3 = \frac{1}{2}\, V_{XX} + \, V_{XZ} \,, \tag{4.46}$$

$$\mathcal{C}_4 = 2\, V_Z \,, \tag{4.47}$$

$$\mathcal{C}_5 = -2\, V_{ZZ} - V_Z - V_{XZ} \,. \tag{4.48}$$

In these expressions, the X, Z- derivatives of V are evaluated on the undeformed configuration. Moreover, by obtaining the relation between $V(X, Z)$ and the stress-strain curve (such as *e.g.* Eq. (4.27)) one can relate all these $V(X, Z)$ derivatives

to derivatives of the stress strain curve at the origin, $\sigma_S'(0)$, $\sigma_S''(0)$, etc, which are measurable quantities. For instance, the bulk modulus is $\mathcal{K} = 4V_{ZZ}+2V_Z+4V_{XZ}+V_{XX}$, $\mathcal{G} = V_X$ and $\epsilon + p = V_X + 2V_Z$.

This illustrates that the realization of symmetries implies nontrivial relations between distinct low energy observables. In this example, the strength of the phonon cubic interactions are determined by the shape of the stress-strain curves.

We can write the 5 $\mathcal{C}$'s as a function of these quantities and we would just need two independent new parameters

$$\mathcal{C}_1 = \frac{\mathcal{K}}{2} + \mathcal{N}\,, \tag{4.49}$$

$$\mathcal{C}_2 = \frac{1}{2}\left(3\,\mathcal{G} - \mathcal{K} - 3\,(\epsilon + p)\right)\,, \tag{4.50}$$

$$\mathcal{C}_3 = \frac{1}{4}\left(\mathcal{G} + \mathcal{K} - (\epsilon + p)\right) + \mathcal{M}\,, \tag{4.51}$$

$$\mathcal{C}_4 = \epsilon + p - \mathcal{G}\,, \tag{4.52}$$

$$\mathcal{C}_5 = \frac{1}{4}\left(\mathcal{G} - \mathcal{K} - (\epsilon + p)\right) + \mathcal{M}\,. \tag{4.53}$$

where the independent new parameters are

$$\mathcal{N} = \frac{1}{6}\left(8\,V_{ZZZ} + 12\,V_{XZZ} + 6\,V_{XXZ} + V_{XXX}\right) - 2\,V_{ZZ} - \frac{1}{2}\,V_{XX}\,, \tag{4.54}$$

$$\mathcal{M} = \frac{1}{4}\,V_{XX} - V_{ZZ}\,. \tag{4.55}$$

We can compare our results with Ref. [139]. There he concludes that there are 3 independent new parameters, but we think the difference comes from the fact that he is working in 3 space-dimensions instead of 2. Moreover, in Ref. [139] there are 6 independent operators in the cubic expansion. It is trivial to check that in two dimensions the extra operator can be expressed as a function of the others

$$(\partial_i\pi_j)\,(\partial_i\pi_k)\,(\partial_j\pi_k) = (\partial_i\pi^i)\,(\partial_j\pi_k)^2 + \frac{(\partial_i\pi^i)}{2}\,\left((\partial_j\pi_k)(\partial_k\pi_j) - (\partial_i\pi^i)^2\right)\,. \tag{4.56}$$

In the case of scale invariance these terms simplify considerably. Allow us to foresee the form of the potential in the case of a solid action with a spontaneously broken SI, which will be presented in (5.4). The potential will have the next form $V_{SBSI}(X, Z) = Z^{\frac{1}{2}+\omega}\, f\left(\frac{X}{\sqrt{Z}}\right)$, therefore we can express the parameters $\mathcal{C}_i$ as

$$\mathcal{C}_1 = \frac{\omega}{3}\left((2+6\,\omega+4\,\omega^2)f(1)-3f'(1)\right)\,, \tag{4.57}$$

$$\mathcal{C}_2 = \frac{1}{2}\left(-(3+8\,\omega+4\,\omega^2)\,f(1)+3\,f'(1)\right)\,, \tag{4.58}$$

$$\mathcal{C}_3 = \omega\,f'(1)\,, \tag{4.59}$$

$$\mathcal{C}_4 = (1+2\omega)\,f(1)-f'(1)\,, \tag{4.60}$$

$$\mathcal{C}_5 = \omega\,(f'(1)-(1+2\,\omega)\,f(1))\,. \tag{4.61}$$

This implies that for a scale invariant potential there are no free parameters: we can identify $f(1)$, $f'(1)$ and ω with $\mathcal{K}$, $\mathcal{G}$ and $\epsilon+p$

$$\mathcal{G} = f'(1)\,, \tag{4.62}$$

$$\mathcal{K} = 2\,\omega\,(1+2\,\omega)\,f(1)\,, \tag{4.63}$$

$$\epsilon+p = (1+2\,\omega)\,f(1)\,. \tag{4.64}$$

Therefore cubic interactions are all fixed by these background or linear elasticity quantities. This is true both for general SI as well as conformal solid limit (which, as we shall see, is just a particular value of ω).

Chapter 5

Scale invariant solids

In Chapter 4 we described how the elastic response of a solid can be described through EFT methods. In this chapter, however, we will go beyond these methods in order to describe certain types of solid systems, which we will name as scale invariant solids. This type of solid exhibits scale invariance (SI) in addition to the broken symmetries of a regular solid system. The question of whether we can describe the behaviour of these solids is interesting per se, but this SI solids seem to be quite close to real world materials that exhibit criticality in the form of a quantum critical point (see Section 3.3). As we will see, in order to deal with these kind of materials we will employ both the solid EFT methods and the AdS/CFT correspondence.

When we cope with a scale invariant system we may consider two possible ways in which SI can be realized generically. The main division that we can think of between different SI solids is whether their low energy dynamics are controlled by a nontrivial infrared fixed point (IRFP). In such a case, at low energies we would have an unbroken symmetry of SI due to this IRFP. However, in the absence of this fixed point, the SI can only be a spontaneously broken symmetry which is non-linearly realized, as we discussed in Section 3.2.1.

Following this logic we assume that generically there are two possible cases of SI solids, which are:

- **Solids with spontaneously broken SI:** In this kind of SI solids we expect to have a gapped spectrum, thus at low energies phonons can be considerate as isolated degrees of freedom. Due to existence of this energy gap EFT methods should be applicable in order to describe the lightest excitations in the mechanical sector as the Goldstone bosons of the spontaneously broken spacetime symmetries. The methods necessary for this are summarized in Chapter 4 but in Section 5.1 we will expand on aspects related to this SI behavior.

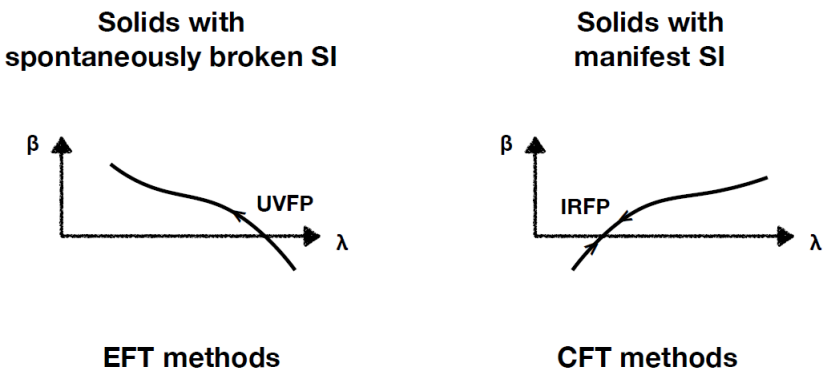

Figure 5.1: Generically we can divide scale invariant (SI) solids in two separate groups using the beta function $\beta = \mu\, d\lambda/d\mu$ where λ is some coupling of the theory. We indicate the direction of the flow towards low energies with an arrow.

- **Solids with manifest SI:** Here we will assume that there is a dynamical IRFP. Contrary to the spontaneously broken case, here the spectrum is a continuum rather than being gapped. Thus phonons cannot be treated as isolated degrees of freedom and we expect that the dispersion relation of these phonons develop an imaginary part. To cope with this type of solid we employ bottom-up AdS/CFT methods, which are helpful to construct models with these kind of properties. This will be fully developed in Section 5.2.

Due to we are talking about fixed points it comes very handy using renormalization group (RG) terminology. One of the most important parameters in RG is so-called beta function, which we already introduced in (2.2), which is

$$\beta_g(\mu) = \frac{\partial}{\partial \log \mu} g(\mu)\,, \tag{5.1}$$

where μ is the energy scale and g is some coupling of the theory.

The two different cases of solids that realize SI can be identified depending on how this function behaves as a function of the coupling. On the one hand the spontaneously broken SI case can be understood as an RG flow from some UV fixed point caused by the vacuum expectation value of some operator that breaks the SI symmetry. This case is depicted in the left part of Fig. 5.1. On the other hand we have the case of the solids with manifest SI, which can be linked to the presence of an IR fixed point. This case is depicted in the right part of Fig. 5.1.

One could propose a third option to the list, which would be a combination of both cases, that is, a combination of both IR and UV fixed points. In this case we would have some UV fixed point where the SI is spontaneously break but when going towards a low energy regime we would encounter another fixed point, i.e. an IR fixed point which would realize some emergent SI. Thus, we would have a combination of spontaneous breaking and a manifest realization of SI. There are different examples that realize this possibility in various ways including both Lorentz invariant and non-invariant theories which are easily constructed through bottom-up holographic models.

In the case of Lorentz invariant theories we find both spontaneously broken SI, such as in [45, 150], and a mixing of spontaneous breaking and emergent SI, like in [31, 113]. These examples of Lorentz invariant theories have a particular feature that non-Lorentz invariant theories lack, which is the appearance of a massless dilaton. The appearance of this massless dilaton requires some fine-tuning of the theory, but assuming this tuning it can be found that the dilaton pole must show up.

However, in condensed matter set-ups we do not consider theories that respect Lorentz invariance, as symmetries such as Lorentz boosts are broken, and therefore, in such scenarios, the dilaton will not appear even if SI is broken spontaneously [79, 141]. These theories realize conformal symmetry nonlinearly without this dilaton, as the phonon fields π^I will play the role of Goldstone bosons for various broken symmetries[1] [164]. As far as we know, the only previous example of a SI solid effective theory is presented in [79], but this model has a crucial problem which is that the speeds of phonons are necessarily relativistic. If we are trying to study a real world material we need to solve such issue.

The cases we study in this text are of the second nature: we will consider realizations of SI in solid materials, which break Lorentz invariance, at low energies, with either a SI spontaneously broken or as an emergent symmetry.

5.1 Solids with spontaneously broken scale invariance

This type of solids can be implemented with the solid EFT described in Chapter 4 without much effort. We will demand that the solid EFT Lagrangian respects scale invariant transformations, which will not be respected by the ground state of the theory. In this model we can differentiate between two objects that will play the role of coordinates in scale transformations: the ("external") spatial coordinates x^μ and the

[1] Generally when we are spontaneously breaking space-time symmetries there will be fewer Goldstone modes than broken symmetries [141].

internal space coordinates (the solid element positions) Φ^I. Scale transformations act on coordinates as a rescaling and in this scenario we will consider the possibility that the scale transformations act differently depending on the coordinate itself, meaning that the way external and internal coordinates transform might be distinct. Specifically let us define the scale transformation as

$$x^\mu \to \lambda^{-1}\, x^\mu\,, \tag{5.2}$$

$$\Phi^I \to \lambda^{\Delta}\, \Phi^I \tag{5.3}$$

where Δ is some weight of the scale transformation on the internal coordinates Φ^I.

The solid EFT that we considered in Chapter 4 demanded that the Lagrangian describing the solid must be constructed out of the matrix B^{IJ} which for a d dimensional space-time can form $d-1$ independent terms as we see in equation (3.37). Imposing that the Lagrangian must be invariant under the scale transformations (5.2) and (5.3) we find that the potential has to be of the next form[2]

$$V_{SBSI} = Z^{\frac{1+\omega}{2}}\, F(x_1, \ldots, x_n) \quad , \quad n = d-2 \tag{5.4}$$

where ω is some constant value that will depend on the weight Δ and $x_n \equiv X_n/Z^{n/(d-1)}$, which was already introduced in (4.2) to simplify the expressions. The virtue of the terms x_n is that they are already manifestly SI for any value of Δ, so we will only need to play with ω and Δ to define a potential that respects SI. Moreover, the function $F(x_n)$ is an arbitrary function (up to consistency and stability conditions that we will apply afterwards).

In order to have a SI potential we need to fulfill a specific relation between ω and Δ. Demanding SI uniquely fixes ω as a function of Δ by the relation $(1+\omega)\,(d-1)\,(1+\Delta) = d$, which can be expressed in two ways, depending on what we want,

$$\omega = \frac{1-(d-1)\,\Delta}{(d-1)\,(\Delta+1)} \quad \text{or} \quad \Delta = \frac{1-(d-1)\,\omega}{(d-1)\,(\omega+1)}\,. \tag{5.5}$$

The relation between the two terms is displayed in Figure 5.2 for the case of $d = 4$.

The ω parameter has a physical meaning that can be readily found by computing the ratio between the pressure p and the energy density ρ

$$\frac{p}{\rho} = \frac{-V + 2\,Z\,V_Z}{V} = \omega\,. \tag{5.6}$$

[2]As we shall see below, this theory represents a new example of SI theory that does not realize conformal invariance, other examples of these type of theories can be found in [159].

Therefore ω plays the role of the equation of state of the system. Note that this relation is true for arbitrary values of the pressure and the energy density and even out of the equilibrium configuration of the scalar, thus the relation between p and ρ will always be a linear relation

$$p(\rho) = \omega\,\rho\,. \tag{5.7}$$

Let us now apply consistency conditions to this equation of state parameter, such as the Null Energy Condition (NEC), which demands that we must have $\omega > -1$, as a condition to be free of any ghost instability. This can be easily confirmed checking equation (4.12).

Interestingly, the equation of state can be used to relate the speeds of the phonon modes (4.13) and (4.14) as

$$c_L^2 = \omega + 2\,\frac{d-2}{d-1}\,c_T^2\,. \tag{5.8}$$

From here we derive how ω and Δ are restricted by stability constraints on the phonon speeds. Demanding these constraints to the transverse sector places no constraints on ω or Δ, only that

$$0 < \mathcal{G} < \rho + p\,. \tag{5.9}$$

However, if we require that $c_L^2 > 0$ then we obtain that

$$\omega > -2\frac{d-2}{d-1}\,c_T^2 \tag{5.10}$$

which for the Δ parameter translates to an upper bound $\Delta < 1/(d-1)$.

Requiring also that this speed is not superluminal, $c_L^2 < 1$, we find that we need $\omega < 1$ (or $\Delta > -\frac{d-2}{2\,(d-1)}$). Altogether we summarize the bounds for the weight Δ as

$$-\frac{d-2}{2(d-1)} < \Delta < \frac{1}{d-1}\,. \tag{5.11}$$

Focusing now on the weight Δ we may also interpret it as a parameter that plays a similar role as the scaling dimension for the field Φ^I, just like scalar operators in a CFT (see Eq.(2.47)). However we need to be careful when we compare this theory with a CFT because is not in any way clear that (5.4) is actually defining a relativistic CFT, as we shall see.

Thus, we wonder whether we can apply standard logic and results from CFTs. The potential defined in (5.4) is formally relativistic and the fields Φ^I play the role of some scalar operator, so maybe we are actually dealing with a relativistic CFT. Nevertheless, our impression is that this it not actually true.

Firstly, this theory does not have a well defined Poincaré invariant ground state, such as $\Phi^I = 0$ (or, using the shift symmetry of the theory, $\Phi^I = \text{const.}$). Studying perturbations around this vacuum we realize that there is no analytic kinetic term for the field Φ^I (see the perturbation expansion in (4.10)). Thus, we need to demand that the ground states have some finite gradient $\partial\Phi^I$ in order to be able to quantize the theory. The ground state that we take is of the form $\Phi^I = \alpha\, x^I\, \delta^i_I$, where now due to SI the parameter α has only two possible values: either $\alpha = 1$, which breaks part of the Poincaré group but admits perturvative quantization, or $\alpha = 0$, which would be relativistic but is not well-defined. Therefore, we cannot approach the unbroken symmetry case continuously in a controllable way by varying the parameter α and we are restricted to take the non-relativistic solution.

Secondly, but related to the first point, there is an inquiring detail of the EFT that makes us realize is not a relativistic CFT. By taking this configuration for the scalar field we are in some way making the field Φ^I play the role of spatial coordinates. Thus, to some extent, for $\Delta \neq 0$ we have that time and space transform differently for scale transformations, which is in contradiction to what one would expect from a CFT.

Beyond these aspects about the non-relativistic nature of the theory we may also look at the trace of the stress-energy tensor, which is related to the equation state by

$$T^\mu_\mu = (1 - (d-1)\,\omega)\,\rho\,. \tag{5.12}$$

This trace is generically non-zero, as it must be in a CFT (see (2.37)). As we already pointed out in Section 2.2.2 it is not true that all scale invariant theories must have a traceless stress energy tensor, whereas conformal invariant theories do. In order to see this, let us consider a conformal transformation in D dimensions of the type $\delta x^\mu = v^\mu(x)$ that obeys

$$\partial_\mu v_\nu + \partial_\nu v_\mu = \frac{2}{D}\, g_{\mu\nu}\, \partial\cdot v\,. \tag{5.13}$$

This conformal symmetry leads to the current (for $D \geq 3$) [171, 173]

$$J^{(v)\,\mu} = v^\nu T^\mu_\nu + \partial\cdot v K^\mu + \partial_\nu\, \partial\cdot v L^{\mu\nu} \tag{5.14}$$

where K^μ and $L^{\mu\nu}$ are constructed of local operators. The conservation of this current is equivalent to

$$T^\mu_\mu = -\partial_\mu K^\mu \quad \text{and} \quad K^\mu = -\partial_\nu L^{\nu\mu} \tag{5.15}$$

which combined lead us to

$$T^\mu_\mu = \partial_\mu\partial_\nu L^{\mu\nu}\,. \tag{5.16}$$

The interesting point is that the stress-energy tensor is not unique, we can propose another tensor that still defines the same four-momentum and Lorentz generators. Specifically

$$T'_{\mu\nu} = T_{\mu\nu} + \partial^\sigma \partial^\rho Y_{\mu\sigma\nu\rho} \tag{5.17}$$

where $Y_{\mu\sigma\nu\rho}$ is antisymmetric on $\mu\sigma$ and on $\nu\rho$, but symmetric under the exchange of $\mu\sigma$ and $\nu\rho$. Thus, as long as our stress energy tensor trace has the form of (5.16) we can promote our stress-energy tensor to an *improved* tensor [55,62,75,124,159,173,185] of the form

$$\Theta_{\mu\nu} = T_{\mu\nu} + \tag{5.18}$$

$$\frac{1}{D-2}\left(\partial_\mu\partial_\alpha L^\alpha_\nu + \partial_\nu\partial_\alpha L^\alpha_\mu - \partial^2 L_{\mu\nu} - g_{\mu\nu}\partial_\alpha\partial_\beta L^{\alpha\beta}\right) + \tag{5.19}$$

$$\frac{1}{(D-2)(D-1)}\left(g_{\mu\nu}\partial^2 L^\alpha_\alpha - \partial_\mu\partial_\nu L^\alpha_\alpha\right) \tag{5.20}$$

which will obey $\Theta^\mu_\mu = 0$.

Let us now consider the current of the dilatation transformation, which has the form of

$$J^D_\mu = x^\rho\, T_{\mu\rho} - V_\mu\,. \tag{5.21}$$

The conservation of this current implies that the trace of the stress energy tensor must be

$$T^\mu_\mu = \partial^\mu V_\mu \tag{5.22}$$

where V_μ is known as the virial current [62] and is the same as K^μ plus some conserved current. Therefore, we may have a theory that is scale but not conformal invariant with a non-traceless stress-energy tensor if we have some current V_μ that is not conserved, $\partial_\mu V^\mu \neq 0$, and that cannot be expressed as a total derivative, like in (5.15). In scalar theories where the ground state is Poincaré invariant and are perturvative around it this cannot happen [173], as the only $D-1$ dimensional term that we can write is $\sim \partial_\mu\phi^2$, which is indeed a total derivative. However, this is not our case, just like in the potential discussed in [171], where they find that that for a particular potential $V(X) = X^n$ the virial current is

$$K^\mu = \Delta n\, X^{n-1}\,\partial^\mu\Phi^2 \tag{5.23}$$

which is not a total derivative (except for the case $n = 1$) and is only zero for $\Delta = 0$. In their case they consider a SI superfluid where the scalar field's vev is $\Psi = \alpha t$, but the solutions can be considered analogous, as the computations do not differ much.

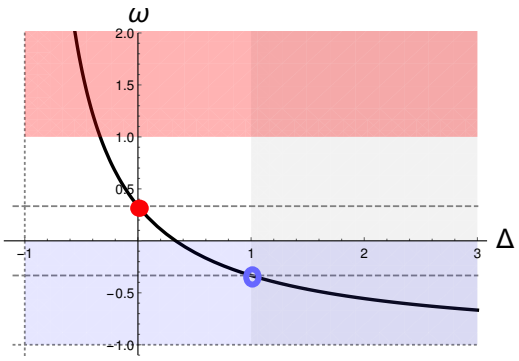

Figure 5.2: Equation of state parameter ω as a function of the weight of the scalars Δ for $d = 4$, following the relation (5.5). The gray shaded area on the right is where by the naive unitarity bound $\Delta > 1$ is fulfilled. In the red shaded area we have that the longitudinal speed c_L is superluminal and should be excluded. The red dot corresponds to the Weyl invariant case, i.e. $T^\mu_\mu = 0$, where $\Delta = 0$. The blue circle includes the free theory, where an improved stress-energy tensor that is traceless is admitted. In the blue region the theory suffers from gradient instability in the longitudinal mode if $c_T \ll 1$.

Before discussing this SI superfluid theory let us mention that the case of $\Delta = 0$ (and therefore $\omega = 1/(d-1)$) in our model is a special one indeed. We can verify that this case is invariant under conformal (or Weyl) transformations of the metric

$$g_{\mu\nu} \to \Lambda^2(x^\sigma) g_{\mu\nu} \tag{5.24}$$

where Λ is an arbitrary function. This theory is the one considered in [79], and here is just a particular case which we point with a red dot in Fig. 5.2.

Next in order we have the case of $n = 1$ in (5.23), which in our model can be generalized to $\Delta = \frac{d-2}{2}$ (and thus $\omega = -\frac{d-3}{d-1}$) with $F(x_i) = x_1$, where the theory admits an improved stress tensor that is traceless. This type of potential is basically the one of a free theory of scalar fields and is marked with a blue disk in Fig. 5.2, which is known to admit this improved stress tensor [124, 159, 185]. Indeed, in equation (5.23) we see that the current is a total derivative in the case of $n = 1$.

In Figures 5.2 and 5.3 we have another shaded region, in grey, for the cases where $\Delta > 1$. This area shows how large the scaling dimension of the scalars should be if this theory was actually a true CFT in order to obey unitarity conditions. For a general d-dimensional CFT this bound is $\Delta > (d-2)/2$. It is interesting to notice that

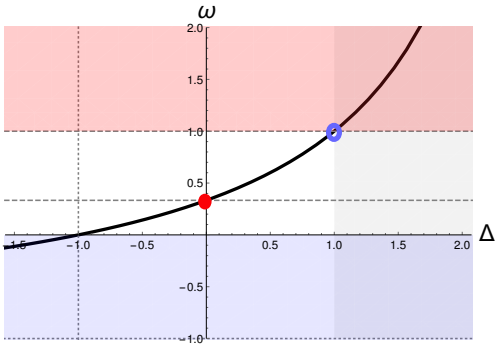

Figure 5.3: Here we show the same relation displayed in Figure 5.2 for a SI superfluid.

the range where our potential obeys the NEC and the absence of gradient instability corresponds to a considerable range in $\Delta < 1$. Moreover, not even the conformal solid case ($\Delta = 0$ or $\omega = 1/(d-1)$) is safe from this constraint. However, we must not take this condition to be strictly necessary for us due to this theory does not have full Lorentz invariance nor conformal invariance, which indicates that we should alleviate this bound.

For completeness and in order to include the case discussed in [171] let us comment that we can easily realize an "SI relativistic superfluid" by just considering a different ground state for the scalar fields. In particular we take a single scalar field with $\Psi = t + \psi$ whose most general action at leading order in derivatives is

$$S = \int d^d x P(X_\Psi) \tag{5.25}$$

where $X_\Psi \equiv \partial^\mu \Psi \partial_\mu \Psi$. Due to scaling invariance we need to restrict this potential to just power laws of X_Ψ, i.e. $P(X_\Psi) = X_\Psi^n$ and this invariance allows us to define a scaling dimension of Ψ, Δ_Ψ. The relations between the scaling dimension Δ_Ψ, ω and the power n follows a different relation to what we have for the solid case. Similarly to the solid case, the action must have a power $n = \frac{1+\omega}{2}$ and a relation between the equation of state and the scaling dimension

$$\Delta_\Psi = \frac{(d-1)\,\omega - 1}{\omega + 1}, \quad \text{or} \quad \omega = \frac{1 - (d-1)\,\Delta_\Psi}{(d-1)\,(\Delta + 1)}, \tag{5.26}$$

which we show in 5.3 for the case of $d = 4$ dimensions. In this case we also need to demand that $\Delta = 0$ in order to have Weyl/conformal-invariance, outside the naive

bound of unitarity. To end the comparison we can look at the sound speed of sound, which only consists of one speed $c_s = \omega$. Therefore, restricting the potential to one that has neither gradient instabilities nor superluminal modes we need $0 < \omega < 1$, and thus $-1 < \Delta < \frac{d-2}{2}$.

5.1.1 Benchmark potentials and non-linear elasticity

Here we will concentrate in the case of a two dimensional solid system and particularly in its non-linear elastic regime.

Firstly, the non-linear bulk scaling is determined by ω and is completely independent of the function $F(x)$. This scaling is given by

$$\nu_B = 2\,(1+\omega)\ . \tag{5.27}$$

Moreover, the bulk strain κ is unconstrained, as opposed to the shear strain ε.

The results related to the shear response are potential dependent, so we will need to specify what type of potential we want to study. In particular, we will take the two cases considered in [7], which are:

1. The first possibility we will study is the case where $F(x)$ is a monomial, *i.e.*

$$F(x) = x^{\nu_S/2} \tag{5.28}$$

   with ω as a free parameter. This simple potential realizes a power-law scaling in the stress for large deformations. This potentials will display a power-law behaviour in the stress-strain relation for the shear channel, which will be determined by ν_S, i.e. we will have that at large deformations $\sigma_S \sim \epsilon^{\nu_S}$.

2. The second possibility we are going to consider is taking both

$$F(x) = 1 + v^2 x^{\nu_S/2} \tag{5.29}$$

   and the limit $\omega \to 0$. The advantage of this potential is that the speeds of the phonon modes will be realistic (i.e. much smaller than the speed of light) as long as $v^2 \ll 1$, whereas the monomial potential has relativistic modes for generic values of ν_S and ω. The shear response will only come from the x-dependent term, so the power-scaling of the shear response will be determined by ν_S.

Looking at Fig. 5.4, we can see that the case of a monomial potential the bulk scaling is restricted to satisfy $2 < \nu_B < 4$. For a more general $F(x)$, we can find that

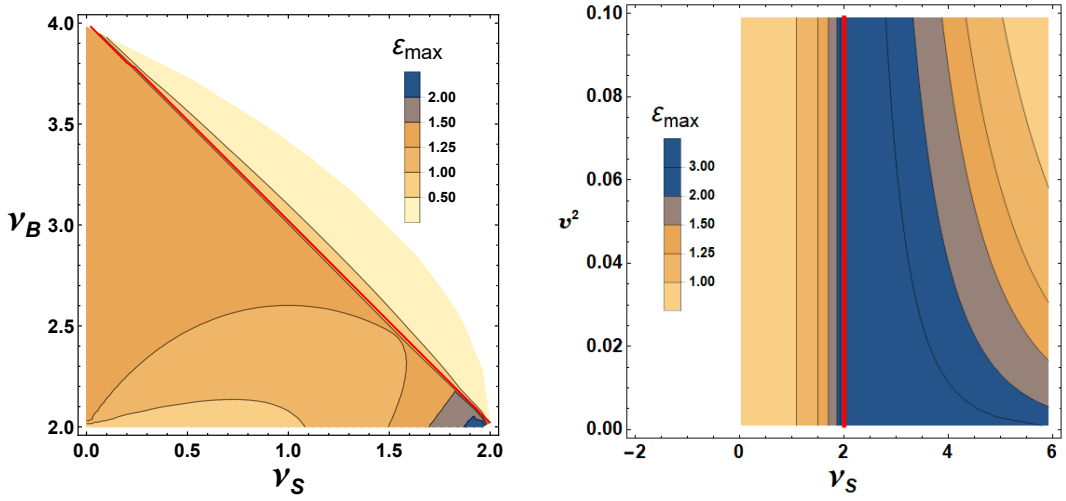

Figure 5.4: **Left:** The maximum allowed strain ε_{max} within the allowed region for the monomial EFT case $F(x) = x^{\nu_S/2}$. The left, bottom and right edges are respectively given by: gradient instability, positivity of the bulk modulus and subluminality. The red line separates the region where ε_{max} is controlled by gradient instability and subluminality. This figure is the same as Fig. 4.2. **Right:** The maximum allowed strain ε_{max} within the allowed region. SSB case in the particular case where $\omega = 0$ and $F(x) = 1 + v^2\, x^{\nu_S/2}$. The left and bottom edges are respectively given by: gradient instability and positivity of the bulk modulus. The maximum shear strain is determined by gradient instability for $\nu_S < 2$, subluminality for $\nu_S > 2$ and unconstrained for $\nu_S = 2$.

the limit is still the same, *i.e.* we cannot have $\omega > 1$ without gradient instabilities or superluminal modes. Thus, neither the non-linear bulk scaling nor the constraints of it depend on the shape of $F(x)$.

The discussion about the shear scaling ν_S of the spontaneous broken scale invariance (SBSI) case is of course sensitive to the form of the function $F(x)$. The simplest non-trivial example of potential one can think of is a monomial, ie. $F(x) = x^{\nu_S/2}$, which is shown in Fig.5.4. In this particular scenario both the bulk and shear scalings are constrained, in particular we find that $2 < \nu_B < 4$ and $0 < \nu_S < 2$. The most elastic region is found close to $\nu_S \sim 2$ and we find that for this scaling ε_{max} reads as

$$\varepsilon_{max} \simeq \sqrt{2}\left(\frac{1}{2-\nu_S}\right)^{1/4} \quad \text{for} \quad \nu_S \lesssim 2\,. \tag{5.30}$$

As we saw in Chapter 4 the problem with this kind of potentials is that the speeds of the phonons are excessively large. Typically one would expect that the speeds of these modes are not bigger than $\sim 10^{-4}$ times the light speed in 'earthly' materials. This constrains very much the possible scalings one can realize in a realistic scenario, specifically we would be restricted to ν_S and $\nu_B - 2$ not bigger than 10^{-8}.

If we do not restrict ourselves to the most simple case, we can describe a solid with slower phonon modes. For this, we are going to take $\omega \to 0$ and $F(x) = 1 + v^2\, x^{\nu_S/2}$ with $v^2 \ll 1$ as proposed in Chapter 4.2.2. Because we are taking the limit $\omega \to 0$ we see from (5.27) that the bulk scaling is forced to be $\nu_B = 2$. Moreover, this form of potential ensures that the speed of the phonon modes are small at least for small shear strain. The shear scaling is forced to be positive $\nu_S > 0$ and the maximum shear scaling is

$$\nu_S^{max} = \frac{2\,(1+v^2)}{v^2}, \tag{5.31}$$

thus $\nu_S^{max} \gg 1$ for $v^2 \ll 1$. The region with ϵ_{max} large is found around $\nu_S \lesssim 2$ and also in the region where $\nu_S > 2$ and $v^2 \ll 1$, specifically

$$\varepsilon_{max} \simeq \sqrt{2}\left(\frac{1}{2-\nu_S}\right)^{1/4} \quad \text{for} \quad \nu_S \lesssim 2\,, \tag{5.32}$$

$$\varepsilon_{max} \simeq \sqrt{2}\left(\frac{2}{v^2\,(\nu_S-2)}\right)^{\frac{1}{\nu_S}} \quad \text{for} \quad \nu_S \gtrsim 2\,, \tag{5.33}$$

where we have taken the limit $\omega \to 0$ and the last ϵ_{max} is valid for $\nu_S > 2$ not necessarily close to $\nu_S = 2$ as long as $v^2 \ll 1$, as can be seen in Fig.5.4.

5.2 Solids with manifest scale invariance

So far we have focused on EFTs that describe the behavior of solid systems, but in order to realize a solid with manifest scale invariance we are going to employ the holographic tools that we introduced in Chapter 2. This is because the low energy dynamics of solids with manifest scale invariance are controlled by an IRFP, and therefore EFTs lose their strength. It is a necessary condition for an EFT to work having a gapped spectrum in order to integrate out heavier modes. However in a CFT the energy spectrum is a continuum and the analysis gets more complex. Due to this the phonon modes are not isolated energy modes we thus expect them to show some diffusive behaviour. This

translates into the dispersion relation of the phonons acquiring an imaginary part

$$\omega = c_s k - i\,\Lambda(k), \tag{5.34}$$

where the diffusive part, $\Lambda(k)$, scales as k^2 at low momentum and thus in this limit we can consider this dispersion relation as real, linear and propagating[3]. Therefore we will assume phonons to propagate without taking into account diffusive modes[4]

5.2.1 The holographic model

Similarly to what we did with the EFT solid here we would like our theory to realize some sort of translation symmetry breaking to describe our solid. It has been long known [8] that in the bottom-up gravitational duals that can easily accomplish this are massive gravity theories and more precisely Lorentz violating massive gravity.

The massive gravity theory that we are going to consider can be expressed as a theory of general relativity coupled to some scalar fields. This type of formalism used in these holographic theories was initiated in [17, 207] and was contributory to identifying these scalar degrees of freedom to phonon modes [6, 28], as we shall see below. These models were originally proposed, however, to introduce momentum relaxation in the holographic theories in order to obtain a finite DC conductivity.

The scalar fields that we will introduce in the gravity theory are some set of fields Φ^I which live and propagate in the bulk space. For simplicity we are going to consider that the CFT that describes the solid is $2+1$ dimensional, and thus we are going to need an (asymptotic) AdS_4 gravity dual. The scalar fields Φ^I have an equilibrium configuration $\Phi^I = \delta^I_i\, x^i$ that breaks the $2+1$ Poincaré group as in the EFT case, breaking both translations and rotations, and also breaking SI.

The action of this gravity theory is given by

$$S = \int d^4x\sqrt{-g}\,\left[\frac{R}{2} - \Lambda - m^2\, W(X,Z)\right] \tag{5.35}$$

with $\mathcal{B}^{IJ} = \partial_\mu\Phi^I\partial^\mu\Phi^J$, $X = \frac{1}{2}\,\mathrm{Tr}\mathcal{B}$, $Z = \det\mathcal{B}$ and a cosmological constant fixed to $\Lambda = -3$.

[3]This will be true until the momentum reaches some value which depends on how strong is the dissipation. See [12] for more details.

[4]Using hydrodynamic techniques this modes can be considered to include these dissipative terms. See [10, 72, 146] for more details.

Let us then consider that the gravitational theory (5.35) lives in a space-time with the metric of some some AdS black brane geometry

$$ds^2 = \frac{1}{u^2}\left(-f(u)\,dt^2 + \frac{du^2}{f(u)} + dx_i dx^i\right) \tag{5.36}$$

$$f(u) = u^3 \int_u^{u_h} dv\, \frac{3 - m^2\, W(v^2, v^4)}{v^4} \tag{5.37}$$

where we have assumed that this function $f(u)$ vanishes at some $u = u_h$ where the event horizon of a black brane is located, while the boundary is located at $u = 0$. We have also taken the AdS radius to be $\ell = 1$.

Following (2.145) we can determine the temperature as

$$T = -\left.\frac{f'(u)}{4\,\pi}\right|_{u=u_h} = \frac{3 - m^2\, W(u_h^2, u_h^4)}{4\,\pi\, u_h} \tag{5.38}$$

and the entropy density is, according to (2.148), $s = 2\,\pi/u_h^2$.

It has been confirmed in [5, 6, 10, 25] the presence of gapless phonon modes in this theory by computing the quasi normal modes (QNMs) of the system in both shear and longitudinal sectors. These phonons modes coincide with the poles of the $T_{ij}T_{kl}$ retarded's Green function at finite momentum k. The conclusion that they arrive to is that for potentials that fall-off faster than[5] $W \sim u^5$ the theory contains gapless phonons with a dispersion relation of the form of (5.34) for both transverse and longitudinal modes. Moreover, it will be necessary that potentials fall off faster than $W \sim u^3$ in order to have positive shear modulus.

For some particular forms of the potential $W(X, Z)$ the holographic interpretation of the Lorentz and SI breaking is that it is spontaneous [6]. This holographic model, constructed through an AdS dual, represents the IRFP that controls the quantum critical material at low energies. Thus, the AdS dual is acting as the effective theory that controls the low energy dynamics where a new symmetry emerges, i.e. scale invariance.

5.2.2 Linear elasticity

In Section 2.4.1 we introduced a gravitational theory consisting on an AdS Schwarzschild black brane, which was useful to study the nature of conformaly invariant fluids. This

[5]This requirement might be avoided using alternative quantization [11, 20, 27].

kind of gravity theories, however, are not suitable for solid systems due to their response to static shear deformations is zero. The system only has a finite response in the stress-energy tensor for dynamical shear deformations due to the shear viscosity η, i.e. the shear response came from

$$\sigma_{ij} \sim \eta\, \dot{\epsilon}_{ij} \tag{5.39}$$

where ϵ_{ij} is the strain tensor (3.2).

As we shall see now, the gravity theory (5.35) does have a finite response to static shear deformations, in this case due to the shear elastic modulus $\mathcal{G}$. In such a case, for a static deformation we would essentially have

$$\sigma_{ij} \sim \mathcal{G}\, \epsilon_{ij} \quad \text{for} \quad i \neq j\,. \tag{5.40}$$

Just like we did in the case of the shear viscosity, here we may also derive the so-called Green-Kubo formula for the shear modulus, which according to [8] is given by the retarded two-point function of $T_{xy}\, T_{xy}$

$$\mathcal{G} = \lim_{\omega,k\to 0} \mathrm{Re}\, \langle T_{xy}\, T_{xy}\rangle^R\,. \tag{5.41}$$

In order to compute this correlator we are going to need to study the perturbation that sources T_{xy} which is $h \equiv u^2 \delta g_{xy}$. The quadratic action for this perturbation of the metric for an homogeneous mode is

$$S^{(2)} = \int d^4x \frac{1}{4}\frac{1}{u^2}\left(\frac{1}{f(u)}\,(\dot{h})^2 - f(u)\,(h')^2 - 2\,m^2\, W_X(u^2,u^4)\, h^2\right)\,. \tag{5.42}$$

From here we can derive the equation of motion for this metric perturbation

$$h'' + \left(\frac{f'}{f} - \frac{2}{u}\right) h' - \frac{2\,m^2\, W_X(u^2,u^4)}{f}\, h = 0 \tag{5.43}$$

where we have taken the limit of static perturbation, i.e. $\omega = 0$. In order to extract the retarded Green's function we need to impose infalling boundary conditions, like we explained in (2.179) (see [9] for details). Near the AdS boundary the shear perturbation goes as

$$h(u) = h_0\,(1 + \dots) + h_3\, u^3 (1 + \dots)\,. \tag{5.44}$$

On the one hand we can identify h_0, the leading mode of this shear perturbation, with the source of the T_{xy} operator, and on the other hand the subleading mode h_3 plays

the role of the expectation value of such an operator, i.e. the vev of the stress tensor $\langle T_{xy} \rangle$. Finally we can use (2.132) to determine the Green function

$$\mathcal{G} = \frac{2\Delta - d}{2} \frac{h_3}{h_0} = \frac{3}{2} \frac{h_3}{h_0} \tag{5.45}$$

where the conformal dimension is $\Delta = 3$. What this relation is telling us is that the shear modulus of the system is derived by considering some geometrical deformation h_0. However, from the physical point of view we would like to consider the response of the stress-energy tensory h_3 in terms of the mechanical shear deformation ϵ_{xy} that we defined in (3.2). In [28] they find that there is actually not much difference between the two notions of shear deformation. This is a consequence of the fact that the gauge invariant shear strain is in fact a combination of ϵ_{xy} and h_0. In particular we may use the next change of variables

$$\frac{h_3}{h_0} \to -\frac{h_3}{2\,\epsilon_{xy}} \,. \tag{5.46}$$

Thus, we can choose between both interpretations of the shear deformations, either coming from geometrical or mechanical origin. When we study deformations at the non-linear level it will be much more convenient to treat the shear perturbations just from the scalar perturbations and thus we will fix $h_0 = 0$, but for the moment we will stick to the linear level.

In the limit where $m = 0$ we know that the shear modulus is zero, therefore we can compute this elastic modulus perturbatively in the limit $m \ll T$

$$\mathcal{G} = m^2 \int_0^{u_h} \frac{W_X(\zeta^2, \zeta^4)}{\zeta^2} \, d\zeta + \mathcal{O}(m^4) \,, \tag{5.47}$$

where the potential must fall-off faster than ζ^3 in order to have a positive shear modulus. To compute the shear modulus out of this small m/T regime we are going to need to employ numerical computations.

In the case of the elastic bulk modulus the computation is much more trivial. First we need to take into account that the pressure ($T_{ii} \equiv p$) and the energy density ($T_{tt} \equiv \rho$) in a conformal system are related as

$$p = \frac{\rho}{2} \tag{5.48}$$

due to the tracelessness condition of the stress-energy tensor. This fixes the equation of state of the system to be $\omega = 1/2$. With this information we can already derive what the bulk modulus is going to be. In general, we may consider an homogeneous

system with equation of state ω and box volume $\mathcal{V}$. In an adiabatic process the energy density scales with the volume as $\rho \propto \mathcal{V}^{-1-\omega}$. Thus, in our case we should have

$$\rho \propto \mathcal{V}^{-3/2} \,. \tag{5.49}$$

Finally, we can use (3.7), which leads us to

$$\mathcal{K} = \frac{3}{4}\,\rho \,. \tag{5.50}$$

These elastic moduli determine the speed at which the phonon modes travel through the system, according to (3.15). Therefore, the speeds that are found in the QNMs of the $T_{ij}T_{ij}$ should coincide with these values. Indeed this is what is found [5, 6, 10, 25] and is what allow us to identify these modes as phonons.

In equation (3.15) we can restore the dimension of the speeds in the phonon speed formulas by taking back the speed of light c. Thus, using the result in (5.50) we get

$$c_T^2 = \frac{\mathcal{G}}{\rho + p}\, c^2, \quad c_L^2 = c_T^2 + \frac{\mathcal{K}}{\rho + p}\, c^2 = c_T^2 + \frac{c^2}{2} \,. \tag{5.51}$$

In the form of the longitudinal speed we already detect a similar issue to what we found in the solid EFT: we will have relativistic phonon speeds. Thus, we have considered a possible way-out to this issue.

It is reasonable to consider that SI is not the only symmetry that emerges at low energies, but we could also contemplate the possibility of having Lorentz symmetry as an emergent symmetry in the low energy regime. Such a possibility has been already studied in the past (see [14, 36, 58, 87, 91, 117, 165, 179, 213]), where the field theory is characterized by a well defined light-cone c_e, which in principle can be different from the speed of light c but always $c_e < c$ in order to obey the fundamental principles of relativity. We will not prove that this is the case here but rather assume that it is a reasonable premise in order to construct our model.

Consequently we may consider that the theory does not only have the usual Minkowski metric $\eta_{\mu\nu}$ but it also contains (or is produced dynamically) a spin-2 object, that we may call $\eta^e_{\mu\nu}$, such that all CFT operators couple to it, acting as an emergent Minkowski metric. This object allows us to define an emergent light-cone structure as

$$ds^2 = -c_e^2 dt^2 + dx_i\, dx^i \,. \tag{5.52}$$

We may re-define this light-cone with the usual space-time coordinates $x^\mu = \{c\,t, x^i\}$ where all components have the same dimensions. In such a coordinate system the

space-time metric will then be

$$\eta^e_{\mu\nu} = \text{diag}\left(-\frac{c_e^2}{c^2}, 1, \ldots, 1\right) . \tag{5.53}$$

When we say that the CFT is invariant under this emergent Minkowski metric we mean that, for instance, the operators of the theory will be constructed by objects such as the distance as $\Delta x^\mu \Delta x^\nu \eta^e_{\mu\nu}$. This has evident consequences when defining operations such as the trace, where now would be defined through this emergent metric. Let us take as an example the trace of the stress-energy tensor $T_{\mu\nu}$. This particularity lead us to re-define the notion of tracelessness in a conformaly invariant, due to now this traceless now is defined through the new metric

$$T^{\mu\nu}\, \eta^e_{\mu\nu} = 0 . \tag{5.54}$$

Using this we want to know how this new Lorentz invariance would affect the speeds of the phonons. We can translate the result to the new Minkowski metric (5.52) by re-scaling the time coordinate in the dispersion relation as[6]

$$\frac{\partial}{\partial t} \to \frac{\partial}{\partial t}\frac{c}{c_e}, \quad \omega \to \omega\, \frac{c}{c_e} . \tag{5.56}$$

Using this we can get to the conclusion that

$$c_{L,T} \to c_{L,T}\, \frac{c_e}{c} , \tag{5.57}$$

from where it follows that the relation between the transverse and the longitudinal phonon speeds now are related between each other as

$$c_L^2 = \frac{1}{2}\, c_e^2 + c_T^2 . \tag{5.58}$$

The re-scaling (5.56) also affects the form of the stress-energy tensor in the momentum and energy density terms but not the pressure ones. Therefore, the speeds take the next form

$$c_T^2 = \frac{\mathcal{G}}{(c_e/c)^2\, \rho + p}\, c_e^2, \quad c_L^2 = \frac{\mathcal{G} + \mathcal{K}}{(c_e/c)^2\, \rho + p}\, c_e^2 . \tag{5.59}$$

[6]We may also derive this result by noticing that the denominator of the phonon speed is the momentum susceptibility χ_{PP} [6], which is computed as

$$\chi_{PP} = \lim_{\omega,k\to 0} \langle T_{tx} T_{tx} \rangle^R \tag{5.55}$$

and therefore would scale as $\chi_{PP} \to (c/c_e)\, \chi_{PP}$, while the elastic moduli remain constant.

Let us now re-express this speed in terms of the physical mass density, which is commonly defined as

$$\rho_m \equiv \rho/c^2 \,. \tag{5.60}$$

This definition allows us to re-express (5.59) as

$$c_T^2 = \frac{\mathcal{G}}{\rho_m + p/c_e^2}, \quad c_L^2 = \frac{\mathcal{G}+\mathcal{K}}{\rho_m + p/c_e^2} \,. \tag{5.61}$$

In the case of the solids with spontaneously broken scale invariance this expression has a similar form

$$c_T^2 = \frac{\mathcal{G}}{\rho_m + p/c^2}, \quad c_L^2 = \frac{\mathcal{G}+\mathcal{K}}{\rho_m + p/c^2} \,. \tag{5.62}$$

Comparing (5.61) and (5.62) we notice that in the case of a manifest SI solid with a small emergent light-cone speed $c_e \ll c$ the pressure contribution in the denominator of the sound speed formulas gets considerably enhanced, which ultimately means that the sound speeds get reduced. On the contrary, the spontaneously broken SI solid gets a large suppression on the pressure p.

This is the moment to go back to the tracelessness condition (5.54) with the emergent Minkowski metric. In such a metric the tracelessness condition for a homogeneous solid, which has a stress-energy tensor of the form of $T^{\mu\nu} = \mathrm{diag}(\rho, p, \ldots, p)$, is

$$T^{\mu\nu}\,\eta^e_{\mu\nu} = -\frac{c_e^2}{c^2}\,\rho + (d-1)\,p = 0 \,, \tag{5.63}$$

where in our case we have been working in $d = 3$ dimensions. Using this relation the transverse speed of the phonons simplifies to

$$c_T^2 = \frac{d-1}{d}\,\frac{\mathcal{G}}{\rho_m} = \frac{2}{3}\,\frac{\mathcal{G}}{\rho_m} \quad \text{for the manifest SI solid.} \tag{5.64}$$

On the other hand, let us consider the spontaneously broken SI solid in the non-relativistic limit where the speeds of the phonons are small. In this limit the pressure is much smaller than the mass density ρ_m (i.e. the equation of state must be very small $\omega \ll 1$ as we can see from (5.8)) we obtain

$$c_T^2 = \frac{\mathcal{G}}{\rho_m + p/c^2} \simeq \frac{\mathcal{G}}{\rho_m} \quad \text{for the spontaneously broken SI solid,} \tag{5.65}$$

up to corrections of the order of $\mathcal{O}(p/\rho_m c^2)$, which are small in the non-relativistic limit.

The difference between the expressions in (5.64) and (5.65) is completely independent of the value of the emergent speed c_e. This could indicate that discrepancy in the form of the two speeds depends on how SI is realized in the system. It is an intriguing question whether from the relation among the values $\mathcal{G}$, ρ_m and c_T from a SI solid one could actually infer how SI is realized in the IR. Moreover, we should note that this type of discrepancy between the speeds is also present in the longitudinal sector.

There is one possibility that we have not considered yet. It is conceivable that in the framework of the EFT solid we might also have a Lorentz invariance with some light-cone speed c_e different from the light speed c. In such a case the coset construction of the theory would be build up taking this different Lorentz group as the one that is ultimately broken by the ground state. This scenario is beyond our scope, but we would expect to have a speed of the form of (5.61). However, in the spontaneous broken SI case the pressure is not determined by the tracelessness of the stress-energy tensor, although its value would be enhanced by the c_e^{-2} factor that comes with it.

Benchmark potential

After having discussed the model for generic potentials $W(X, Z)$ now we would like to have some quantitative results. We are going to consider a monomial potential as the benchmark potential throughout this section

$$W(X, Z) = X^{\mathfrak{a}}\, Z^{\frac{\mathfrak{b}-\mathfrak{a}}{2}}\,. \tag{5.66}$$

Just like we did with the solid EFT, here we are going to demand some requirements to the potential in order to be valid. We must demand that the theory has no ghost and no gradient instabilities. The study of these stability conditions are analogous to the ones performed for the monomial EFT case, i.e. we need

$$\mathfrak{a} \geq 0 \quad \text{and} \quad \mathfrak{b} \geq 1\,. \tag{5.67}$$

As we shall see, in order to have positive energy density and elastic moduli (see (5.70) and (5.71)) we must impose more restrictive conditions on $\mathfrak{b}$

$$\mathfrak{b} \geq \frac{3}{2}\,. \tag{5.68}$$

Furthermore, as we said earlier, the potential should fall-off faster than $\sim u^5$ close to the boundary in order to have gapless phonon modes, which in this potential translates to

$$\mathfrak{b} \geq \frac{5}{2}\,. \tag{5.69}$$

For potentials with smaller $\mathfrak{b}$ the phonons will acquire some finite mass and thus the dispersion relation (5.34) will have some gap. The presence of this mass in the phonon modes might be due to the presence of some explicit breaking of translational invariance [12].

These are requirements that we demand to the bulk fields, but on top of this conditions we must also take into account that the phonon modes on the boundary should obey $1 > c_{L,T}^2 > 0$, i.e. no gradient instabilities and no superluminal propagation (e.g. see 5.7). Notice however that we are allowing bulk modes to be superluminal as they do not give a physical phonon speed.

We can finally compute different physical properties of the system for the benchmark potential (5.66). The expressions for the energy density and the pressure are

$$\rho = \frac{1}{u_h^3} + m^2 \, \frac{u_h^{2\,\mathfrak{b}-3}}{2\,\mathfrak{b}-3}, \quad p = \frac{1}{2}\,\rho \tag{5.70}$$

where the energy density is derived from the emblackening factor as $\rho = -f'''(u_h)/6$. The elastic moduli, on the other hand, may only be derived (analytically) in the limit of small m/T for the case of the shear modulus

$$\mathcal{G} = \frac{\mathfrak{a}}{2\,\mathfrak{b}-3}\, m^2\, u_h^{2\,\mathfrak{b}-3} + \mathcal{O}\,(m^4), \quad \mathcal{K} = \frac{3}{4}\,\rho\,. \tag{5.71}$$

From this result we may already derive an interesting conclusion: the $\mathfrak{a}$ parameter determines whether the system is describing a solid of a fluid, as for $\mathfrak{a} = 0$ we have a zero shear elastic modulus. We may also determine the form of the Poisson's ratio $\mathcal{R}$, defined in (3.11), for this holographic model. In Fig.5.5 we can see how the Poisson's ratio $\mathcal{R}$ depends on the values of $\mathfrak{a}, \mathfrak{b}$ in the low temperature limit, where we need to compute $\mathcal{G}$ numerically.

In the limit $T/m \gg 1$ the Poisson's ratio generically goes to $\mathcal{R} = 1$, which means that the system goes to a fluid state. This indicates that independently of the potential $W(X, Z)$ the systems tends to become a fluid at large temperatures. This can be explained by noticing that in the limit $T/m \gg 1$ the mass of the graviton, and thus the additional structure provided by the scalar fields Φ^I, become negligible in this limit and then the gravity theory passes to be the dual theory of some strongly coupled fluid system. On the other hand, in the low temperature regime the Poisson's ratio is highly dependent on the form of the potential $W(X, Z)$, taking it away from the fluid limit $\mathcal{R} = 1$. We can see this in Fig.5.6, where the values of the Poisson's ratio for different values of $(\mathfrak{a}, \mathfrak{b})$ are represented. In this figure we also see that the value of the ratio $\mathcal{G}/\mathcal{K}$

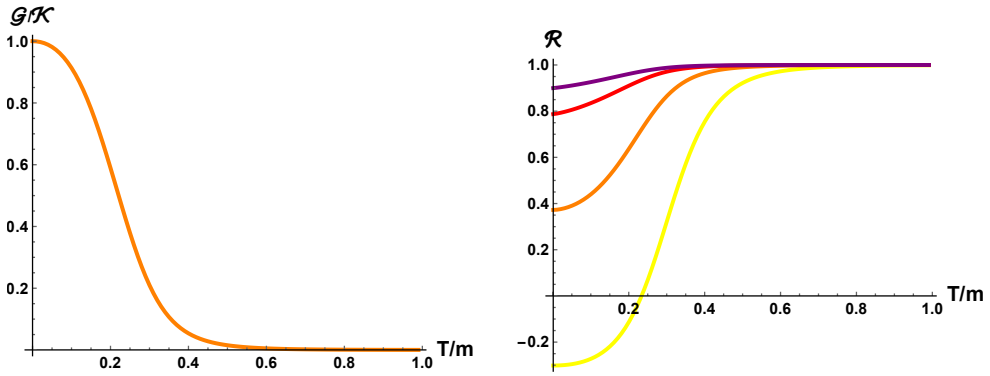

Figure 5.5: **Left:** Elastic moduli ratio $\mathcal{G}/\mathcal{K}$ for a potential with $(\mathfrak{a},\mathfrak{b}) = (3,3)$, i.e. $W(X,Z) = X^3$, as a function of T/m. **Right:** The value of the Poisson's ratio for different potentials as a function of T/m. The values of $(\mathfrak{a},\mathfrak{b})$ are indicated by the color of the lines just like in Fig.5.6. In the large temperature limit the Poisson's ratios go to the fluid limit $\mathcal{R} = 1$.

goes to zero as we increase the ratio T/m, so we can consider this as some "melting" process that the system goes through.

From Fig.5.6 we may derive some conclusions about the properties of the system depending on the $(\mathfrak{a},\mathfrak{b})$ parameters:

- For small $\mathfrak{a}$ we have the Poisson's ratio close to the upper fluid-like limit $\mathcal{R} = 1$. These type of models represent thus incompressible and elastic materials such as rubber.

- For values $\mathfrak{a} \sim \mathfrak{b}$ the Poisson's ratio is of order $-0.5 < \mathcal{R} < 0.5$. This Poisson's ratio is typical in steels and rigid polymers.

- In the large $\mathfrak{a}$ and small $\mathfrak{b}$ we find the most auxetic materials, i.e. we get closer and closer to the lower limit of $\mathcal{R} = -1$. As we can see in Fig.5.7 in this region we generically have to deal with superluminal phonon modes.

The classification of different materials depending on their Poisson's ratio presented above is based on [89, 156].

The elastic moduli are related with the phonon speeds, as we have explained above. However, in a narrow sense, the formulae presented in (5.51) is only applicable for massless phonon modes, with a dispersion relation $\omega = c_{L,T}\, k$, which is only the case for $\mathfrak{b} > 5/2$. In Fig.5.7 we can see how these speeds depend on the ratio T/m and on

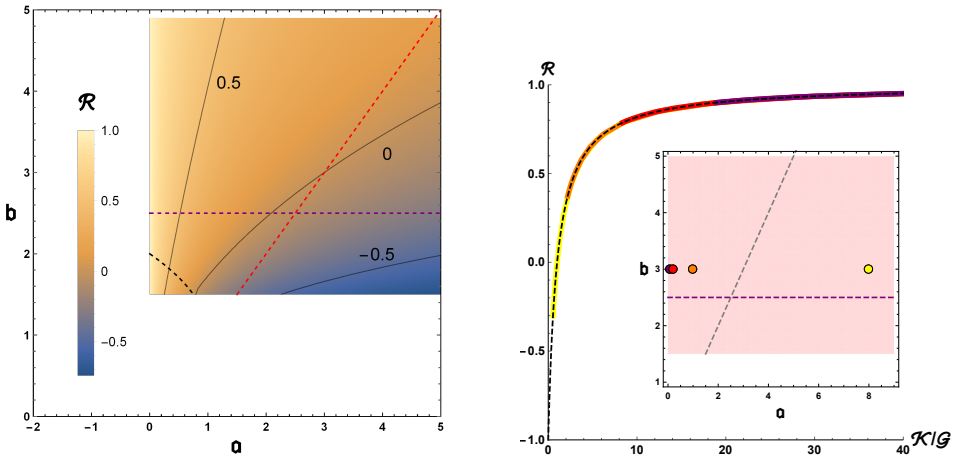

Figure 5.6: **Left:** Poisson's ratio $\mathcal{R}$ for the benchmark potential (5.66) at low temperatures $T/m \ll 1$. From orange to blue, the ratio becomes smaller and smaller, to the point it gets negative and thus auxetic. Above the purple line the phonons are gapless. The red dashed line represents the potential $W(X, Z) = X^{\mathfrak{a}}$. Below the black-dashed line the bulk fields are sub-luminal (see Fig.5.7 for the boundary speed values). **Right:** Poisson's ratio as a function of $\mathcal{K}/\mathcal{G}$ for the benchmark potential (5.66). These plots are made by varying T/m for some fixed $(\mathfrak{a}, \mathfrak{b})$ and all lines eventually get to the fluid limit $\mathcal{R} = 1$. In the inset we show, with colored dots, the values of $(\mathfrak{a}, \mathfrak{b})$ for its correspondent plot.

the parameters $(\mathfrak{a}, \mathfrak{b})$. The first result that we can remark is that there is a relation between the speeds that is conserved at all temperatures, which is

$$c_L^2 = \frac{1}{2} + c_T^2 \,. \tag{5.72}$$

This relation can be explained as a consequence of the theory being conformaly invariant, as already proved in [79]. Therefore, this means that the longitudinal speed has a minimum given by $c_L^2 = 1/2$, which as we can see is found at $\mathfrak{a} = 0$ and any $\mathfrak{b}$, exactly where the shear modulus vanishes. At the same time, we may also find this result in the large temperature limit, $T/m \gg 1$, where the speeds will change towards $c_L^2 \to 1/2$ and $c_T^2 \to 0$.

There is also a white region depicted in the right Fig.5.7 which shows where the phonon speeds get superluminal, i.e. $c_L^2 > 1$. Interestingly, it is also in this white region where the materials get more and more auxetic. This restriction can be surpassed if we take into account that the light-cone speed can be the emergent one c_e, and thus

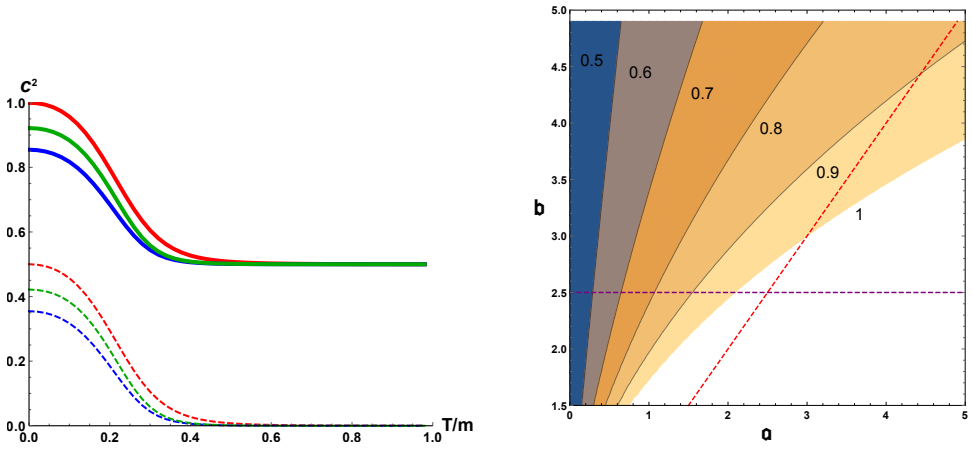

Figure 5.7: **Left:** We show the longitudinal (thick) and transverse (dashed) speeds as a function of the ratio T/m. We take three different cases of $(\mathfrak{a}, \mathfrak{b})$: $(3,3)$, $(3,4)$ and $(4,4)$ for the red, blue and green lines. **Right:** Longitudinal speed as a function of $\mathfrak{a}$ and $\mathfrak{b}$ for the limit $T/m \ll 1$. The purple dashed line indicates the limit of massless phonons, $\mathfrak{b} = 5/2$. The red dashed line indicates the potentials $V(X,Z) = X^{\mathfrak{a}}$. In the white region we have $c_L > 1$.

we may consider as a possibility that $c_L > c_e$. The relation between the longitudinal speed and the Poisson's ratio can be found to be

$$c_L^2 = \frac{c_e^2}{\mathcal{R}+1}\,. \tag{5.73}$$

This shows us that in order to have an auxetic solid we will need to consider $c_e < c$, otherwise the theory would have superluminal phonon modes. The limit on how much auxetic the material can be is then restricted by the value of c_e/c. This relation is shown in Fig.5.8, where we show the relation between c_L and $\mathcal{R}$ depending on the value of c_e. A similar plot could be done for the case of spontaneously broken SI solid, but replacing the ratio c_e^2/c^2 with the equation of state ω (e.g. see (5.8)).

5.2.3 Non-linear elasticity

Next in order we are going to proceed as we did with the solid with spontaneous broken SI, analyzing the behavior of the system when deformed by a finite strain. The strain configuration will be determined by the scalar fields Φ^I as

$$\Phi^I(u, x^i) = O^I_j\, x^j \tag{5.74}$$

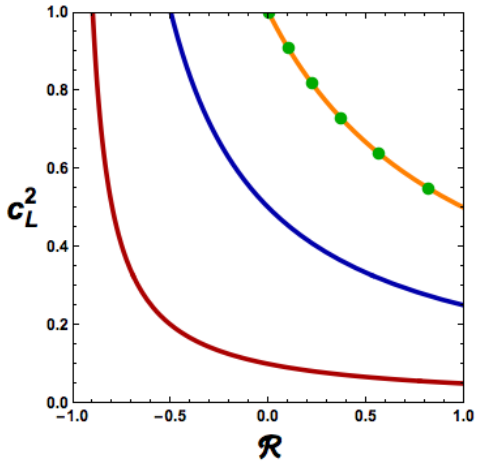

Figure 5.8: The longitudinal speed c_L^2 as a function of the Poisson's ratio $\mathcal{R}$ for different emergent speeds c_e. The ratios are $c_e/c = 1, 1/\sqrt{2}, 1/\sqrt{10}$ for the orange, blue and red lines, respectively. The orange line coincides with the values expected for a conformal solid EFT, shown in green dots. Negative values of $\mathcal{R}$ are achieved for $c_e/c < 1$. A similar plot could be obtained by varying ω instead of c_e/c for a spontaneously broken SI solid.

where O_j^I is the same matrix we used in (4.26). Just like in the linear case, we must now find what is the stress-tensor produced by this strain deformation O_j^I. In order to do this we must find the solutions to our gravity + scalars theory with a nonzero tensor mode, which plays the role of the strain tensor in the gravity theory. Thus, the spatial part of the metric g_{ij} can no longer be just $\sim \delta_{ij}$ so that it contains finite shear deformations.

This system can be solved by using an ansatz of the space-time metric for a non-linear static[7] deformation, which has the form of

$$ds^2 = \frac{1}{u^2}\left(-f(u)\, e^{-\chi(u)}\, dt^2 + \frac{du^2}{f(u)} + \gamma_{ij}(u) dx^i dx^j\right) \tag{5.75}$$

where γ_{ij} is a $d-1$ dimensional tensor with unitary matrix. We are interested in the $d = 3$ case, thus we can parametrize γ_{ij} in terms of the usual tensor polarizations $\times$ and $+$, i.e.

$$\hat{\gamma} = \exp\left[h_+(u)\,\hat{\sigma}_+ + h_\times(u)\,\hat{\sigma}_\times\right] \tag{5.76}$$

where $\hat{\sigma}_{\times,+}$ are the Pauli matrices, which are commonly called $\hat{\sigma}_{1,3}$ respectively and thus the only u-dependent terms are the $h_{\times,+}$ functions.

[7]For a case of non-linear oscillatory deformations see [26].

These two polarizations $\times$ and $+$ are coupled only at the non-linear level, this is why we could just focus on one of the two polarizations when treating the shear deformations as infinitesimal. In order to simplify the problem we can switch variables to

$$h_+ = h\,\sin\theta \quad , \quad h_\times = h\,\cos\theta \tag{5.77}$$

where both h and θ depend on the coordinate u. This variables are handy if we want to separate the direction of the spin-2 mode polarization, dictated by θ, and the magnitude, dictated by the function h. Physical solutions must have a vanishing leading mode of $h(u)$ at the boundary, while the subleading mode will encode the stress tensor. We will see below that this leads us to a constant function of $\theta(u)$. Thus, in this variables θ will be the polarization direction of the stress tensor and h the magnitude of the response.

This same parametrization can be applied to the strain matrix O^I_j of the scalar field

$$\hat{O} = \alpha\,\exp\left[\frac{\Omega}{2}\left(\cos\theta_0\,\hat{\sigma}_\times + \sin\theta_0\,\hat{\sigma}_+\right)\right], \tag{5.78}$$

where the α term determines the bulk strain whereas the magnitude and direction of the shear strain are encoded in Ω and θ_0, respectively. In particular, the shear strain for the case $\theta_0 = 0$ is given by

$$\epsilon = 2\,\sinh(\Omega/2)\,. \tag{5.79}$$

The equations of motion for the metric (5.75) in $d = 3$ take the form of

$$2\,\chi' \,-\, u\,\left(\sinh^2(h)\,\theta'^2 \,+\, h'^2\right) \,=\, 0, \tag{5.80}$$

$$u\,f' - \Lambda \,-\, m^2\,W(\bar{X},\bar{Z}) - (6 + u\,\chi')\,f/2 = \,0\,, \tag{5.81}$$

$$\begin{aligned} &f\,\left(2\,u^2\,h'' \,-\, u^2\,\sinh(2\,h)\,\theta'^2 - u\,h'\,(4 + u\,\chi')\right) \,+\, 2\,u^2\,f'\,h' \\ &-\, 4\,m^2\,W_h(\bar{X},\bar{Z}) \,=\, 0\,, \end{aligned} \tag{5.82}$$

$$\begin{aligned} &f\,\left(2\,u^2\,\theta'' + 4\,u^2\,\coth(h)\,\theta'\,h' - u\,\theta'\,(4 \,+\, u\,\chi')\right) \,+\, 2\,u^2\,f'\,\theta' \\ &-\, 4\,m^2\,W_\theta(\bar{X},\bar{Z})\,\mathrm{cosech}^2(h) \,=\, 0\,, \end{aligned} \tag{5.83}$$

where we have fixed the cosmological constant to $\Lambda = -3$ and indicate the derivatives with respect to θ and h with subscripts. The potential W is evaluated at the background values

$$\bar{Z} \,\equiv\, \alpha^4 u^4\,, \qquad \bar{X} \,\equiv\, \alpha^2 u^2(\cosh\Omega\,\cosh h \,-\, \cos(\theta_0 - \theta)\,\sinh\Omega\,\sinh h).$$

From equations (5.80) and (5.81) we notice that the functions $h(u)$ and $\theta(u)$ determine the form of the functions $\chi(u)$ and $f(u)$. Moreover, we can check that equation (5.82) reduces to (5.43) when the function $h(u)$ is treated as infinitesimal, as expected. We assume there is a horizon located at $u = u_h$ defined by $f(u_h) = 0$ where the function $h(u)$ reaches a value $h(u_h) \equiv h_H$. The entropy density does not vary from the one in the linear regime (i.e. $s = 2\pi/u_h^2$) but the temperature changes due to the new function in the time metric component

$$T = -\frac{f'(u_h)}{4\pi}\, e^{-\chi(u_h)/2}\,. \tag{5.84}$$

On the boundary we impose that $f(0) = 1$ and $\chi(0) = 0$. When approaching the boundary the function $h(u)$ takes the form of (5.44), i.e. there will be a constant component h_0 as a leading term and a cubic component h_3 as the subleading term. We will consider that the leading term is zero in order to have zero external space-time deformation source, thus

$$h_0 = 0\,. \tag{5.85}$$

Taking this as a condition the only source of strain for the system will come from the scalar field Φ^I, encoded in the terms α, Ω and θ_0.

As mentioned above, we expect that for a zero space-time deformation we must have a constant polarization direction $\theta(u)$. This is what one expects from a homogeneous and isotropic material, where the elastic response is such that the strain and stress are aligned in the same polarization direction. In our holographic model this translates to having $\theta = \theta_0$.

Let us look at the $\theta(u)$ equation (5.83). Because there is a cross-coupling between h and θ in the second term, the two modes of θ near the AdS boundary will depend on the value that h takes at the boundary, i.e. on the value of h_0. In the case of $h_0 \neq 0$ the θ function has a constant mode and a cubic mode, like the h function. On the other hand, if we have $h_0 = 0$ the boundary mode changes and we would find that θ has a constant mode and a u^{-3} mode. Demanding regularity at the AdS boundary requires that the coefficient of the u^{-3} mode vanishes. In such a case we are left with a constant mode and from (5.83) it is easy to notice that this constant function is forced to be $\theta(u) = \theta_0$. This result indicates that the elastic response in this model is isotropic, since the strain in a given polarization only sources stress tensor in the same polarization.

Thus, from now on we are going to consider $\theta = \theta_0 = 0$ as a condition. Using this

result the equations (5.80)-(5.83) are simplified substantially

$$
\begin{aligned}
&2\,\chi' \,=\, u\,h'^2,\\
&2\left(\,u\,f' - \Lambda \,-\, m^2\,W(\bar{X},\bar{Z})\,\right) - f\,\left(6 + u^2\,h'^2/2\right) \,=\, 0\,,\\
&f\,\left(2\,u^2\,h'' - u\,h'\,(4\,+\,u^2\,h'^2/2)\right) + 2\,u^2\,h'\,f' \,-4\,m^2\,W_h(\bar{X},\bar{Z}) = 0,
\end{aligned}
\tag{5.86}
$$

where now $\bar{X}$ is

$$
\bar{X} \equiv u^2\alpha^2\cosh(h-\Omega),
\tag{5.87}
$$

which indicates more clearly that Ω acts as a 'source' term for the function h.

We are going to consider the same potential we presented in (5.66) which we expect to display a power-law scaling stress-strain relation, $\sigma \sim \epsilon^\nu$, as the one we considered for the spontaneously broken SI solid. We will see below that there appears two different scalings for both the bulk and shear deformations, which for the sake of clarity we are going to specify here as

$$
\nu_1^S, \quad \nu_2^S, \quad \nu_1^B, \quad \nu_2^B,
\tag{5.88}
$$

where the 1 and 2 subscripts denote which one appears first and second and the superscripts B and S denote that these are scalings for the bulk and shear strains, respectively.

On top of the restrictions we imposed on the potential at zero shear deformation (e.g. no ghosts, no gradient instabilities) we are also going to demand that this remains to be true at finite shear deformations $\epsilon \neq 0$, similarly to what we did in Chapter 4 for the longitudinal and transverse speeds of the phonon modes.

Shear deformation

The nonlinear shear response is derived from the metric off-diagonal component g_{xy} from its subleading term

$$
T_{xy} = \sigma_S = \frac{3}{2}\,g_{xy}^{(3)}
\tag{5.89}
$$

when expressed in Fefferman-Graham coordinates, where the holographic coordinate must be replaced with the next coordinate transformation

$$
\frac{dz^2}{z^2} = \frac{du^2}{u^2\,f(u)}\,.
\tag{5.90}
$$

It can be checked in Appendix C that the final result for the case $h_0 = 0$ is

$$\sigma_S = \frac{3}{2} h_3 \,. \tag{5.91}$$

where h_3 is the subleading term of the function $h(u)$ close to the AdS boundary (5.44). On the other hand the shear strain is produced by the difference between the background configuration of the scalar field (5.78) and its equilibrium configuration $\Phi^I = \delta^I_i x^i$. Using the definition of the strain tensor (3.2) we get to

$$\epsilon = 2\,\epsilon_{xy} = 2\,\sinh\left(\frac{\Omega}{2}\right) . \tag{5.92}$$

Now we can already derive an analytic expression of the shear response in the limit of small m^2, similar to what we did in (5.47), which should be a good approximation to the shear response for not very large strains $\Omega \gtrsim 1$. At first order in m^2 we find that

$$\sigma_S = \frac{1}{2} m^2\, \epsilon\, \sqrt{4+\epsilon^2} \int_0^{u_h} \frac{W_X\left(\frac{1}{2}(2+\epsilon^2)\,\zeta^2, \zeta^4\right)}{\zeta^2}\, d\zeta + \mathcal{O}(m^4)\,. \tag{5.93}$$

As we mentioned, for the benchmark potential we are going to find two different scalings for the shear stress-strain relation. Let us compute the integral for the benchmark potential

$$\sigma_S(\epsilon) \simeq \frac{\mathfrak{a}}{2^{\mathfrak{a}}(2\,\mathfrak{b}-3)}\, m^2 \alpha^{2\,\mathfrak{b}}\, u_h^{2\mathfrak{b}-3}\, \epsilon\, \sqrt{4+\epsilon^2}\, (2+\epsilon^2)^{\mathfrak{a}-1} \tag{5.94}$$

which in order to have a convergent integral we must demand $\mathfrak{b} > 3/2$, the same condition we demand for the positivity of the linear bulk modulus. In fact, in the limit of infinitesimal shear strain $\epsilon \ll 1$ we obtain the same result as in (5.47).

In (5.94) we can deduce that if u_h does not vary significantly with ϵ then we must find that the shear scaling is

$$\sigma_S \sim \epsilon^{2\mathfrak{a}} \equiv \epsilon^{\nu_1^S} \tag{5.95}$$

but numerically, for larger values of ϵ, a second scaling will show up, which this approximation does not anticipate, as we can see in Figure 5.9.

In order to obtain the full non-linear response we need to use numerical methods. To do so we are going to use shooting methods, integrating from the IR horizon towards the UV boundary. At the horizon we are going to impose as a boundary condition, to ensure regularity, that $[2\,u^2\,h'\,f' - 4\,m^2\,W_h(\bar{X},\bar{Z})]_{u_h} = 0$ and $h(u_h) = h_H$, which will play the role of the shooting parameter.

The numerical results are shown in Figure 5.9 for different potentials at different values of m/T. At infinitesimal values of the strain we find that the shear response

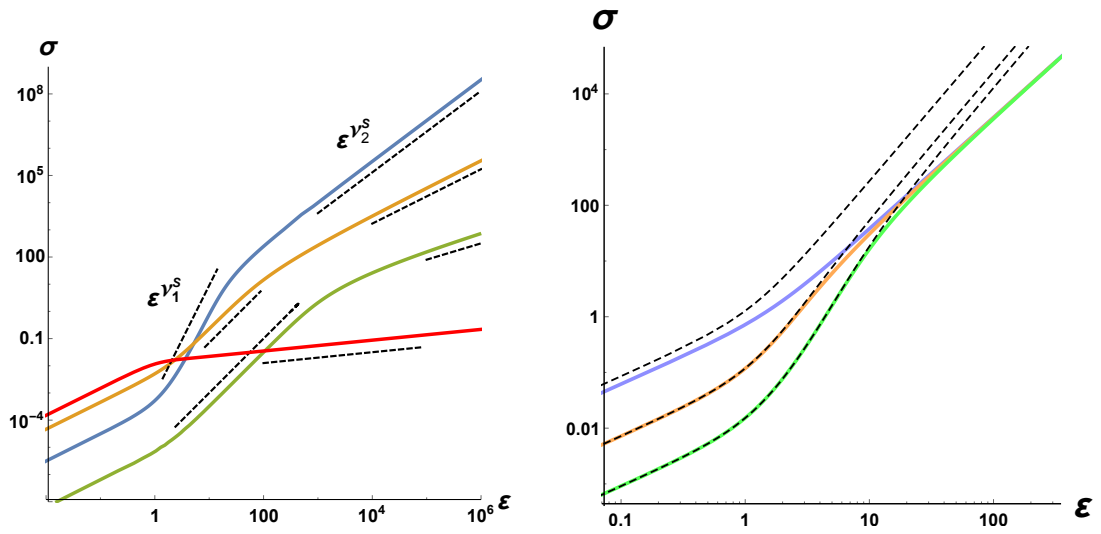

Figure 5.9: **Left:** Shear stress-strain relations for different potentials at fixed $m/T = 1$. The chosen potentials display both stiffening and softening: $\nu_1^S = 2\,\mathfrak{a} = 4, 2, 2, 0.2$ and $\nu_2^S = 3\,\mathfrak{a}/\mathfrak{b} = 3/2, 1, 3/5, 1/7$. The black dashed lines show these scalings. Here we do not impose constraints on the potential. **Right:** Shear stress-strain relations for a potential with $\mathfrak{a} = 2$ and $\mathfrak{b} = 3$ for different values of T/m ($T/m = 0.1, 0.5, 1$ for blue, orange and green, respectively). Black dashed lines show the analytic result derived in (5.94). As we expected, it coincides the closer we are to the limit $m/T \ll 1$ for some finite range of ϵ.

scales linearly with the shear modulus $\mathcal{G}$ (5.47) as the slope. For larger values we find an intermediate power-law scaling $\sigma_S \sim \epsilon^{\nu_1^S}$ of the shear response with

$$\nu_1^S = 2\,\mathfrak{a}. \tag{5.96}$$

For much larger values of the strain we encounter a second power-law scaling $\sigma_S \sim \epsilon^{\nu_2^S}$, in this case with

$$\nu_2^S = 3\,\frac{\mathfrak{a}}{\mathfrak{b}}. \tag{5.97}$$

Interestingly, the intermediate scaling does only show up when the temperature is high enough, whereas at low T/m the shear stress-strain plot interpolates directly from a linear relation to the second scaling ν_2^S as we see in Figure 5.9. Note that the intermediate scaling ν_1^S can be either softening or stiffening (smaller or larger than 1), but the second scaling is always smaller than the first $\nu_1^S > \nu_2^S$ due to the restrictions on the potential (5.68).

Although the second scaling cannot be derived from the analytic approximation in (5.94) we can actually obtain the result taking an asymptotically large strain $\epsilon \gg 1$ in the equations of motion. Applying a large strain translates to taking a large Ω in our system, which in addition implies that the function $h(u)$ must explore a large range of values from the black brane horizon to the AdS boundary, where it vanishes. In order to simplify the analysis we are going to define a new variable

$$\tilde{h}(u) \equiv \Omega - h(u) \tag{5.98}$$

which is the combination the potential depends on. Due to near the boundary $h(u)$ vanishes, we expect that for a $\Omega \gg 1$ we will also have $\tilde{h} \gg 1$. Therefore, taking the limit $\tilde{h} \gg 1$ we may also substitute the expressions $\sinh \tilde{h}$ and $\cosh \tilde{h}$ for its asymptotic limit $\sim e^{\tilde{h}}/2$. Furthermore, we also expect that in this limit the derivative of the function $\tilde{h}'(u)$ must be large (e.g. compared to $f'(u)$) somewhere in the bulk. Taking this into consideration we can assume that there is a region where the function $f(u)$ is mostly constant, which at the same time implies that the shape of the function $\tilde{h}(u)$ must be logarithmic. In particular we find that the equations of motion (5.86) admit a solution close to the boundary as

$$f(u) \simeq f_0 = \frac{3\,\mathfrak{a}^4}{(\mathfrak{a}^2+\mathfrak{b})(3\,\mathfrak{a}^2+\mathfrak{b}^2)}, \quad \tilde{h}(u) \simeq -2\,\frac{\mathfrak{b}}{\mathfrak{a}}\,\log\left(\frac{u}{u_0}\right), \tag{5.99}$$

where $m^2\,u_0^{2\mathfrak{b}} \equiv 3\mathfrak{b}\,2^{\mathfrak{a}}/(\mathfrak{a}^2+\mathfrak{b})$. This behavior for the functions $f(u)$ and $\tilde{h}(u)$ shows up for $\Omega \gg 1$ for some finite region of u, as is clearly displayed in Figure 5.10.

We know that when reaching the boundary the function $h(u)$ vanishes, therefore $\tilde{h}(u)$ must reach a large but finite value determined by $\tilde{h}(0) = \Omega$. Thus, at some value u_* the function $\tilde{h}(u)$ must deviate from the logarithmic shape from (5.99) and stay at a value Ω. Then, let us consider that through the region between u_* and the horizon u_h the $\tilde{h}(u)$ function goes like

$$\tilde{h}(u) \simeq \Omega - 2\,\frac{\mathfrak{b}}{\mathfrak{a}}\,\log\left(\frac{u}{u_*}\right). \tag{5.100}$$

From this equation we can derive what should be the value of the coordinate around the "transition"

$$u_* \simeq u_h \exp\left(\frac{\mathfrak{a}}{2\,\mathfrak{b}}(\tilde{h}(u_h)-\Omega)\right) \simeq u_h \exp\left(-\frac{\mathfrak{a}}{2\,\mathfrak{b}}\,\Omega\right) \tag{5.101}$$

where we have considered $\tilde{h}(u_h) \ll \Omega$, as the function $h(u)$ will go from zero at the AdS boundary to some large value close to the horizon (see Figure 5.10). From (5.101)

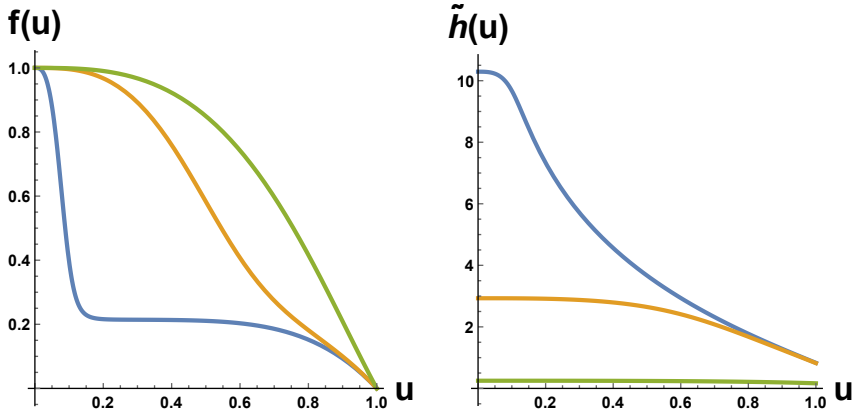

Figure 5.10: Metric functions $f(u)$ and $\tilde{h}(u)$ as a function of u at fixed $u_h = 1$ for the benchmark potential with $\mathfrak{a} = 2$ and $\mathfrak{b} = 4$. We take $\Omega = 0.24, 2.93, 10.29$ and temperatures $T/m = 0.15, 0.02, 10^{-5}$ for green, orange and blue, respectively.

is clear that the larger is the value of Ω, the closer is the transition point u_* to the boundary. Since u_* represents the value where $h(u)$ changes its shape from a constant value to a logarithmic one we then can assume, by dimensional analysis, that the value of the subleading term h_3 must scale as $h_3 \sim u_*^{-3}$. Finally, if the shear strain is $\epsilon = 2 \sinh \Omega/2 \sim \exp(\Omega/2)$ then we arrive to the conclusion that

$$\sigma_S \simeq h_3 \sim u_*^{-3} \simeq \exp\left(-\frac{3\mathfrak{a}}{2\,\mathfrak{b}}\,\Omega\right) \simeq \epsilon^{3\mathfrak{a}/\mathfrak{b}} \tag{5.102}$$

which is precisely the power-law scaling that we found numerically for very large shear strain, i.e. $\nu_2^S = 3\mathfrak{a}/\mathfrak{b}$, as we see in Figure 5.10.

Beyond proving how this intermediate scaling shows up it is also interesting noticing how the space-time metric changes in this limit. Consider the coordinates $\tilde{x}$ and $\tilde{y}$ where the metric is diagonal, then in the limit where $f(u)$ and $h(u)$ asymptote to (5.99) the geometry goes as

$$ds^2 \simeq \frac{1}{u^2}\left(\frac{du^2}{f_0} - u^{-2\mathfrak{b}^2/\mathfrak{a}^2}\,dt^2 + u^{2\mathfrak{b}/\mathfrak{a}}\,d\tilde{x}^2 + u^{-2\mathfrak{b}/\mathfrak{a}}\,d\tilde{y}^2\right)\,. \tag{5.103}$$

We note that in this geometry there is a Lifshitz scaling between time and space and also between the two spatial coordinates $\tilde{x}$ and $\tilde{y}$, namely there is an anisotropic scaling. Due to the large strain applied to the system it is natural to see that this anisotropy

between spatial coordinates shows up. The geometry in (5.103) is acting as a new UV (Lifhitz) fixed point. This fixed point seems to be attractive towards the UV, and the configurations with large strains get close to it for a significant range of $\log u$.

The fact that this Lifshitz scaling between the spatial and time coordinates shows up might be surprising at first glance. We may explain why this happens if we remind ourselves that the gravity theory we are considering a massive gravity theory in (5.35). We can readily see this by going to the unitary gauge, where our scalar field takes the configuration $\Phi^I = \delta^I_i x^i$, thus we get the terms $X = \mathrm{Tr} g^{ij}$ and $Z = \det g^{-1}$ as the variables of our potential $W(X, Z)$, which now will play the role of the the potential of the spatial components of the metric. We know that 1-spin massive theories serve as theories that provide a Lifshitz geometry [66, 129, 206], therefore it does not seems surprising that in a 2-spin massive theory this kind of geometry can also arise.

Having solutions of the type (5.99) is somewhat dependent on the choice of potential $W(X, Z)$. By studying these equations of motion we first see that in order to have $f(u) =$ constant we are going to need a logarithmic $\tilde{h}$ function. As a consequence the potential $W(X, Z)$ has to be either mostly constant or vanishing towards the boundary. Thus, with this condition we take a look at the second equation of motion, which requires that W_h (which at large h we can substitute by $X\, W_X$) also to be constant. In order to keep both $W(X, Z)$ and $X\, W(X, Z)$ to be constant we are going to need a special form for our potential in which the dependence on X and Z goes through the combination $X^p\, Z^q$ with p and q constant values, just like it happens in our benchmark potential (5.66). Nevertheless, any potential of the type $W(X, Z) = W_0(X^p\, Z^q)$, with W_0 an arbitrary function, should also do the work[8]. Although we do not expect this Lifshitz UV fixed point to appear for more generic potentials, it is conceivable that some anisotropic solution might exist and dominate the large form of the response in the large shear strain regime.

Nevertheless, these (near)-Lifshitz solutions are expected to influence other features of the theory such as transport properties like the electric conductivity at finite strain (e.g. see [43]). Such features hint the possibility of testing the appearance of this anisotropic Lifshitz regime on real materials.

Other models where anisotropy has been considered by using a unidirectional scalar field $\Psi = \alpha z$ have been studied broadly in the past [125, 148, 184]. Such models could share some features with the holographic model proposed here in the limit $\Omega \to \infty$ for the scalar field configuration $\Phi^x = \alpha\, e^{\Omega}$ and $\Phi^y = \alpha\, e^{-\Omega}$ as long as we keep $\alpha\, e^{\Omega}$ fixed.

Let us also mention that the models (5.35) have an extremal near-horizon geometry

[8]To be even more general we could also add terms to the potential dependent on Z that vanish when moving closer to the boundary.

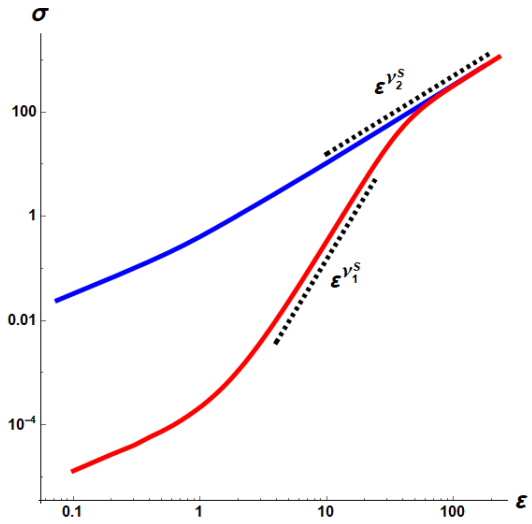

Figure 5.11: Shear stress-strain relation for an adiabatic process where we consider $u_h = 1, 0.2$ (blue, red), which at zero strain have a temperature $T/m = 0.16, 1.19$. We use the benchmark potential with $(\mathfrak{a}, \mathfrak{b}) = (2, 4)$.

of the type $AdS_2 \times \mathbb{R}^2$ (we discussed a similar case in Section 2.4). This represents the additional emergent scale invariance, this one with with Lifshitz dynamical exponent $z \to \infty$, and isotropic character. This scaling is expected to be manifested in the lightest excitations, governed by the near horizon geometry.

Finally, let us comment that the shear deformations that we have considered above have been studied in the case of constant temperature $T/m =$ constant, meaning that we have only considered isothermal processes. We can also apply this shear deformation but instead of maintaining the temperature constant we will take a constant entropy (or adiabatic) process $S/m =$ constant, or equivalently $u_h/m =$ constant. What we find is that the stress-strain relations are equivalent to those taken at constant temperature. As we can see in Figure 5.11 we can observe both the intermediate scaling ν_1^S and the large deformation scaling ν_2^S. While we are increasing the shear strain ϵ the temperature decreases, thus it will depend on the value of u_h that whether we find the intermediate scaling ν_1^S or not: if the initial temperature is low enough, there will not be an intermediate scaling.

Bulk deformation

Just like we have extended the study of shear deformations beyond the linear level we can do the same for the case of bulk deformations. As we just want to consider pure bulk deformations we are going to restrict ourselves to the case of $\epsilon = 0$ and use α as the parameter that controls the bulk strain, or more concretely $\kappa = \partial \cdot \Phi$ which is the bulk strain and is related to α as $\kappa = 2(\alpha - 1)$.

Due to conformal invariance we can relate the pressure to the energy density as $p = T_{xx} = T_{tt}/2$. This will allow us to express the longitudinal stress as a function of the bulk strain. In particular we define this longitudinal response as $\sigma_B = T_{xx} - T_{xx}^{(eq)}$. For the benchmark potential this reduces to

$$\sigma_B = \frac{m^2 \left(\frac{\kappa}{2}+1\right)^{2\mathfrak{b}} u_{u,\kappa}^{2\mathfrak{b}-3} - u_{u,\kappa=0}^{2\mathfrak{b}-3}}{2(2\mathfrak{b}-3)} + \frac{1}{2}\left(\frac{1}{u_{h,\kappa}^3} - \frac{1}{u_{h,\kappa=0}^3}\right), \tag{5.104}$$

where $u_{h,\kappa}$ denotes that the position of the black brane horizon depends on the value of κ, while $u_{h,\kappa=0}$ is the position of the horizon at zero bulk strain, or equivalently $\alpha = 1$. The sign of the bulk strain κ can be either positive (a compression) or negative (an expansion).

At large bulk strain we find a universal power-law scaling in the longitudinal response

$$\sigma_B \sim \kappa^3 \quad \text{at } \kappa \gg 1\,, \tag{5.105}$$

as we see in Figure 5.12. This universal scaling is a consequence of conformal invariance and it can be generalized to D space-time dimensions at the boundary theory as $\sigma_B \sim \kappa^D$. It is straightforward to derive (5.105) by noticing that if we take large κ and we want to keep T/m constant, then we are forced to have $u_h \sim 1/\kappa$. Comparing to the case of the spontaneously broken SI solid the scaling (5.105) coincides exactly if we consider the conformal limit of the EFT (see (5.27), where the conformal limit is $\omega = 1/2$).

Thus, just like it happens for the shear deformation, there are two different scalings that show up when increasing the bulk strain. One of the two scalings is an intermediate scaling that only is present in the case of having a high enough temperature, while the second scaling is always present at large enough deformation. Using the definitions in (5.88) we then conclude that

$$\nu_1^B = 2\,\mathfrak{b} \quad , \quad \nu_2^B = 3\,, \tag{5.106}$$

where due to the constraints on the benchmark potential (5.68) we always have that the bulk response always gets stiffer, i.e. $\nu_1^B > \nu_2^B$.

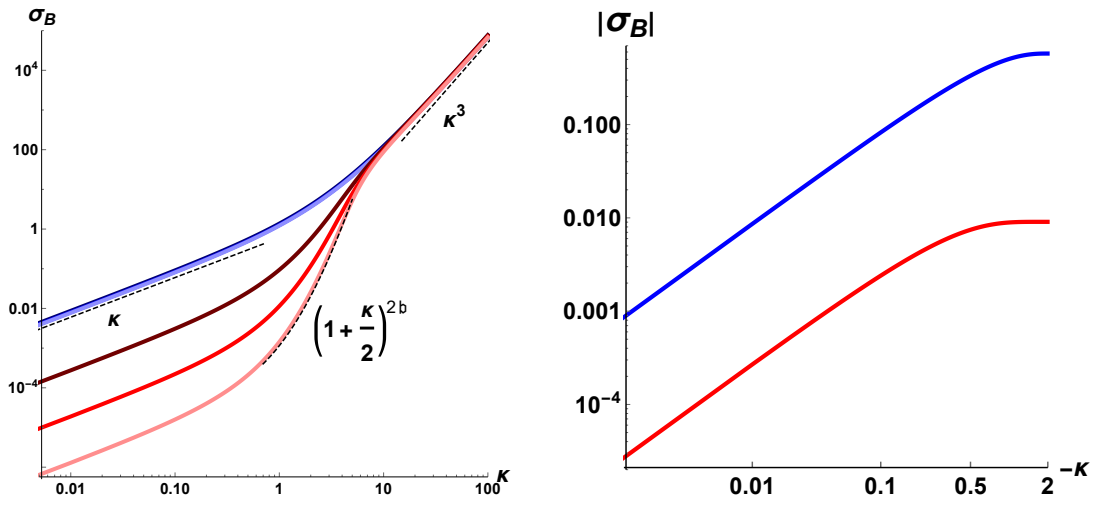

Figure 5.12: **Left:** Nonlinear bulk stress for different temperatures: $T/m = 0.01$ (blue lines) and $T/m = 1$ (red lines). We take different benchmark potentials $(\mathfrak{a}, \mathfrak{b}) = (3,3), (2,4), (1,5)$. At large bulk strain there is a universal scaling $\sim \kappa^3$. At large temperature and finite, but not large, strain the scaling goes as $\sim (\frac{\kappa}{2}+1)^{2\mathfrak{b}} = \alpha^{2\mathfrak{b}}$. **Right:** Absolute value of σ_B for a negative bulk strain κ for $(\mathfrak{a}, \mathfrak{b}) = (3,3)$ at $T/m = 0, 1$ (blue and red lines).

For completeness let us also explore what is the bulk response for the negative bulk deformations (expansions). In this case the range of values that κ can explore is limited by the lower limit $\alpha = 0$, which coincides with $\kappa = -2$. In this case, taking a look at (5.104) we see that at low temperatures we would have a response that scales as $\sigma_B \sim (\alpha^3 - 1) = ((\frac{\kappa}{2}+1)^3 - 1)$, whereas for high temperatures the scaling would be $2\,\mathfrak{b}$ instead of the cubic one. Unfortunately, due to the short range of values where κ can be extended we do not get to see these scalings in the stress strain plots. A couple of examples for high and low temperatures are displayed in Figure 5.12, where a linear response dictated by the bulk modulus determines the small κ regime and the response ultimately gets saturated at some finite value at $\kappa = -2$. Thus, we see that the amount to stress needed to produce a full expansion is finite.

Notice that just like for the shear deformation here we may also consider either an isothermal (T constant) deformation or an adiabatic (S constant) deformation, but the discussion here is a bit trickier. This is because for a bulk deformation there is a difference between the entropy and its density due to the volume of the system is changing (either growing or reducing). To convince ourselves of this we just need to

realize that

$$\Phi^i = x^i \to \Phi^i = \alpha\, x^i \quad \text{and} \quad x^i \to x^i \tag{5.107}$$

is equivalent to the next transformation

$$\Phi^i = x^i \to \Phi^i = x^i \quad \text{and} \quad x^i \to \frac{1}{\alpha}\, x^i, \tag{5.108}$$

as both X and Z (and the equations of motion) will take the same form in either case. Therefore, as the entropy is proportional to the area of the black brane horizon it is easy to find that the total entropy scales as

$$S = \frac{s}{\mathcal{V}} \sim (u_h\, \alpha)^{-2}\ . \tag{5.109}$$

Thus, in order to ensure that this process is adiabatic we must impose that the position of the black brane horizon scales as

$$u_h \sim \frac{1}{\alpha} = \frac{1}{1+\frac{\kappa}{2}}\,. \tag{5.110}$$

Using this relation we can simplify (5.104) to

$$\sigma_B = \frac{u_{h,\kappa=0}^{2\,\mathfrak{b}}}{2}\left(1+\frac{m^2}{2\,\mathfrak{b}-3}\right)\left(\frac{1}{u_{h,\kappa}^3}-\frac{1}{u_{h,\kappa=0}^3}\right)\,, \tag{5.111}$$

where $u_{h,\kappa} \sim \alpha^{-1}$. From this expression it is evident that in the case of the adiabatic bulk deformation the only scaling that appear is the cubic scaling ν_2^B, whereas the intermediate scaling ν_1^B does not appear for any value of u_h. Moreover, from this expression it is evident that the bulk modulus for an adiabatic process is

$$\mathcal{K} = \left.\frac{d\sigma_B}{d\kappa}\right|_S = \frac{3}{4}\,\rho, \tag{5.112}$$

just like we showed in (5.50).

Elasticity bounds

Lastly, after having studied what are the nonlinear relations for both bulk and shear deformations, we want to take a look on whether we can place a limit in the maximum deformation a solid with manifest SI may sustain, just like we did for the EFT description in Chapter 4. The methods that we are going to employ are actually analogous

to the ones presented for that case. We are going to demand to have stable perturbations around our strained configurations and find whether there is a ϵ_{max} where some perturbation becomes unstable.

In order to be completely correct one should compute the dispersion relation of the QNMs for the gravity theory considered. However, this was beyond our scope in [23] and we decided to restrict ourselves to the so-called decoupling limit, which already provides some intuition on what could be the limits for the deformations we can perform on such models.

Therefore, what we will do to extract this limit is, on the one hand, computing the speeds of propagation $c_{(i)}$ of the fields though the bulk. By increasing the shear deformation[9] we will eventually find that $c_i^2 < 0$, i.e. a gradient instability. One could argue that even though we have an instability at some point in the bulk space of the type $c_{(i)} < 0$ this does not necessarily mean that the QNMs are unstable, and thus the physical speeds of the perturbations on the solid. However, we assume that this constraint is expected to place a conservative upper limit on the maximum shear deformation ϵ_{max}.

Due to we are going to work in the decoupling limit we must neglect the mixing between scalar perturbations $\delta\Phi^I$ and the metric perturbations. Therefore, the computations are going to be completely equivalent to those we performed in Chapter 4 for the EFT case. What we found in that case was that there were two different phonon speeds

$$c_{\pm}(\epsilon, \varphi, u) \tag{5.113}$$

where φ is the angle direction in which the perturbation travels (with respect to the principal axes) and the $\pm$ subscript indicates which one is larger and which one is smaller. There is a third speed we could consider, which is the speed at which the perturbations travel through the u direction, which is always 1. Notice that the speeds now could depend on the holographic coordinate u, but because of the benchmark potential that we have chosen is a monomial, the u-dependence disappears from the equations of motion and the speeds become independent of it.

The limit we are going to impose to our speeds is

$$c_-^2 > 0 \tag{5.114}$$

for any direction φ. The dependence of the speeds with respect to the parameters of the potential $\mathfrak{a}$ and $\mathfrak{b}$ are going to be exactly the same as the dependence on A and B for the EFT potential in (4.17), and thus we will have the same relation among

[9] Because we are considering a monomial as our benchmark potential there will not be instabilities due to bulk deformations, as we saw in the case of monomial potentials in Section 4.2.1.

parameters in (5.114). However, the physical role that these parameters represent is different in these two different theories, so the relation to terms such as the scalings ν will differ. Therefore, the discussion and comparison between the relation of ϵ_{max} in the two different SI solids will not be phrased using the parameters $\mathfrak{a}, \mathfrak{b}$ and A, B but with the physical parameters ν^B and ν^S.

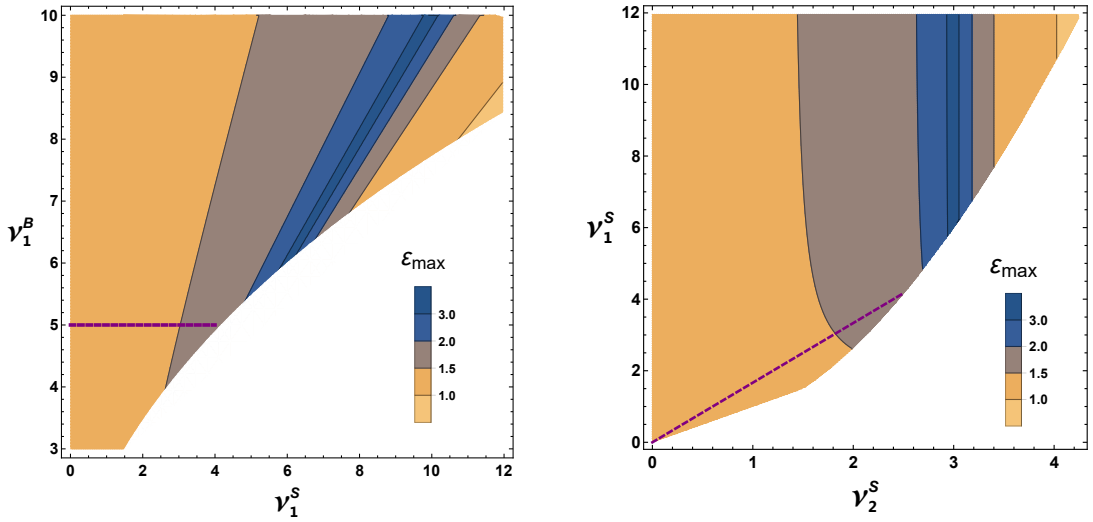

Figure 5.13: **Left:** Maximum shear strain ϵ_{max} as a function of the scalings ν_1^S and ν_1^B. Close to $\nu_1^S = \nu_1^B$ there is a region where ϵ_{max} asymptotically grows. Left and right of this line the maximum shear strain is determined by the absence of gradient instabilities and ghosts, respectively. White area shows where the longitudinal speed becomes superluminal at the boundary. Purple line shows the massless condition of the phonons (5.69). **Right:** Maximum shear strain ϵ_{max} as a function of the scalings ν_1^S and ν_2^S. Close to $\nu_2^S = 3$ there is a region where ϵ_{max} asymptotically grows, see (5.115).

So far we have already mentioned the constraints placed at zero shear strain for $\mathfrak{a}$ and $\mathfrak{b}$ in (5.67) and (5.68) but now we want to place limits on the maximum deformation ϵ_{max} as a function of $(\mathfrak{a}, \mathfrak{b})$. In Figure 5.13 we can see the bounds on this maximum deformation, where the first thing we can comment is that the shear scalings fulfill $\nu_1^S > \nu_2^S$, as we already expected. We can split the regions in this Figures depending on the value of ν_2^S: for $\nu_2^S > 3$ (or $\mathfrak{a} > \mathfrak{b}$) the limit on the shear deformation will be due to the appearance of ghosts, whereas for $\nu_2^S < 3$ (or $\mathfrak{a} < \mathfrak{b}$) it will be determined

by gradient instabilities. There is a special case just in the middle of these two regions: for a scaling $\nu_2^S \sim 3$ the maximum deformation grows asymptotically. More specifically we can find that close to this line the maximum shear strain goes as

$$\epsilon_{\max} \sim \left(\frac{6}{|\nu_2^S - 3|}\right)^{1/4}, \tag{5.115}$$

where we use the relation $\nu_2^S = 3\nu_1^S/\nu_1^B$ in order to explain the large strain region in Figure 5.13 for $\nu_1^S \sim \nu_1^B$. Surprisingly, the expression in (5.115) does not depend on whether we are below or above the $\nu_2^S = 3$ line and does not depend on ν_1^S.

There is a final detail that must be taken into account, as it was done for the EFT case, which is the subluminal constraint on the phonon speeds. Firstly, we allow superluminality on the local bulk speeds (5.113) as they are not strictly giving any physical speeds to the phonons. Again, we should work out the computations on the QNM dispersion relation at finite strain in order to place a more exact limit. What we can do is use the QNM dispersion relation which has been computed at zero strain [10, 25] in order to place some restriction. Thus, we display as a white region in Figure 5.13 where the longitudinal phonon speed c_L travels faster than light. Nevertheless, we can guess what effect could have the more exact computation on the physical phonon speeds. We can assume some continuity between the white area and the colored one, smoothing out the values of $\epsilon_{\max}$ close to this area, such as close to the large strain (blue) area around $\nu_1^S \sim \nu_1^B \sim 6$ for instance. Still, this does not necessarily mean that the whole blue region should vanish, so we expect a large region of hyperelasticity persisting.

5.3 Comparison

Let us end up this chapter comparing the results we have obtained for the case of solids with spontaneous broken SI and manifest SI. For the purpose of simplifying the comparison we are going to use as a comparison the physical non-linear scaling ν, both in the shear and bulk deformations, and compare the bounds we have obtained for both. In the manifest scenario we have found that there are actually two different scaling for both bulk and shear responses, thus let us restrict the comparison to the first (or intermediate) scaling $\nu_1^{B,S}$ as the second scaling will show up at very large deformations (at finite temperature)[10]. We are going to restrict the comparison to the

[10]Moreover, another advantage of restricting to this intermediate scaling is that they allow for a continuum range of bulk exponents ν_1^B whereas the second one is fixed by conformality to be $\nu_2^B = 3$.

monomial potential in the case of the spontaneous broken SI solid, as the model would depend on an extra parameter in the case presented in Section 5.1.1.

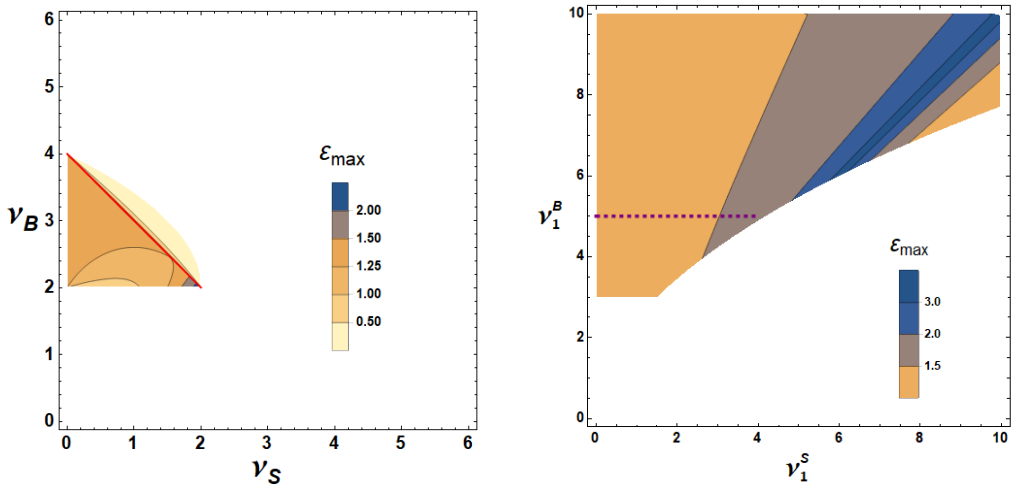

Figure 5.14: Elasticity bounds for a spontaneosly broken (left) and manifest (right) scale invariant solid. In both cases the response displays power-law stress-strain relations $\sigma \sim \epsilon^{\nu}$ for pure-bulk and pure-shear deformations. There is a significant difference between the two cases.

We summarize the results of these scaling and its elastic bound in Figure 5.14, where we basically repeat the plots in Figures 5.4 and 5.13 in a comparable size, in order to facilitate the comparison. It is straightforward to realize that the results found make manifest that the universal elasticity bound that are obtained from low-energy effective methods are significantly different depending on how SI is realized (either as a manifest or spontaneous broken symmetry).

Observing the Figure 5.14 we already notice that there is a significant difference both in the range of possible values for the scaling ν_S and ν_B with a finite maximum deformation ($\epsilon_{\text{max}} \geq 1$) and in the regions where the material becomes hyper-elastic ($\epsilon_{\text{max}} \gg 1$). As a matter of fact, if we limit the analysis of the CFTs to the ones with massless phonons (i.e. $\nu_1^B > 5$) then the the areas allowed for ν_S and ν_B are completely disconnected from the ones found in the EFT example, where the bulk scaling is restricted to be in the range $2 < \nu^B < 4$.

Remember also that the second shear scaling is related to the intermediates as $\nu_2^S = 3\,\nu_1^S/\nu_1^B$

Likewise, in the case of the shear response we find that for the EFT the range is $0 < \nu^S < 2$, whereas for the CFT there seems to be no limit in the shear scaling. Another important discrepancy between the two cases is that the manifest case has a significant area of very elastic models (the blue area in Figure 5.14) which is found near the region where

$$\nu_1^B \sim \nu_1^S \,. \tag{5.116}$$

The solids that are in this region are dubbed as *black rubber* in [23] due to their very large elastic bounds. There are two points that we can highlight from this solutions:

- The area of large elasticity begin around $\nu_1^{B,S} \sim 5$, which is denotes a very stiff behavior. We should note here that this bound might be alleviated if we considered an emergent light speed $c_e \ll 1$, but we will stick with the case of $c_e = 1$ in order to not introduce an extra parameter.

- This area is far away from the free scalar case ($\mathfrak{a} = \mathfrak{b} = 1$, or equivalenty $\nu_1^S = \nu_1^B = 2$). Therefore, black rubbers require the presence of scalar with non-canonical kinetic terms.

On the other hand, in the case of the EFT the area of hyper-elasticity becomes much more narrow and it merely represents a 'dot'-like area. In this case this area could also be enlarged if we considered the second potential of Section 5.1.1. Notice that here the very elastic region is also located where $\nu_S \sim \nu_B$ and in this case the closer we are to the free scalar action, the larger is the maximum deformation sustained by the solid.

Chapter 6

Discussion

The first main result presented in this manuscript is that it is possible to extract non-trivial information and bounds on the nonlinear elastic response of solid materials by using low energy effective methods. We have shown that this is possible basically because the (measurement of the) stress-strain relations already fix the nonlinear Lagrangian for phonon fields, at leading order in a derivative expansion. Among the observables that are fixed once the stress-strain relations are known we may mention: all n-point correlation functions, the phonon-phonon self-interactions[1] and, most remarkably, how these depend on the applied stresses (being the first example of this the acoustoelastic effects, i.e. how the phonon speeds on an elastic material depend on the stress). Such results are most directly relevant for materials that admit large deformations and where dissipative effects are not important[2].

The EFT methods presented in Chapter 4 show how just from the symmetry breaking pattern of a solid system we are able to derive non-trivial bounds on the non-linear elastic properties without any information about the microscopic composition of the material. These effective low energy methods (which usually go under the name of *solid EFT*) allow us to extract elasticity bounds of these solid materials, which we believe is the first time such a computation has been performed. The results we obtain allow us to relate different non-linear physical observables of solids, such as the maximum stress tolerated by the material and the scaling of the stress-strain relation.

We illustrate the predictive power of the EFT methods through a specific type of solid materials, studying how large can be the maximal strain sustained by a given material and how it is constrained by the EFT. In particular we assume a class of

[1] See Section 4.3 where we compute the three-phonon interaction terms for the solid EFT.

[2] For recent EFT-like efforts to include dissipation in fluids and viscoelastic materials, see [18, 37, 38, 68, 70, 88, 92, 96–98, 126, 127, 210, 211].

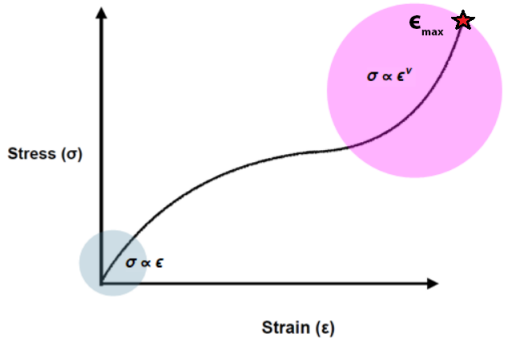

Figure 6.1: As an illustrative example we choose potentials that display a power-law scaling in the stress-strain relations at large deformations. The red star denotes the fracture point of the solid.

materials which display a power-law stress-strain relation at large deformations $\sigma \sim \epsilon^{\nu}$ (such as the one in Figure 6.1). This leads to interesting relations between intrinsically non-linear response parameters, such as the maximum strain $\epsilon_{\max}$ and the strain exponents ν_S and ν_B. We define the maximum strain $\epsilon_{\max}$ of the material as the point where some pathologies (gradient instabilities, ghosts or superluminal propagation) appear in the theory.

We notice in Figures 4.2, 4.6 and 4.7 a result that is common in the different potentials presented, which is that close to the region $\nu_S = \nu_B$ we find the solids with very large maximum stress. Additionally, in the region $\nu_S \lesssim \nu_B$ we see that the maximum stress has a simple form related to the power-law scalings

$$\epsilon_{\max} \sim \left(\frac{2\,\nu_S}{\nu_B - \nu_S} \right)^{1/4} . \tag{6.1}$$

On the other hand, away from this region (at values $\nu_S < \nu_B$) the maximum stress is usually $\epsilon_{\max} \sim \mathcal{O}(1)$. Therefore, solids with this non-linear scaling will not actually display a power-law scaling in their stress-strain relation as we expect them to become unstable before reaching the non-linear strain regime. For example, in (4.31) we find that materials in the limit $\nu_S \to 0$ have a universal maximum stress $\epsilon_{\max} = \sqrt{2}$.

It is worth spending some words on whether this behavior is similar to what is found experimentally, even though a proper analysis of the experimental data on real world solids is well beyond the scope of this work. The classical results summarized in [222] shows some similarities to our results. The fits to the measured stress-strain relations in the most elastic rubber-like materials indeed show properties in agreement with our results. The best fit to rubber materials are the ones that at large deformation

have $\nu_S \sim \nu_B$. This similarity is promising because it confirms that the models near the region $\nu_S = \nu_B$ could actually correspond to these type of rubbers. It would be interesting to check whether (4.40) or (4.42) hold in such materials, but we leave these questions for the future.

We present another computation to exemplify the predictive power of the low energy methods by extracting another non-trivial result of solid materials. In particular we show that from the shape of the stress-strain curve it is trivial to determine the cubic phonon interactions, as we see in (4.44)-(4.48). Interestingly, in the particular case of SI being realized in the EFT we only need information from the linear elastic properties to determine the cubic interactions of phonon modes, as displayed in (4.57)-(4.61).

We should also highlight the difference between the example of the Chiral Lagrangian presented in Section 3.2.1 to the solid EFT construction. In the case of the Chiral Lagrangian we saw that the symmetry breaking pattern fixes the nonlinear Lagrangian up to one (or a few) constants, which are fixed experimentally. Naively, it seems that the solid EFT action cannot be so predictive, as the symmetry arguments seem to fix less the Lagrangian: up to some free functions. Nonetheless, we have realized that the stress-strain curve of the solid fixes this function. Therefore, the solid EFT model is much more predictive than it looks at first sight.

Another topic that we have addressed concerns the non-relativistic limit of phonon modes to obtain realistic speeds. For generic values of ν_S and ν_B in the monomial potential presented in Section 4.2.1 we have speeds of order of the speed of light. However, it is common that phonons propagating in solid materials have speeds much smaller than c. Recall that typical bounds on the phonon speeds are of order $c_{T,L} \sim 10^{-4}\, c$, which would restrict the monomial potential significantly. Thus, in Section 4.2.2 we propose another potential that allow us to control the speeds of the phonons while leaving the stress-strain curve unaltered. This is achieved by introducing a term $\sim \sqrt{Z}$, which is proportional to the mass density of the material. This explains why the coefficient in front of this term must be large in non-relativistic materials. Comparing Figures 4.2 and 4.6-4.7 we see that only in the non-relativistic potential we have a large region of parameters where $\epsilon_{\max} \gg 1$, whereas in the monomial potential the region with very large deformations is reduced to a 'dot' in the area close to $(\nu_S, \nu_B) = (2, 2)$.

Next in order we introduced the scale invariant solids, which we assume to be either solids with spontaneously broken SI or with manifest SI, and studied the mechanical response of such solid materials.

For the first case, it is consistent to consider that the mass-spectrum is gapped

and then use the EFT methods mentioned above to study the gapless phonons as the Goldstone bosons of the spontaneously broken space-time symmetries. The potential of the most general solid with spontaneously broken SI in three space-time dimensions is

$$V_{SBSI} = Z^{\frac{1+\omega}{2}} F(x) \tag{6.2}$$

which is a free function of only one variable ($x = X/\sqrt{Z}$) and the equation of state parameter, ω. This family of EFTs includes the previously studied conformal solid EFT [79] as a particular value of ω, however for other generic values the theory nonlinearly realizes SI but not the full conformal group. We must mention that the theory presented in (5.4) is a novel example of a SI theory that does not realize the full conformal group. This is yet another example of SI theory, such as the ones presented in [159]. The theory of the spontaneously broken SI solid avoids being conformally invariant since its ground state breaks the Poincaré symmetry, as we discussed in Section 5.1.

The sub-case of the manifest SI solid needs to be treated with holographic methods due to the dynamics of the phonon modes are controlled by an IRFP. In particular, we use a massive gravity theory in an asymptotically AdS_4 space-time, whose elastic response was shown to be associated with the presence of massless propagating phonons [6]. Contrary to the spontaneous case, here the phonon modes are part of a continuum spectrum instead of being isolated degrees of freedom. This is the reason why the EFT methods used in the first sub-case cannot be applied here.

We have found that the phonon speeds can be slow compared to the speed of light in the SI solids, as long as we have ω small. In particular, we found that the longitudinal and transverse speeds are related as

$$c_L^2 = \omega\, c^2 + \frac{2\,(d-2)}{d-1}\, c_T^2 \tag{6.3}$$

with ω being the equation of state and d are the space-time dimensions. It is a necessary condition, as we can see, that the equation of state parameter is small in order to have slow phonon speeds, which would be needed if we wanted to describe realistic materials. This result shows that it is possible to have a SI solid with realistic (small) phonon speeds, while conformal solids, such as the one presented in [79], are restricted to have relativistic phonon speeds. Even in the case of the manifest SI solid we have proposed a way to obtain non-relativistic speeds but further research in this direction is needed.

In both SI solids we compute several linear elastic response parameters, such as the elastic moduli, the Poisson ratio or the propagation speed of the phonons in function of the various parameters of the model. We find that in both cases maximally auxetic solids (i.e. most negative Poisson ratio) may only arise in the limit of $\omega \ll 1$, otherwise

the theory will have superluminal phonon modes (e.g. see Figure 5.8).

In the case of the holographic model it is straightforward extract the temperature dependence of elastic properties, which allows us to show that these models interopolate between a fluid phase and a solid phase by decreasing the temperature. The crossover is continous and very analogous to what happens to some extent in glasses and amorphous materials. The behaviour of the vibrational modes in these holographic systems has already produced some developments in the study of the latter [29,30]. In the Appendix A we also discuss some aspects involving the thermodynamic properties of the holographic model, which we would like to extend in the future to introduce more acoustocaloric effects, which seem to be having growing interest recently [78, 118, 140, 166, 221]. Furthermore, it would be desirable to introduce dissipative and thermal effects within the EFT picture of condensed matter systems [77, 210].

In addition to the linear elastic properties we analyzed the non-linear mechanical response of SI solids from both perspectives. In the case of the solids with spontaneously broken SI we already worked out the stress-strain relations and the elasticity bounds in the generic solid EFT case. For the case of the manifest SI solid we showed how the elastic response can be extended to the full non-linear regime by obtaining the full stress-strain curves. To our knowledge, this is the first time that the full non-linear response of an AdS black brane geometry is presented by extracting the corresponding stress-strain curve. Previous studies already discussed the linear approximation of this elastic response, while [15, 26] discussed the viscoelastic oscillatory (i.e. non-static) response and [46] an out-of-equilibrium similar set up. Let us highlight the three main differences between the two SI solids in the non-linear response:

- The elasticity bounds for the two types of solids differ substantially from each other as we clearly see in Figure 5.14. The range of the accepted strain scaling are almost decoupled and the values of the deformability $\epsilon_{\max}$ disagree by $\mathcal{O}(1)$ factors. This discrepancy seems to be physical and due to the fact that SI is realized differently in the two cases considered, thus the non-linear constrains for the theories must be different.

- The holographic model presents an interesting feature in the stress strain curves: it exhibits two different regimes of power-law stress-strain curves. At finite temperature we find a scaling at moderately large deformation (of order $1 < \epsilon < 10$) and a second scaling at very large deformations, which is always smaller than the first one. In the case of very low temperature only the second scaling controls the stress-strain curve. The fact that this scaling appears is because these models

contain a UV anisotropic Lifshitz fixed point. Whether this feature is specific to the present model or whether it would appear in more generic elastic solids with manifest SI remains unclear. However, we should note that for finite temperature this second scaling could be rather irrelevant, as it appears at extremely large deformations (i.e. $\epsilon > 10$) where most solutions show already some instability.

- Similarly to what happens in the case of non-relativistic solid EFTs the holographic models that exhibit highest elasticity share features similar to familiar real-world elastomers. Indeed, we find that the model allows black brane solutions to be stable under large deformations where bulk and shear scalings are of the same order $\nu_B \sim \nu_S$ (see Figure 5.14). This is similar to what happens for natural rubber and other elastomers [81], thus it motivates us to call these type of solutions *black rubber*.

There are some applications that could be derived from the study of these systems. We know that the electric transport properties of quantum critical materials have been subject of recent efforts especially in connection to the anomalous scalings found in strange metals. More recently there has been interest in whether phonons and elastic properties can display surprising and interesting characteristics in these quantum critical materials. In particular there are preliminary indications that phonons in quantum critical systems may exhibit glassy or viscoelastic features [120]. Furthermore, the role of such viscoelastic properties of the materials has been discussed in connection to the possible implications on high-T_c superconductivity [195] and some experimental reasearch has also explored the elastic properties of high-T_c cuprates superconductors [187].

There has been a particular interest recently related to the non-linear mechanical characterization of critical materials (such as the high-T_c superconductors) due to the technological applications these materials have [190, 191]. Hopefully the holographic methods presented here may provide useful insights in the properties of these materials.

Appendix A

Thermodynamic properties of solids with manifest scale invariance

These results are not part of any publication.

Heat capacities

Due to this model of solids with manifest SI has a finite temperature description it is worth taking a look at some of its thermodynamic properties, such as the heat capacities of the system.

In thermodynamics, the heat capacity ratio is the ratio of the heat capacity at constant pressure, C_P, and the heat capacity at constant volume, C_V. The heat capacity of a system tells us how much heat ΔQ we need to add in order to raise its temperature ΔT

$$C = \lim_{\Delta T} \frac{\Delta Q}{\Delta T}. \tag{A.1}$$

This heat capacity can be defined also depending on the kind of process the system is undergoing, whether we are doing it at constant pressure or constant volume. Thus, let us define these two heat capacities (per unit volume) as

$$C_V = \frac{T}{\mathcal{V}} \left(\frac{\partial S}{\partial T}\right)_{\mathcal{V}} = \frac{4\,\pi(3 - m^2\,u_h^{2\,\mathfrak{b}})}{u_h^2\,(3 + (2\,\mathfrak{b} - 1)\,m^2\,u_h^{2\,\mathfrak{b}})}\,, \tag{A.2}$$

$$C_P = \frac{T}{\mathcal{V}} \left(\frac{\partial S}{\partial T}\right)_{p} = \frac{3\,\pi\,u_h^{-2(1+\mathfrak{b})}(3 - m^2\,u_h^{2\mathfrak{b}})(-3 + 2\,\mathfrak{b} + m^2\,u_h^{2\,\mathfrak{b}})}{\mathfrak{b}\,m^2\,(-3 + 3\,\mathfrak{b} + m^2\,u_h^{2\,\mathfrak{b}})} \tag{A.3}$$

where we have used the second law of thermodynamics $\delta Q = T\,dS$. These heat capacities grow with temperature, just like is expected for solid materials, and have a

quadratic scaling for C_V and a scaling of $\nu_1^B + 2 = 2\,(\mathfrak{b}+1)$ for C_P, as we can observe in Figure A.1. However, in solid materials it is also expected that at large temperatures these heat capacities saturate at some constant value as we can see in [22].

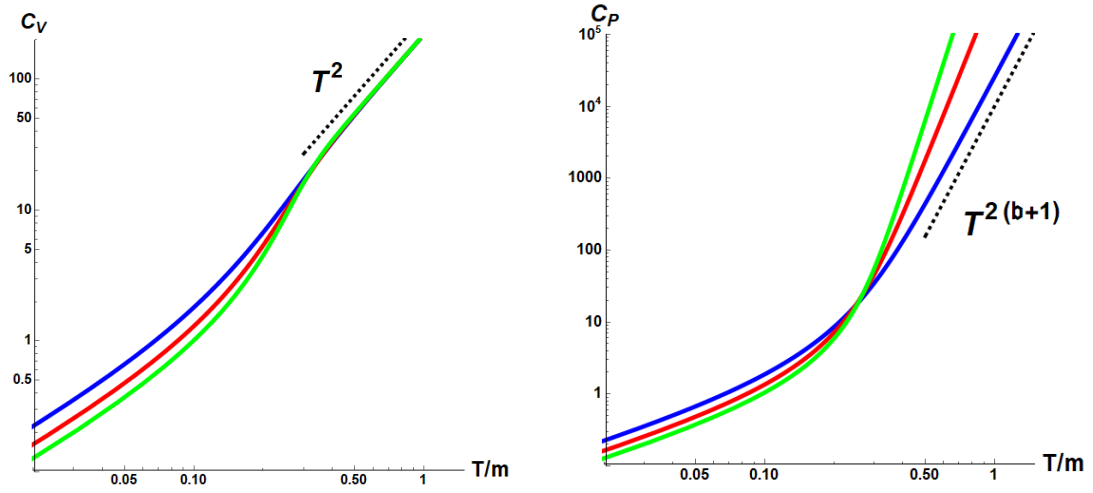

Figure A.1: Heat capacity at constant volume C_V (left) and constant pressure C_P (right) for a benchmark potential with $\mathfrak{b} = 2, 3, 4$ (blue, red, green) as a function of the temperature T/m.

From these two heat capacities we can also construct another interesting thermodynamical relation: the heat capacity ratio γ. The heat capacity ratio is defined as the ratio between the heat capacities and for our benchmark potential we obtain

$$\gamma \equiv \frac{C_P}{C_V} = \frac{3\,(2\,\mathfrak{b} - 3 + m^2\,u_h^{2\,\mathfrak{b}})\,(3 + (2\,\mathfrak{b} - 1)\,m^2\,u_h^{2\,\mathfrak{b}})}{u_h^{2\,\mathfrak{b}}\,4\,\mathfrak{b}\,m^2\,(-3 + 3\,\mathfrak{b} + m^2\,u_h^{2\,\mathfrak{b}})}\,. \tag{A.4}$$

This heat capacity ratio is exactly $\gamma = 1$ for $T/m = 0$, as solids have very similar pressure and volume heat capacities $C_P \sim C_V$, and grows with temperature with a power-law scaling of $\nu_1^B = 2\,\mathfrak{b}$.

Interestingly, this γ is related to two different notions of bulk moduli. Up until now we have just considered the adiabatic bulk modulus (e.g. see (5.49)-(5.50) or (5.112)) -which now we are going to label $\mathcal{K}_S$ to avoid confusion- but there is a second notion of bulk modulus which is the isothermal bulk modulus. This second definition considers a constant temperature process instead of an adiabatic one

$$\mathcal{K}_T = -\mathcal{V}\,\left.\frac{dp}{d\mathcal{V}}\right|_T\,. \tag{A.5}$$

However, the bulk modulus that controls the speed of phonon modes is K_S as noted in [138].
With this definition we can check that both the ratios of the heat capacities and the bulk moduli are exactly the same, as expected,

$$\gamma \equiv \frac{C_P}{C_V} = \frac{\mathcal{K}_S}{\mathcal{K}_T}\,. \tag{A.6}$$

We should note here that the definition we are employing here is in tension with the one considered in [11,19], where the bulk modulus is defined through a so-called lattice pressure p_l, an extra contribution to T_{xx} as a result of working around a uniformly strained equilibrium state. Therefore, using that definition for the bulk modulus the form of the longitudinal speed changes substantially from (3.15).

The interested reader may read [19] for the exact definition of this lattice pressure. Let us point here that p_l is related to T_{xx} and to the so-called *thermodynamic pressure* p_{th} which is defined through the thermodynamic potential Ω as

$$p_{th}\cdot\mathcal{V} \equiv -\Omega = -T\,S_E \tag{A.7}$$

where S_E is the Euclidean on-shell boundary action. This pressure fulfills the thermodynamical relation

$$p_{th} + \rho = s\,T \tag{A.8}$$

and differs from T_{xx} as discussed in [9]. All in all, the relation among these three pressure is

$$p = T_{xx} = p_{th} + p_l\,. \tag{A.9}$$

There is another thermodynamic relation that indicates us that working with the mechanical pressure T_{xx} seems to be the sane choice. According to [138] we should have

$$C_P - C_V = T\,\alpha_T^2\,\mathcal{K}_T \tag{A.10}$$

where α_T is the thermal expansion coefficient

$$\alpha_T \equiv \frac{1}{\mathcal{V}}\left(\frac{\partial\,\mathcal{V}}{\partial\,T}\right)_p = \frac{1}{\mathcal{K}_T}\left(\frac{\partial\,p}{\partial\,T}\right)_V\,. \tag{A.11}$$

It is easy to check that (A.10) only holds if we consider the mechanical pressure $p = T_{xx}$. Using this definition we may obtain the thermal expansion coefficient

$$\alpha_T = -\frac{2\,(2\,\mathfrak{b}-3)\,\pi u_h^{1-2\,\mathfrak{b}}(-3+m^2\,u_h^{2\,\mathfrak{b}})}{\mathfrak{b}\,m^2\,(-3+3\,\mathfrak{b}+m^2\,u_h^{2\,\mathfrak{b}})} \tag{A.12}$$

which is positive and grows with temperature with a power-law scaling of $\nu_1^B - 1 = 2\mathfrak{b} - 1$. This result is completely different from the one in [19], where the thermal expansion they obtain from (A.11) is negative, decreases with temperature as $1/T$ and is independent of the potential chosen.

Grüneisen parameter

In solid state physics, the Grüneisen parameter γ_G was originally introduced to study the effect of varying the volume of a crystal lattice in its vibrational frequency [135] and has been used to investigate the characteristic energy scales of systems with respect to changes of external potentials[1].

The original formulation of γ_G was proposed by E. Grüneisten for the Einstein model [93,94] and it was used to quantify the degree of anharmonicity of the structure of the energy spectrum in volume changes:

$$\gamma_G \equiv -\frac{\mathcal{V}}{\omega_0}\frac{\partial\,\omega_0}{\partial\mathcal{V}} = \frac{\mathcal{V}}{C_V}\left(\frac{\partial S}{\partial\mathcal{V}}\right)_T = \frac{\alpha_T\,\mathcal{V}}{C_V}\,\mathcal{K}_T = -\left(\frac{\partial\log T}{\partial\log\mathcal{V}}\right)_S \tag{A.13}$$

where the excitations in a solid are described by N phonons with the same frequency ω_0 (notice that for an harmonic model phonon frequencies would be volume independent).

The Grüneisen parameter for our model is remarkably simple, it is quite easy to find that

$$\gamma_G = \frac{1}{2} \tag{A.14}$$

so it does not depend on temperature or even the potential.

We should note that in [136,227] it was found that due to the temperature scaling of C_p and α_T the Grüneisen parameter diverges when approaching to a quantum critical point.

[1] See [223] for a review on the Grüneisen parameter.

Appendix B

More on solid EFT in d dimensions

In order to compute the speeds of the phonon modes we need to calculate the quadratic action on the perturbations around the background of the fields $\Phi^I = \alpha\,(x^I + \pi^I)$ which give us

$$\mathcal{I}_{IJ} \;=\; \alpha^2(\delta_{IJ} + \partial_I\pi_J + \partial_J\pi_I + \partial^\mu\pi_I\,\partial_\mu\pi_J). \tag{B.1}$$

The most relevant expressions up to quadratic order are summarized below

$$\begin{aligned}\mathrm{Tr}(\mathcal{I}^n) \;=&\alpha^{2n}\big((d-1) - n\,\dot\pi_i{}^2 + 2\,n\,\partial_i\,\pi_i^L \\ &+ n\,(2n-1)\,(\partial_i\,\pi_i^L)^2 + n^2\,(\partial_i\,\pi_j^T)^2\big),\end{aligned} \tag{B.2}$$

$$Z \;=\; \alpha^{2(d-1)}\left(1 + 2\,\partial_i\,\pi_i^L - \dot\pi_i{}^2 + (\partial_i\,\pi_i^L)^2\right), \tag{B.3}$$

$$x_n \equiv \frac{\mathrm{Tr}(\mathcal{I}^n)}{Z^{\frac{n}{d-1}}} = d - 1 + n^2\,(\partial_i\,\pi_j^T)^2 + \frac{2(d-2)}{d-1}\,n^2\,(\partial_i\,\pi_i^L)^2, \tag{B.4}$$

where we have split the perturbation into longitudinal and transverse modes

$$\partial_i\,\pi_i^T \;=\; 0 \quad , \quad \partial_{[i}\,\pi_{j]}^L \;=\; 0. \tag{B.5}$$

The action at second order is then

$$\delta S^{(2)} = -\int d^dx\left(-N\,\dot\pi_i{}^2 + c_1^2\,(\partial_i\,\pi_i^L)^2 + c_2^2\,(\partial_i\,\pi_j^T)^2\right) \tag{B.6}$$

where

$$N = Z\,V_Z\,, \tag{B.7}$$

$$c_L^2 = \frac{c_1^2}{N} = 1 + \frac{2\,V_{ZZ}\,Z}{V_Z} + \frac{2(d-2)}{d-1}\,c_T^2\,, \tag{B.8}$$

$$c_T^2 = \frac{c_2^2}{N} = \sum_{n=1}^{d-2} \frac{n^2\,V_{x_n}}{Z\,V_Z}. \tag{B.9}$$

We would like to relate this to the bulk and shear moduli. The stress-energy tensor is

$$T_{\mu\nu} = -\frac{2}{\sqrt{-g}}\frac{\delta S}{\delta g^{\mu\nu}} = -\eta_{\mu\nu}\,V + 2\,\frac{\partial V}{\partial \mathcal{I}^{IJ}}\,\partial_\mu\Phi^I\,\partial_\nu\Phi^J. \tag{B.10}$$

Our potential is a function of Z and x_n, so

$$\begin{aligned}\frac{\partial V}{\partial \mathcal{I}^{IJ}} &= \frac{\partial Z}{\partial \mathcal{I}^{IJ}}\,\frac{\partial V}{\partial Z} \\ &+ \sum_{n=1}^{d-2}\Big(\frac{\partial \mathrm{Tr}(\mathcal{I}^n)}{\partial \mathcal{I}^{IJ}}\,\frac{1}{Z^{n/d-1}} - \frac{\partial Z}{\partial \mathcal{I}^{IJ}}\,\frac{n}{d-1}\,\frac{x_n}{Z}\Big)\frac{\partial V}{\partial x_n}\,.\end{aligned} \tag{B.11}$$

Let us start computing the shear modulus. The shear strain changes our background to

$$\Phi^I = x^I + \varepsilon^I_k x^k \tag{B.12}$$

where we can take $\varepsilon^I_J = \varepsilon^J_I$ with no loss of generality. We assume that $\varepsilon^j_i \neq 0$ for $i \neq j$ and look at the component T_{ij} at first order in ε^j_i, and extract the shear modulus comparing with equation (3.6). Notice that the term $\frac{\partial Z}{\partial \mathcal{I}^{IJ}}$ cancels with $\partial_i\Phi^I\partial_j\Phi^J$. To check this, first we make the derivative of Z with respect to $\mathcal{I}^{IJ}$ using Jacobi's formula

$$\frac{\partial Z}{\partial \mathcal{I}^{IJ}} = \mathrm{adj}^T(\mathcal{I})_{IJ}. \tag{B.13}$$

Contracting this with

$$\partial_i\Phi^I\partial_j\Phi^J = (\delta^I_i\delta^J_j + \delta^I_i\varepsilon^J_j + \delta^J_j\varepsilon^I_i)\,\alpha^2 + \mathcal{O}(\varepsilon^2). \tag{B.14}$$

At linear order we find that $\mathrm{adj}^T(\mathcal{I})_{ij} = -2\,\varepsilon_{ij}\,\alpha^{2d-4}$ (with $i \neq j$) and $\mathrm{adj}^T(\mathcal{I})_{ii} = \alpha^{2d-4}(1+\mathcal{O}(\varepsilon))$. Therefore

$$\begin{aligned}&\frac{\partial Z}{\partial \mathcal{I}^{IJ}}\,(\delta^I_i\delta^J_j + \delta^I_i\varepsilon^J_j + \delta^J_j\varepsilon^I_i)\,\alpha^2 \\ &= \mathrm{adj}^T(\mathcal{I})_{ij}\,\alpha^2 + 2\,\alpha^{2(d-1)}\,\varepsilon_{ij} = 0.\end{aligned} \tag{B.15}$$

The only non-zero term is then

$$T_{ij} \,=\, 2\sum_{n=1}^{d-2}\frac{\partial V}{\partial x_n}\,\frac{\partial \mathrm{Tr}((\mathcal{I}^{KL})^n)}{\partial \mathcal{I}^{IJ}}\,\frac{1}{Z^{n/d-1}}\,\partial_i\Phi^I\,\partial_j\Phi^J. \tag{B.16}$$

For the derivative of the traces,
$\mathrm{Tr}(\mathcal{I}^n)=\mathcal{I}^{I_1\,I_2}\,\mathcal{I}^{I_2\,I_3}\,\ldots\,\mathcal{I}^{I_{n-1}\,I_n}\,\mathcal{I}^{I_n\,I_1}$, one finds

$$\frac{\partial \mathrm{Tr}(\mathcal{I})}{\partial \mathcal{I}^{IJ}}=\delta_{IJ}\,,\qquad \frac{\partial \mathrm{Tr}(\mathcal{I}^2)}{\partial \mathcal{I}^{IJ}}=2\,\mathcal{I}_{IJ}\,,$$

and

$$\frac{\partial \mathrm{Tr}(\mathcal{I}^n)}{\partial \mathcal{I}^{IJ}} \,=\, n\,\mathcal{I}^{I\,I_3}\,\mathcal{I}^{I_3\,I_4}\,\ldots\,\mathcal{I}^{I_{n-1}\,I_n}\,\mathcal{I}^{I_n\,J} \tag{B.17}$$

for $n>2$, where we have used the cyclic property of the trace. Since $\mathcal{I}^{IJ}=\alpha^2(\delta_{IJ}+\varepsilon^I_J+\varepsilon^J_I)$, finally we can find that at linear order

$$T_{ij} \,=\, 4\,\varepsilon_{ij}\sum_{n=1}^{d-2} n^2\,\frac{\partial V}{\partial x_n} \,=\, 2\,\varepsilon_{ij}\,\mathcal{G}. \tag{B.18}$$

For the bulk modulus we consider a purely volume deformation (zero shear), which can be parametrized as

$$\alpha=1+\frac{\kappa}{d-1} \tag{B.19}$$

where κ is the bulk strain, and we look at T_{ii}.

Notice that V_{x_n} does not appear here as we can easily check using $\partial_i\Phi^I\,\partial_i\Phi^J=\alpha^2\delta^I_i\,\delta^J_i$

$$\left(\frac{\partial \mathrm{Tr}(\mathcal{I}^n)}{\partial \mathcal{I}^{ii}}\,\frac{1}{Z^{n/d-1}}\,-\,\frac{\partial Z}{\partial \mathcal{I}^{ii}}\,\frac{n}{d-1}\,\frac{x_n}{Z}\right)\alpha^2 \,=\, 0. \tag{B.20}$$

Therefore we arrive to

$$T_{ii} \,=\, -V+2\,Z\,V_Z \tag{B.21}$$

and from the equation above we can already find the important result

$$\rho+p=2\,Z\,V_Z\,. \tag{B.22}$$

Finally, using the definition of the bulk modulus (3.7) together with $\mathcal{V}\propto\alpha^{1-d}$ and (B.19), one arrives at

$$\mathcal{K}\equiv-\mathcal{V}\,\frac{dp}{d\mathcal{V}}=\,\frac{dp}{d\kappa}\,=\,\frac{dT_{ii}}{d\kappa} \tag{B.23}$$

From (B.21), then, one finds

$$\mathcal{K} \,=\, 2\,Z\,V_Z \,+\, 4\,Z^2\,V_{ZZ} = 4\,Z^{3/2}\,\partial_Z\left(\sqrt{Z}\,V_Z\right). \tag{B.24}$$

It is also possible to rewrite, the bulk modulus in terms of the equation of state of the solid, understood as the functional dependence of the pressure on the energy density, that is $P(\rho)|_{\square}$, by changing only the density – that is at zero shear strain. Note that

$$\mathcal{K} \,=\, \frac{dp}{d\rho}\,\frac{d\rho}{dZ}\,\frac{dZ}{d\kappa} \,=\, \frac{dp}{d\rho}\,2\,Z\,V_Z, \tag{B.25}$$

where we use $\rho = V$. Therefore we find

$$\frac{\mathcal{K}}{\rho + p} \,=\, \frac{dp}{d\rho}\Big|_{\square}\,, \tag{B.26}$$

which leads to (5.8). The subscript $|_{\square}$ stands to recall that the derivative is at vanishing shear deformation.

Appendix C

Holographic Stress Tensor

We can explicitely compute the boundary stress tensor $T^{\mu\nu}$ following [32]. In particular, for asymptotic AdS_4 spacetime, we have:

$$T^{\mu\nu} = \frac{1}{8\,\pi\,G}\left(\Theta^{\mu\nu} - \Theta\,\Xi^{\mu\nu} - 2\,\Xi^{\mu\nu} - G^{\mu\nu}_{\Xi}\right), \tag{C.1}$$

where we set the AdS length $l = 1$. The metric $\Xi_{\mu\nu}$ is the boundary metric and $\Theta^{\mu\nu}$ the extrinsic curvature of the boundary surface, with Θ its trace. Our boundary metric is given by

$$\Xi_{ij} = \frac{1}{u^2}\begin{pmatrix} e^{-\chi(u)}\,f(u) & 0 & 0 \\ 0 & \cosh h(u) & \sinh h(u) \\ 0 & \sinh h(u) & \cosh h(u) \end{pmatrix} \tag{C.2}$$

and it is clearly flat, implying $G^{\mu\nu}_{\Xi} = 0$. We can define the normal vector to the boundary as:

$$n_\mu = \left(0\,,\,0\,,\,0\,,\,\frac{1}{\sqrt{g^{uu}}}\right), \tag{C.3}$$

where $g^{uu} = u^2 f(u)$. The extrinsic curvature can be defined as usual

$$\theta_{\mu\nu} = \frac{1}{2}\left(\nabla_\mu n_\nu + \nabla_\nu n_\mu\right), \tag{C.4}$$

and it reads

$$\theta = \frac{u\,f'(u) - f(u)\,(6 + u\chi'(u))}{2\sqrt{f(u)}}. \tag{C.5}$$

Close to the boundary, we can expand the function $h(u)$ as in (5.44) and $f(u) = 1 - M(u)u^3$ (where $M(0)$ would correspond to the energy density of the system) and

find that the off-diagonal component of the stress-energy tensor is

$$T_{xy} \;=\; \frac{1}{2}\left(3\,\mathcal{C}_3\cosh\left(\mathcal{C}_0\right) \;+\; M(0)\sinh(\mathcal{C}_0)\right) \tag{C.6}$$

This result is a direct manifestation of the presence of a strain deformation in our background and it will encode the corresponding response, *i.e.* the shear component of the stress.
Interestingly one can also notice that

$$T_x{}^y \;=\; \frac{3}{2}\mathcal{C}_3. \tag{C.7}$$

Using the standard holographic renormalization techniques [197] we can also identify

$$T_{\mu\nu} \;=\; \frac{3}{2}g^{(3)}_{\mu\nu}, \tag{C.8}$$

where $g^{(3)}_{\mu\nu}$ is the sub-leading term of the induced metric expressed in Fefferman-Graham coordinates. As a first step we have to rewrite our ansatz in the FG form using the coordinate transformation

$$\frac{dz^2}{z^2} \;=\; \frac{du^2}{u^2\,f(u)} \tag{C.9}$$

where z will now be the holographic (FG) coordinate.

Again, using that the asymptotic behaviour of $f(u)$ is $1-M(u)u^3$ we can find that for small z we have $u = z - \frac{M(z)z^4}{6}$. Now we can already look at our metric and derive the stress-energy tensor. For instance, for the off-diagonal term, we are interested in, we have

$$g_{xy}(z) \;=\; \frac{1}{u(z)^2}\sinh(h(u(z))) = \tag{C.10}$$

$$= \;\frac{1}{z^2}\left(\sinh(\mathcal{C}_0) + \left(3\,\mathcal{C}_3\cosh\left(\mathcal{C}_0\right) \;+\; M(0)\sinh(\mathcal{C}_0)\right)z^3\right), \tag{C.11}$$

where higher orders in z have been suppressed. We can identify T_{xy} easily in this expression and see that the result is the same we found before in C.6. This result give us a robust definition of the non-linear stress in our system which can be indeed identified as:

$$\sigma \;=\; \frac{1}{2}\left(3\,\mathcal{C}_3\cosh\left(\mathcal{C}_0\right) \;+\; M(0)\sinh(\mathcal{C}_0)\right) \tag{C.12}$$

Since we impose the boundary condition $\mathcal{C}_0 = 0$ the stress, we use in all our computations, is simply defined by $\sigma \;=\; \frac{3}{2}\,\mathcal{C}_3$.

Bibliography

[1] Z. Abiza, M. Destrade, and R.W. Ogden. Large acoustoelastic effect. Wave Motion, 49(2):364 – 374, 2012.

[2] Allan Adams, Nima Arkani-Hamed, Sergei Dubovsky, Alberto Nicolis, and Riccardo Rattazzi. Causality, analyticity and an IR obstruction to UV completion. JHEP, 10:014, 2006.

[3] Ofer Aharony, Yaron E. Antebi, Micha Berkooz, and Ram Fishman. 'Holey sheets': Pfaffians and subdeterminants as D-brane operators in large N gauge theories. JHEP, 12:069, 2002.

[4] Ofer Aharony, Oren Bergman, Daniel Louis Jafferis, and Juan Maldacena. N=6 superconformal Chern-Simons-matter theories, M2-branes and their gravity duals. JHEP, 10:091, 2008.

[5] Lasma Alberte, Martin Ammon, Matteo Baggioli, Amadeo Jiménez, and Oriol Pujolàs. Black hole elasticity and gapped transverse phonons in holography. JHEP, 01:129, 2018.

[6] Lasma Alberte, Martin Ammon, Amadeo Jiménez-Alba, Matteo Baggioli, and Oriol Pujolàs. Holographic Phonons. Phys. Rev. Lett., 120(17):171602, 2018.

[7] Lasma Alberte, Matteo Baggioli, Victor Cancer Castillo, and Oriol Pujolas. Elasticity bounds from Effective Field Theory. Phys. Rev., D100(6):065015, 2019.

[8] Lasma Alberte, Matteo Baggioli, Andrei Khmelnitsky, and Oriol Pujolas. Solid Holography and Massive Gravity. JHEP, 02:114, 2016.

[9] Lasma Alberte, Matteo Baggioli, and Oriol Pujolas. Viscosity bound violation in holographic solids and the viscoelastic response. JHEP, 07:074, 2016.

[10] Martin Ammon, Matteo Baggioli, Seán Gray, and Sebastian Grieninger. Longitudinal Sound and Diffusion in Holographic Massive Gravity. JHEP, 10:064, 2019.

[11] Martin Ammon, Matteo Baggioli, Seán Gray, Sebastian Grieninger, and Akash Jain. On the Hydrodynamic Description of Holographic Viscoelastic Models. Phys. Lett. B, 808:135691, 2020.

[12] Martin Ammon, Matteo Baggioli, and Amadeo Jiménez-Alba. A Unified Description of Translational Symmetry Breaking in Holography. JHEP, 09:124, 2019.

[13] Martin Ammon and Johanna Erdmenger. Gauge/gravity duality. Cambridge University Press, Cambridge, 2015.

[14] Mohamed M. Anber and John F. Donoghue. The Emergence of a universal limiting speed. Phys. Rev., D83:105027, 2011.

[15] Tomas Andrade, Matteo Baggioli, and Oriol Pujolàs. Linear viscoelastic dynamics in holography. Phys. Rev. D, 100(10):106014, 2019.

[16] Tomas Andrade and Donald Marolf. AdS/CFT beyond the unitarity bound. JHEP, 01:049, 2012.

[17] Tomas Andrade and Benjamin Withers. A simple holographic model of momentum relaxation. JHEP, 05:101, 2014.

[18] Jay Armas, Jakob Gath, Akash Jain, and Andreas Vigand Pedersen. Dissipative hydrodynamics with higher-form symmetry. 2018.

[19] Jay Armas and Akash Jain. Hydrodynamics for charge density waves and their holographic duals. Phys. Rev. D, 101(12):121901, 2020.

[20] Jay Armas and Akash Jain. Viscoelastic hydrodynamics and holography. JHEP, 01:126, 2020.

[21] Ellen M. Arruda and Mary C. Boyce. A three-dimensional constitutive model for the large stretch behavior of rubber elastic materials. Journal of the Mechanics and Physics of Solids, 41(2):389–412, 1 1993.

[22] B. M. Askerov and M. Cankurtaran. Isobaric specific heat and thermal expansion of solids in the debye approximation. physica status solidi (b), 185(2):341–348, October 1994.

[23] Matteo Baggioli, Victor Cancer Castillo, and Oriol Pujolas. Black Rubber and the Non-linear Elastic Response of Scale Invariant Solids. 6 2020.

[24] Matteo Baggioli, Victor Cancer Castillo, and Oriol Pujolas. Scale invariant solids. Phys. Rev., D101(8):086005, 2020.

[25] Matteo Baggioli and Sebastian Grieninger. Zoology of Solid & Fluid Holography : Goldstone Modes and Phase Relaxation. 2019.

[26] Matteo Baggioli, Sebastian Grieninger, and Hesam Soltanpanahi. Nonlinear Oscillatory Shear Tests in Viscoelastic Holography. Phys. Rev. Lett., 124(8):081601, 2020.

[27] Matteo Baggioli and Wei-Jia Li. Universal Bounds on Transport in Holographic Systems with Broken Translations. 5 2020.

[28] Matteo Baggioli and Oriol Pujolas. Electron-Phonon Interactions, Metal-Insulator Transitions, and Holographic Massive Gravity. Phys. Rev. Lett., 114(25):251602, 2015.

[29] Matteo Baggioli and Alessio Zaccone. Universal origin of boson peak vibrational anomalies in ordered crystals and in amorphous materials. Phys. Rev. Lett., 122(14):145501, 2019.

[30] Matteo Baggioli and Alessio Zaccone. Low-energy optical phonons induce glassy-like vibrational and thermal anomalies in ordered crystals. Journal of Physics: Materials, 3(1):015004, January 2020.

[31] Borut Bajc and Adrian R. Lugo. On the matching method and the Goldstone theorem in holography. JHEP, 07:056, 2013.

[32] Vijay Balasubramanian and Per Kraus. A Stress tensor for Anti-de Sitter gravity. Commun. Math. Phys., 208:413–428, 1999.

[33] J. Bardeen, L. N. Cooper, and J. R. Schrieffer. Microscopic theory of superconductivity. Physical Review, 106(1):162–164, April 1957.

[34] J. Bardeen, L. N. Cooper, and J. R. Schrieffer. Theory of superconductivity. Physical Review, 108(5):1175–1204, December 1957.

[35] Paulo Bedaque and Andrew W. Steiner. Sound velocity bound and neutron stars. Phys. Rev. Lett., 114(3):031103, 2015.

[36] Grigory Bednik, Oriol Pujolàs, and Sergey Sibiryakov. Emergent Lorentz invariance from Strong Dynamics: Holographic examples. JHEP, 11:064, 2013.

[37] Aron J. Beekman, Jaakko Nissinen, Kai Wu, Ke Liu, Robert-Jan Slager, Zohar Nussinov, Vladimir Cvetkovic, and Jan Zaanen. Dual gauge field theory of quantum liquid crystals in two dimensions. Phys. Rept., 683:1–110, 2017.

[38] Aron J. Beekman, Jaakko Nissinen, Kai Wu, and Jan Zaanen. Dual gauge field theory of quantum liquid crystals in three dimensions. Phys. Rev., B96(16):165115, 2017.

[39] J. D. Bekenstein. Black holes and the second law. Lett. Nuovo Cim., 4:737–740, 1972.

[40] Jacob D. Bekenstein. Black holes and entropy. Phys. Rev., D7:2333–2346, 1973.

[41] Jacob D. Bekenstein. Generalized second law of thermodynamics in black hole physics. Phys. Rev., D9:3292–3300, 1974.

[42] Micha Berkooz, Amit Sever, and Assaf Shomer. 'Double trace' deformations, boundary conditions and space-time singularities. JHEP, 05:034, 2002.

[43] Jyotirmoy Bhattacharya, Sera Cremonini, and Blaise Goutéraux. Intermediate scalings in holographic RG flows and conductivities. JHEP, 02:035, 2015.

[44] Sayantani Bhattacharyya, Veronika E Hubeny, Shiraz Minwalla, and Mukund Rangamani. Nonlinear Fluid Dynamics from Gravity. JHEP, 02:045, 2008.

[45] Massimo Bianchi, Daniel Z. Freedman, and Kostas Skenderis. How to go with an RG flow. JHEP, 08:041, 2001.

[46] Anxo Biasi, Javier Mas, and Alexandre Serantes. Gravitational wave driving of a gapped holographic system. JHEP, 05:161, 2019.

[47] Dima Bolmatov, Vadim Brazhkin, and Kostya Trachenko. The phonon theory of liquid thermodynamics. 2012.

[48] Raphael Bousso. The Holographic principle. Rev. Mod. Phys., 74:825–874, 2002.

[49] Peter Breitenlohner and Daniel Z. Freedman. Positive energy in anti-de sitter backgrounds and gauged extended supergravity. Physics Letters B, 115(3):197–201, September 1982.

[50] Peter Breitenlohner and Daniel Z. Freedman. Positive Energy in anti-De Sitter Backgrounds and Gauged Extended Supergravity. Phys. Lett., 115B:197–201, 1982.

[51] Peter Breitenlohner and Daniel Z Freedman. Stability in gauged extended supergravity. Annals of Physics, 144(2):249–281, December 1982.

[52] Peter Breitenlohner and Daniel Z. Freedman. Stability in Gauged Extended Supergravity. Annals Phys., 144:249, 1982.

[53] Mauro Brigante, Hong Liu, Robert C. Myers, Stephen Shenker, and Sho Yaida. Viscosity Bound Violation in Higher Derivative Gravity. Phys. Rev. D, 77:126006, 2008.

[54] Curtis G. Callan, Sidney Coleman, J. Wess, and Bruno Zumino. Structure of phenomenological lagrangians. ii. Phys. Rev., 177:2247–2250, Jan 1969.

[55] Curtis G. Callan, Jr., Sidney R. Coleman, and Roman Jackiw. A New improved energy - momentum tensor. Annals Phys., 59:42–73, 1970.

[56] B. Carter. Axisymmetric Black Hole Has Only Two Degrees of Freedom. Phys. Rev. Lett., 26:331–333, 1971.

[57] Jorge Casalderrey-Solana, Hong Liu, David Mateos, Krishna Rajagopal, and Urs Achim Wiedemann. Gauge/String Duality, Hot QCD and Heavy Ion Collisions. 2011.

[58] S. Chadha and Holger Bech Nielsen. LORENTZ INVARIANCE AS A LOW-ENERGY PHENOMENON. Nucl. Phys., B217:125–144, 1983.

[59] P. M. Chaikin and T. C. Lubensky. Principles of Condensed Matter Physics. Cambridge University Press, 1995.

[60] Geoffrey F. Chew and S. C. Frautschi. Principle of equivalence for all strongly interacting particles within the *s*-matrix framework. Phys. Rev. Lett., 7:394–397, Nov 1961.

[61] S. Coleman, J. Wess, and Bruno Zumino. Structure of phenomenological lagrangians. i. Phys. Rev., 177:2239–2247, Jan 1969.

[62] Sidney R. Coleman and Roman Jackiw. Why dilatation generators do not generate dilatations? Annals Phys., 67:552–598, 1971.

[63] Xin Cong, Qiao-Qiao Li, Xin Zhang, Miao-Ling Lin, Jiang-Bin Wu, Xue-Lu Liu, P. Venezuela, and Ping-Heng Tan. Probing the acoustic phonon dispersion and sound velocity of graphene by raman spectroscopy. Carbon, 149:19 – 24, 2019.

[64] Wikiwand contributors. Spontaneous symmetry breaking. `https://www.wikiwand.com/en/Spontaneous_symmetry_breaking`, 2020. [Online; accessed 8-April-2020].

[65] Sera Cremonini. The Shear Viscosity to Entropy Ratio: A Status Report. Mod. Phys. Lett. B, 25:1867–1888, 2011.

[66] Sera Cremonini, Xi Dong, Junchen Rong, and Kai Sun. Holographic RG flows with nematic IR phases. JHEP, 07:082, 2015.

[67] Sera Cremonini, Umut Gursoy, and Phillip Szepietowski. On the Temperature Dependence of the Shear Viscosity and Holography. JHEP, 08:167, 2012.

[68] Michael Crossley, Paolo Glorioso, and Hong Liu. Effective field theory of dissipative fluids. JHEP, 09:095, 2017.

[69] Jin Dai, R. G. Leigh, and Joseph Polchinski. New Connections Between String Theories. Mod. Phys. Lett., A4:2073–2083, 1989.

[70] Jan de Boer, Michal P. Heller, and Natalia Pinzani-Fokeeva. Effective actions for relativistic fluids from holography. JHEP, 08:086, 2015.

[71] P. Debye. Zur theorie der spezifischen wärmen. Annalen der Physik, 344(14):789–839, 1912.

[72] Luca V. Delacrétaz, Blaise Goutéraux, Sean A. Hartnoll, and Anna Karlsson. Theory of hydrodynamic transport in fluctuating electronic charge density wave states. Phys. Rev. B, 96(19):195128, 2017.

[73] Oliver DeWolfe. TASI Lectures on Applications of Gauge/Gravity Duality. PoS, TASI2017:014, 2018.

[74] S. Dubovsky, T. Gregoire, A. Nicolis, and R. Rattazzi. Null energy condition and superluminal propagation. JHEP, 03:025, 2006.

[75] Anatoly Dymarsky, Zohar Komargodski, Adam Schwimmer, and Stefan Theisen. On Scale and Conformal Invariance in Four Dimensions. JHEP, 10:171, 2015.

[76] D. Ebert, R. N. Faustov, and V. O. Galkin. Mass spectra and Regge trajectories of light mesons in the relativistic quark model. Phys. Rev., D79:114029, 2009.

[77] Solomon Endlich, Alberto Nicolis, Rafael A. Porto, and Junpu Wang. Dissipation in the effective field theory for hydrodynamics: First order effects. Phys. Rev., D88:105001, 2013.

[78] Kurt Engelbrecht. Future prospects for elastocaloric devices. Journal of Physics: Energy, 1(2):021001, may 2019.

[79] A. Esposito, S. Garcia-Saenz, A. Nicolis, and R. Penco. Conformal solids and holography. JHEP, 12:113, 2017.

[80] Thomas Faulkner, Hong Liu, John McGreevy, and David Vegh. Emergent quantum criticality, Fermi surfaces, and AdS(2). Phys. Rev., D83:125002, 2011.

[81] Y. B. Fu and R. W. Ogden, editors. Nonlinear Elasticity. Cambridge University Press, May 2001.

[82] Matthias R. Gaberdiel. An Introduction to conformal field theory. Rept. Prog. Phys., 63:607–667, 2000.

[83] David Garfinkle, Gary T. Horowitz, and Andrew Strominger. Charged black holes in string theory. Phys. Rev. D, 43:3140–3143, May 1991.

[84] A. N. Gent. A new constitutive relation for rubber. Rubber Chemistry and Technology, 69(1):59–61, 1996.

[85] G. W. Gibbons and S. W. Hawking. Action Integrals and Partition Functions in Quantum Gravity. Phys. Rev., D15:2752–2756, 1977.

[86] G. W. Gibbons and Kei-ichi Maeda. Black Holes and Membranes in Higher Dimensional Theories with Dilaton Fields. Nucl. Phys., B298:741–775, 1988.

[87] Gian F. Giudice, Martti Raidal, and Alessandro Strumia. Lorentz Violation from the Higgs Portal. Phys. Lett., B690:272–279, 2010.

[88] Paolo Glorioso and Hong Liu. Lectures on non-equilibrium effective field theories and fluctuating hydrodynamics. 2018.

[89] G. N. Greaves, A. L. Greer, R. S. Lakes, and Tanguy Rouxel. Poisson's ratio and modern materials. Nature Materials, 10(11):823–837, 2011.

[90] Michael B. Green, J. H. Schwarz, and Edward Witten. SUPERSTRING THEORY. VOL. 1: INTRODUCTION. Cambridge Monographs on Mathematical Physics. 1988.

[91] Stefan Groot Nibbelink and Maxim Pospelov. Lorentz violation in supersymmetric field theories. Phys. Rev. Lett., 94:081601, 2005.

[92] Sašo Grozdanov and Janos Polonyi. Viscosity and dissipative hydrodynamics from effective field theory. Phys. Rev., D91(10):105031, 2015.

[93] E. Grüneisen. Über die thermische ausdehnung und die spezifische wärme der metalle. Annalen der Physik, 331(6):211–216, 1908.

[94] E. Grüneisen. Theorie des festen zustandes einatomiger elemente. Annalen der Physik, 344(12):257–306, 1912.

[95] S. S. Gubser, Igor R. Klebanov, and Alexander M. Polyakov. Gauge theory correlators from noncritical string theory. Phys. Lett., B428:105–114, 1998.

[96] Felix M. Haehl, R. Loganayagam, and Mukund Rangamani. The eightfold way to dissipation. Phys. Rev. Lett., 114:201601, 2015.

[97] Felix M. Haehl, R. Loganayagam, and Mukund Rangamani. Two roads to hydrodynamic effective actions: a comparison. 2017.

[98] Felix M. Haehl, R. Loganayagam, and Mukund Rangamani. Effective Action for Relativistic Hydrodynamics: Fluctuations, Dissipation, and Entropy Inflow. 2018.

[99] Mark F. Hamilton, Yurii A. Il'inskii, and Evgenia A. Zabolotskaya. Nonlinear surface acoustic waves in crystals. The Journal of the Acoustical Society of America, 105(2):639–651, 1999.

[100] Sean A. Hartnoll. Lectures on holographic methods for condensed matter physics. Class. Quant. Grav., 26:224002, 2009.

[101] Sean A. Hartnoll. Theory of universal incoherent metallic transport. Nature Phys., 11:54, 2015.

[102] S. W. Hawking. Gravitational radiation from colliding black holes. Phys. Rev. Lett., 26:1344–1346, 1971.

[103] S. W. Hawking. Black holes in general relativity. Commun. Math. Phys., 25:152–166, 1972.

[104] S. W. Hawking. Black hole explosions. Nature, 248:30–31, 1974.

[105] S. W. Hawking. Particle Creation by Black Holes. Commun. Math. Phys., 43:199–220, 1975. [,167(1975)].

[106] S. W. Hawking and Don N. Page. Thermodynamics of Black Holes in anti-De Sitter Space. Commun. Math. Phys., 87:577, 1983.

[107] Marc Henneaux, Cristian Martinez, Ricardo Troncoso, and Jorge Zanelli. Asymptotically anti-de Sitter spacetimes and scalar fields with a logarithmic branch. Phys. Rev., D70:044034, 2004.

[108] Peter Hertel. Linear Response Theory, pages 57–85. 05 2012.

[109] Thomas Hertog and Kengo Maeda. Black holes with scalar hair and asymptotics in N = 8 supergravity. JHEP, 07:051, 2004.

[110] Shahar Hod. Bekenstein's generalized second law of thermodynamics: The role of the hoop conjecture. Phys. Lett., B751:241–245, 2015.

[111] Petr Horava. Strings on World Sheet Orbifolds. Nucl. Phys., B327:461–484, 1989.

[112] Gary T. Horowitz and Andrew Strominger. Black strings and P-branes. Nucl. Phys., B360:197–209, 1991.

[113] Carlos Hoyos, Uri Kol, Jacob Sonnenschein, and Shimon Yankielowicz. The holographic dilaton. JHEP, 10:181, 2013.

[114] Zheng Ming Huang, S. Ramakrishna, and A.A.O. Tay. Modeling the stress/strain behavior of a knitted fabric-reinforced elastomer composite. Composites Science and Technology, 60(5):671 – 691, 2000.

[115] Veronika E. Hubeny, Shiraz Minwalla, and Mukund Rangamani. The fluid/gravity correspondence. In Theoretical Advanced Study Institute in Elementary Particle Physics: String theory and its Applications: From meV to the Planck Scale, pages 348–383, 2012.

[116] D. S. Hughes and J. L. Kelly. Second-order elastic deformation of solids. Phys. Rev., 92:1145–1149, Dec 1953.

[117] Roberto Iengo, Jorge G. Russo, and Marco Serone. Renormalization group in Lifshitz-type theories. JHEP, 11:020, 2009.

[118] M. S. Ikeda, J. A. W. Straquadine, A. T. Hristov, T. Worasaran, J. C. Palmstrom, M. Sorensen, P. Walmsley, and I. R. Fisher. AC elastocaloric effect as a probe for thermodynamic signatures of continuous phase transitions. Review of Scientific Instruments, 90(8):083902, August 2019.

[119] ASM International. Atlas of Stress-strain Curves. ASM International, 2002.

[120] Y. Ishii, Y. Ouchi, S. Kawaguchi, H. Ishibashi, Y. Kubota, and S. Mori. Glassy anomalies in the lattice heat capacity of a crystalline solid caused by ferroelectric fluctuation. Physical Review Materials, 3(8), August 2019.

[121] Werner Israel. Event horizons in static vacuum space-times. Phys. Rev., 164:1776–1779, 1967.

[122] Werner Israel. Event horizons in static electrovac space-times. Commun. Math. Phys., 8:245–260, 1968.

[123] Y. Liu J. Zaanen, Y.W. Sun and K. Schalm. The AdS/CMT manual for plumbers and electricians. 2012.

[124] R. Jackiw and S.-Y. Pi. Tutorial on Scale and Conformal Symmetries in Diverse Dimensions. J. Phys. A, 44:223001, 2011.

[125] Sachin Jain, Nilay Kundu, Kallol Sen, Aninda Sinha, and Sandip P. Trivedi. A Strongly Coupled Anisotropic Fluid From Dilaton Driven Holography. JHEP, 01:005, 2015.

[126] Kristan Jensen, Raja Marjieh, Natalia Pinzani-Fokeeva, and Amos Yarom. A panoply of Schwinger-Keldysh transport. 2018.

[127] Kristan Jensen, Natalia Pinzani-Fokeeva, and Amos Yarom. Dissipative hydrodynamics in superspace. 2017.

[128] D. F. Jones and L. R. G. Treloar. The properties of rubber in pure homogeneous strain. Journal of Physics D Applied Physics, 8:1285–1304, August 1975.

[129] Shamit Kachru, Xiao Liu, and Michael Mulligan. Gravity duals of Lifshitz-like fixed points. Phys. Rev. D, 78:106005, 2008.

[130] Leo P. Kadanoff. Scaling laws for ising models near T_c. Physics Physique Fizika, 2:263–272, Jun 1966.

[131] Youngman Kim and Deokhyun Yi. Holography at work for nuclear and hadron physics. Adv. High Energy Phys., 2011:259025, 2011.

[132] Charles Kittel. Introduction to Solid State Physics. Wiley, 8 edition, 2004.

[133] Igor R. Klebanov and Edward Witten. AdS / CFT correspondence and symmetry breaking. Nucl. Phys., B556:89–114, 1999.

[134] Manfred Klüppel and Joachim Schramm. A generalized tube model of rubber elasticity and stress softening of filler reinforced elastomer systems. Macromolecular Theory and Simulations, 9(9):742–754, 2000.

[135] Anton Krivtsov and Vitaly Kuzkin. Derivation of equations of state for ideal crystals of simple structure. Mechanics of Solids, 46:387–399, 06 2011.

[136] R. Küchler, N. Oeschler, P. Gegenwart, T. Cichorek, K. Neumaier, O. Tegus, C. Geibel, J. A. Mydosh, F. Steglich, L. Zhu, and Q. Si. Divergence of the grüneisen ratio at quantum critical points in heavy fermion metals. Physical Review Letters, 91(6), August 2003.

[137] R. Lakes and K. W. Wojciechowski. Negative compressibility, negative poisson's ratio, and stability. Physica Status Solidi (b), 245(3):545–551.

[138] L.D. Landau, E.M. Lifshitz, A.M. Kosevich, J.B. Sykes, L.P. Pitaevskii, and W.H. Reid. Theory of Elasticity: Volume 7. Course of theoretical physics. Elsevier Science, 1986.

[139] H. Leutwyler. Phonons as goldstone bosons. Helv. Phys. Acta, 70:275–286, 1997.

[140] P. Lloveras, A. Aznar, M. Barrio, Ph. Negrier, C. Popescu, A. Planes, L. Mañosa, E. Stern-Taulats, A. Avramenko, N. D. Mathur, X. Moya, and J.-Ll. Tamarit. Colossal barocaloric effects near room temperature in plastic crystals of neopentylglycol. Nature Communications, 10(1), April 2019.

[141] Ian Low and Aneesh V. Manohar. Spontaneously broken space-time symmetries and Goldstone's theorem. Phys. Rev. Lett., 88:101602, 2002.

[142] Matthew Luzum and Paul Romatschke. Conformal Relativistic Viscous Hydrodynamics: Applications to RHIC results at s(NN)**(1/2) = 200-GeV. Phys. Rev. C, 78:034915, 2008. [Erratum: Phys.Rev.C 79, 039903 (2009)].

[143] F. H. MacDougall. Kinetic theory of liquids. by j. frenkel. The Journal of Physical and Colloid Chemistry, 51(4):1032–1033, 1947.

[144] Gerald D. Mahan. Condensed Matter in a Nutshell. Princeton University Press, 2011.

[145] Juan Martin Maldacena. The Large N limit of superconformal field theories and supergravity. Int. J. Theor. Phys., 38:1113–1133, 1999. [Adv. Theor. Math. Phys.2,231(1998)].

[146] P. C. Martin, O. Parodi, and P. S. Pershan. Unified hydrodynamic theory for crystals, liquid crystals, and normal fluids. Phys. Rev. A, 6:2401–2420, Dec 1972.

[147] David Mateos. String Theory and Quantum Chromodynamics. Class. Quant. Grav., 24:S713–S740, 2007.

[148] David Mateos and Diego Trancanelli. The anisotropic N=4 super Yang-Mills plasma and its instabilities. Phys. Rev. Lett., 107:101601, 2011.

[149] John McGreevy. Holographic duality with a view toward many-body physics. Adv. High Energy Phys., 2010:723105, 2010.

[150] Eugenio Megias and Oriol Pujolas. Naturally light dilatons from nearly marginal deformations. JHEP, 08:081, 2014.

[151] Shiraz Minwalla. Restrictions imposed by superconformal invariance on quantum field theories. Adv. Theor. Math. Phys., 2:783–851, 1998.

[152] Prasanta K. Misra. Chapter 2 - phonons and lattice vibrations. In Prasanta K. Misra, editor, Physics of Condensed Matter, pages 37 – 69. Academic Press, Boston, 2012.

[153] M. Mooney. A theory of large elastic deformation. Journal of Applied Physics, 11(9):582–592, 1940.

[154] B. Moore, T. Jaglinski, D. S. Stone, and R. S. Lakes. Negative incremental bulk modulus in foams. Philosophical Magazine Letters, 86(10):651–659, 2006.

[155] M. Moratalla, P. Bejarano, J. Castilla, and Miguel Ramos. Residual entropy in the zero-temperature limit of toluene glass. Low Temperature Physics, 45:331–336, 03 2019.

[156] P. H. Mott and C. M. Roland. Limits to poisson's ratio in isotropic materials. Phys. Rev. B, 80:132104, Oct 2009.

[157] F. D. Murnaghan. Finite deformations of an elastic solid. American Journal of Mathematics, 59(2):235–260, 1937.

[158] James L. Nagle, Ian G. Bearden, and William A. Zajc. Quark-Gluon Plasma at RHIC and the LHC: Perfect Fluid too Perfect? New J. Phys., 13:075004, 2011.

[159] Yu Nakayama. Scale invariance vs conformal invariance. Phys. Rept., 569:1–93, 2015.

[160] H. Nastase. String Theory Methods for Condensed Matter Physics. Cambridge University Press, 2017.

[161] Horatiu Nastase. Introduction to AdS-CFT. 2007.

[162] Makoto Natsuume. AdS/CFT Duality User Guide. Lect. Notes Phys., 903:pp.1–294, 2015.

[163] Alberto Nicolis, Riccardo Penco, Federico Piazza, and Riccardo Rattazzi. Zoology of condensed matter: Framids, ordinary stuff, extra-ordinary stuff. JHEP, 06:155, 2015.

[164] Alberto Nicolis, Riccardo Penco, and Rachel A. Rosen. Relativistic Fluids, Superfluids, Solids and Supersolids from a Coset Construction. Phys. Rev. D, 89(4):045002, 2014.

[165] Holger Bech Nielsen and M. Ninomiya. Beta Function in a Noncovariant Yang-Mills Theory. Nucl. Phys., B141:153–177, 1978.

[166] Kodai Niitsu, Yuta Kimura, Toshihiro Omori, and Ryosuke Kainuma. Cryogenic superelasticity with large elastocaloric effect. NPG Asia Materials, 10(1):e457–e457, January 2018.

[167] R. W. Ogden. Large deformation isotropic elasticity – on the correlation of theory and experiment for incompressible rubberlike solids. Proceedings of the Royal Society of London A: Mathematical, Physical and Engineering Sciences, 326(1567):565–584, 1972.

[168] R. W. Ogden. Non-Linear Elastic Deformations. WILEY-VCH Verlag, 1985.

[169] R W Ogden. Non-linear elastic deformations. Dover civil and mechanical engineering. Dover Publications, New York, NY, 1997.

[170] R.W. Ogden, Giuseppe Saccomandi, and Ivonne Sgura. Fitting hyperelastic models to experimental data. Computational Mechanics, 34, 11 2004.

[171] Enrico Pajer and David Stefanyszyn. Symmetric Superfluids. JHEP, 06:008, 2019.

[172] J. Polchinski. String theory. Vol. 2: Superstring theory and beyond. Cambridge Monographs on Mathematical Physics. Cambridge University Press, 2007.

[173] Joseph Polchinski. Scale and conformal invariance in quantum field theory. Nuclear Physics B, 303(2):226 – 236, 1988.

[174] Joseph Polchinski. String Theory. Cambridge University Press, October 1998.

[175] G. Policastro, Dan T. Son, and Andrei O. Starinets. The Shear viscosity of strongly coupled N=4 supersymmetric Yang-Mills plasma. Phys. Rev. Lett., 87:081601, 2001.

[176] Giuseppe Policastro, Dam T Son, and Andrei O Starinets. From AdS/CFT correspondence to hydrodynamics. II. sound waves. Journal of High Energy Physics, 2002(12):054–054, dec 2002.

[177] Massimo Porrati and Rakibur Rahman. Causal Propagation of a Charged Spin 3/2 Field in an External Electromagnetic Background. Phys. Rev. D, 80:025009, 2009.

[178] Massimo Porrati and Rakibur Rahman. Notes on a Cure for Higher-Spin Acausality. Phys. Rev. D, 84:045013, 2011.

[179] Oriol Pujolas and Sergey Sibiryakov. Supersymmetric Aether. JHEP, 01:062, 2012.

[180] Joshua D. Qualls. Lectures on Conformal Field Theory. 11 2015.

[181] Alfonso V. Ramallo. Introduction to the AdS/CFT correspondence. Springer Proc. Phys., 161:411–474, 2015.

[182] Mukund Rangamani. Gravity and Hydrodynamics: Lectures on the fluid-gravity correspondence. Class. Quant. Grav., 26:224003, 2009.

[183] Pia Ray. Structural investigation of La(2-x)Sr(x)CuO(4+y) - Following staging as a function of temperature. PhD thesis, 11 2015.

[184] Anton Rebhan and Dominik Steineder. Violation of the Holographic Viscosity Bound in a Strongly Coupled Anisotropic Plasma. Phys. Rev. Lett., 108:021601, 2012.

[185] Slava Rychkov. EPFL Lectures on Conformal Field Theory in D¿= 3 Dimensions. SpringerBriefs in Physics. 2016.

[186] Subir Sachdev. Quantum Phase Transitions. Cambridge University Press, 2 edition, 2011.

[187] Sudhir Kumar Sahu, Digambar Jangade, Arumugam Thamizhavel, Mandar M. Deshmukh, and Vibhor Singh. Elastic properties of few unit cell thick superconducting crystals of bi2sr2cacu2o8. Applied Physics Letters, 115(14):143102, September 2019.

[188] A.N. Schellekens. Introduction to conformal field theory. Fortschritte der Physik/Progress of Physics, 44:605 – 705, 01 1996.

[189] C. Scheuerlein, F. Lackner, F. Savary, B. Rehmer, M. Finn, and C. Meyer. Thermomechanical Behavior of the HL-LHC 11 Tesla Nb3Sn Magnet Coil Constituents During Reaction Heat Treatment. IEEE Transactions on Applied Superconductivity, 28(3):2792485, April 2018.

[190] C. Scheuerlein, F. Lackner, F. Savary, B. Rehmer, M. Finn, and C. Meyer. Thermomechanical behavior of the HL-LHC 11 tesla nb3sn magnet coil constituents during reaction heat treatment. IEEE Transactions on Applied Superconductivity, 28(3):1–6, April 2018.

[191] Christian Scheuerlein, Friedrich Lackner, Frederic Savary, Birgit Rehmer, Monika Finn, and Patrick Uhlemann. Mechanical properties of the HL-LHC 11 t nb3sn magnet constituent materials. IEEE Transactions on Applied Superconductivity, 27(4):1–7, June 2017.

[192] Thomas Schäfer and Derek Teaney. Nearly Perfect Fluidity: From Cold Atomic Gases to Hot Quark Gluon Plasmas. Rept. Prog. Phys., 72:126001, 2009.

[193] Matthew D. Schwartz. Quantum Field Theory and the Standard Model. Cambridge University Press, 2014.

[194] T. Senthil. Critical fermi surfaces and non-fermi liquid metals. 2008.

[195] Chandan Setty. Glass-induced enhancement of superconducting tc : Pairing via dissipative mediators. Physical Review B, 99(14), April 2019.

[196] Chun Shen, Ulrich Heinz, Pasi Huovinen, and Huichao Song. Radial and elliptic flow in Pb+Pb collisions at the Large Hadron Collider from viscous hydrodynamic. Phys. Rev. C, 84:044903, 2011.

[197] Kostas Skenderis. Lecture notes on holographic renormalization. Class. Quant. Grav., 19:5849–5876, 2002.

[198] D. T. Son. Quantum critical point in graphene approached in the limit of infinitely strong Coulomb interaction. Phys. Rev., B75(23):235423, 2007.

[199] Dam T. Son and Andrei O. Starinets. Minkowski space correlators in AdS / CFT correspondence: Recipe and applications. JHEP, 09:042, 2002.

[200] Julian Sonner. Solvay Lectures On Applied Holography. 2016.

[201] Wieland Staessens and Bert Vercnocke. Lectures on Scattering Amplitudes in String Theory. In 5th Modave Summer School in Mathematical Physics Modave, Belgium, August 17-21, 2009, 2010.

[202] Leonard Susskind. The World as a hologram. J. Math. Phys., 36:6377–6396, 1995.

[203] Gerard 't Hooft. A Planar Diagram Theory for Strong Interactions. Nucl. Phys., B72:461, 1974. [,337(1973)].

[204] Gerard 't Hooft. Dimensional reduction in quantum gravity. Conf. Proc., C930308:284–296, 1993.

[205] Sam Tang. Wave propagation in initially-stressed elastic solids. Acta Mechanica, 4(1):92–106, Mar 1967.

[206] Marika Taylor. Non-relativistic holography. 12 2008.

[207] Marika Taylor and William Woodhead. Inhomogeneity simplified. Eur. Phys. J. C, 74(12):3176, 2014.

[208] M. F. Thorpe and I. Jasiuk. New results in the theory of elasticity for two-dimensional composites. Proceedings of the Royal Society of London Series A, 438(1904):531–544, September 1992.

[209] R. A. Toupin and B. Bernstein. Sound waves in deformed perfectly elastic materials. acoustoelastic effect. The Journal of the Acoustical Society of America, 33(2):216–225, 1961.

[210] K. Trachenko. Lagrangian formulation and symmetrical description of liquid dynamics. pre, 96(6):062134, December 2017.

[211] K. Trachenko and V. V. Brazhkin. Collective modes and thermodynamics of the liquid state. Reports on Progress in Physics, 79(1):016502, January 2016.

[212] L. R. G. Treloar. Stress-strain data for vulcanised rubber under various types of deformation. Trans. Faraday Soc., 40:59–70, 1944.

[213] O. Vafek, Z. Tesanovic, and M. Franz. Relativity restored: Dirac anisotropy in QED(3). Phys. Rev. Lett., 89:157003, 2002.

[214] Giorgio Velo and Daniel Zwanzinger. Noncausality and other defects of interaction lagrangians for particles with spin one and higher. Phys. Rev., 188:2218–2222, Dec 1969.

[215] Vinod Wadhawan. Understanding natural phenomena 9: Symmetry is supreme. http://nirmukta.com/2012/10/27/understanding-natural-phenomena-9-symmetry-is-supreme/, 2012. [Online; accessed 8-April-2020].

[216] Y. C. Wang and R. S. Lakes. Composites with inclusions of negative bulk modulus: Extreme damping and negative poisson's ratio. Journal of Composite Materials, 39(18):1645–1657, 2005.

[217] Steven Weinberg and Edward Witten. Limits on Massless Particles. Phys. Lett., 96B:59–62, 1980.

[218] Wikipedia contributors. Quantum phase transition. [Online; accessed 31-March-2020].

[219] Edward Witten. Anti-de Sitter space and holography. Adv. Theor. Math. Phys., 2:253–291, 1998.

[220] Edward Witten. Multitrace operators, boundary conditions, and AdS / CFT correspondence. 2001.

[221] Sheng Xu, Hai-You Huang, Jianxin Xie, Shouhei Takekawa, Xiao Xu, Toshihiro Omori, and Ryosuke Kainuma. Giant elastocaloric effect covering wide temperature range in columnar-grained cu71.5al17.5mn11 shape memory alloy. APL Materials, 4(10):106106, October 2016.

[222] Y.B.Fu and R.W. Ogden. Nonlinear Elasticity: Theory and Applications. Number 283 in London Mathematical Society lecture note series. Cambridge University Press, Cambridge, UK, 2001.

[223] Yi-Cong Yu, Shizhong Zhang, and Xi-Wen Guan. Gr\"{u} neisen parameters: origin, identity and quantum refrigeration. arXiv preprint arXiv:1909.05754, 2019.

[224] J. Zaanen. Superconductivity - why the temperature is high. Nature, 430:512–3, 08 2004.

[225] Jan Zaanen, Ya-Wen Sun, Yan Liu, and Koenraad Schalm. Holographic Duality in Condensed Matter Physics. Cambridge Univ. Press, 2015.

[226] A. Zaffaroni. Introduction to the AdS-CFT correspondence. Class. Quant. Grav., 17:3571–3597, 2000.

[227] Lijun Zhu, Markus Garst, Achim Rosch, and Qimiao Si. Universally diverging grüneisen parameter and the magnetocaloric effect close to quantum critical points. Physical Review Letters, 91(6):066404, 2003.

[228] Barton Zwiebach. A First Course in String Theory, 2nd Edition. Cambridge University Press, jan 2009.